Investigation of the Influence of Magnetostriction and Magnetic Forces on Transformer Core Noise and Vibration

Teeraphon Phophongviwat

A thesis submitted to the Cardiff University in candidature for the degree of Doctor of Philosophy

Wolfson Centre for Magnetics
Cardiff School of Engineering, Cardiff University
Wales, United Kingdom

August 2013

DECLARATION

This work has not previously been accepted in substance for any degree and is not concurrently submitted in candidature for any degree.

Signed ……. (candidate) Date ……...

STATEMENT 1

This thesis is being submitted in partial fulfillment of the requirements for the degree of PhD.

Signed ……. (candidate) Date ……...

STATEMENT 2

This thesis is the result of my own independent work/investigation, except where otherwise stated. Other sources are acknowledged by explicit references.

Signed ……. (candidate) Date ……...

STATEMENT 3

I hereby give consent for my thesis, if accepted, to be available for photocopying and for inter-library loan, and for the title and summary to be made available to outside organisations.

Signed ……. (candidate) Date ……...

Acknowledgements

The research presented in this thesis has been carried out at the Wolfson Centre for Magnetics, Institute of Energy, Cardiff School of Engineering, Cardiff University, under the supervision of Professor Anthony Moses and Dr Philip Anderson. I wish to express my deepest gratitude to them for the guidance, encouragement, patience and support they has given me in the past few years.

I would like to thank all sponsors: ABB AB, AK Steel Corp., Alstom Grid, Brush Transformers Ltd, CG Holdings Belgium N.V., Cogent Power Ltd, Kolektor Etra Energetski transformatorji d.o.o., Koncar Distribution and Special Transformers Inc., Legnano Teknoelectric Company S.p.A., Nuova Eletrofer S.p.A., SGB Starkstrom-Gerätebau GmbH, and ThyssenKrupp Electrical Steel GmbH for the financial support which allowed the successful completion of this research project.

Sincere thanks go to Dr Yevgen Melikhov and Dr Hugh Stanbury for valuable discussion during the investigation. Thanks also to all recent and present members of Wolfson Centre for Magnetics for a friendly environment they have created for me. In particular, I would like to thank Dr Sakda Somkun, Mr Tomasz Kutrowski Mr Lukasz Mierczak and Mr Mahesh Mani for the intimate friendship also my colleague Mr Shervin Tabrizi for fulfilling this project.

I am grateful for helping and supporting from staff of the Cardiff School of Engineering, particularly Mr Alan Jauncey and Mr Paul Farrugia of the electrical and electronic workshop, Mr Malcolm Seaborne and Mr Stephen Mead of the mechanical workshop, Mrs Aderyn Reid and Mrs Chris Lee of the research office.

Deepest thanks to my parents Satien and Suree, my brother Phornphot, and my sister Aporn who have believed in me. Without their love and support this work would have never been possible. Finally, I am greatly indebted to my girlfriend Ruetima for her love, encouragement, support and patience she always has for me.

Summary

Transformer noise is of increasing environmental concern so continued efforts are being made by electrical steel and transformer producers to satisfy users by reducing the noise. Magnetostriction and magnetic forces are the main causes of transformer core noise and vibration. Understanding of the relationship from the core material to core structure and core vibration to core noise can help the design of low noise transformer cores.

The most appropriate parameter for investigating the relationship between noise and vibration is sound pressure (in the unit of Pascals) in the frequency domain because it is not A-weighted. In this study, the side surfaces of transformer cores were found to emit higher noise than front and top surfaces at low magnetic induction. When the magnetic induction was increased, the effect of magnetic force increased and caused the front surfaces to emit higher noise.

For three phase three limb transformer cores, the front surface of the middle limb generated higher noise than the outer limbs due to the effect of T-joint. However this does not translate higher noise level because of the phase difference of the vibration between the limbs. Due to this A-weighted sound power level of three phase, three limb transformer cores were shown to be lower than single phase transformer cores, although at the same cross sectional area and core window size the three phase cores has larger size.

A model, developed to separate the effects of magnetostriction and magnetic forces on transformer core vibration, showed that at low induction, magnetostriction is more significant than magnetic forces. The magnetic forces become more significant than magnetostriction when the induction is increased. Magnetostriction primarily depends on material and stress but magnetic forces principally depend on core building. Louder noise can be generated from a core built with low magnetostriction material than higher magnetostriction if the building tolerances are worse. The effect of magnetic forces on transformer core vibration can be reduced by using a bonding technique.

List of Abbreviations and Symbols

Abbreviations

C	Chord
CGO	Conventional grain oriented
GO	Grain oriented
H	Height
HGO	High permeability grain oriented
L	Length
LDR	Laser scribed domain refined
LDV	Laser Doppler Vibrometer
MSL	Multistep lap
R	Radius
stdev	Standard deviation
SSL	Single step lap
SWG	Standard wire gauge
VI	Virtual Instrument
W	Width

Symbols

a	Overlap length
A	Maximum amplitude of the wave
A_c	Cross sectional area
A_w	Coefficient for the A-weighting scale
b	Instantaneous magnetic flux density
b_{total}	Total localised magnetic flux
$b_{r.d.}$	Localised magnetic flux in the rolling direction
$b_{t.d.}$	Localised magnetic flux in the transverse direction
B	Magnetic flux density
B_8	Magnetic flux density at magnetic field 800 A/m, 50 Hz
B_c	Critical induction
B_g	In-plane magnetic flux flow through the gap
B_m	Maximum magnetic flux density
B_{sat}	Saturation induction of the material
B_z	Magnetic flux flow through the gap in normal direction
c	Sound velocity in air
c_i	Sensitivity coefficient of measurement uncertainties

d	Lamination thickness
d_b	Bolt diameter
e_n	Induced voltage from needle probe
e_s	Induced voltage from search coil
f	Frequency
f_n	n^{th} harmonic frequency
f_1	Coherent light source frequency
f_D	Frequency resulting from the Doppler effect
F	Force
g	Gap length between the lamination joints
h	A half the height of the core
H	Magnetic field
J	Torque coefficient
k	Core stacking height
k_{95}	Coverage factor at confidence 95 %
K	Environmental correction
l	Length of the material
l_m	Length in metres of the prescribed contour
L_{bgA}	Average A-weighted background sound pressure level
L_p	Sound pressure level
L_{pA}	Corrected average A-weighted sound pressure level
L_{pAi}	A-weighted sound pressure level
L_{pA0}	Average A-weighted sound pressure level
L_w	Sound power level
L_{wA}	A-weighted sound power level
m	Wave number
n	Number of measurement
N	Number of step
N_{mic}	Total number of measuring position

p	Sound pressure
P	A-weighted magnetostrictive vibration acceleration level
p_g	Attractive stress between the laminations in in-plane direction
p_n	Harmonic components of magnetostrictive vibration acceleration
p_o	Magnetostriction vibration acceleration reference level
p_{ref}	Reference pressure
p_{rms}	Measured root mean square sound pressure
p_z	Attractive interlaminar stress between the lamination in the normal direction
r_c	Radius of curvature
s	Length of overlap shift
S_0	Reference area
S_{w}	Sound power
$S_{\text{w,ref}}$	Reference sound power
S_v	Total area of the surface of the test room
t	Time coordinate
t_L	Thickness of the lamination
T	Torque
u_A	Type A uncertainty
u_B	Type B uncertainty
U	Uncertainty
v	Instantaneous induced voltage
$W_{17/50}$	Core loss at magnetic flux density, 1.7 T, 50 Hz
x	Space coordinate
y	Measured value
Z	Self-transparent mirror
Z_1	Reflector
α	Average acoustic absorption coefficient
χ_x	Displacements along the rolling direction

χ_y	Displacements along the transverse direction
χ_z	Displacements along the normal direction
δ	Phase shift
Δl	Change in length
Δl_{total}	Total deformation
Δl_{λ}	Deformation due to magnetostriction
Δl_M	Deformation due to magnetic forces
ε_b	Bending strain
λ	Magnetostriction
$\lambda_{r.d.}$	Magnetostriction in the rolling direction
λ_n	Magnetostriction harmonic component
$\lambda_{\text{p-p}}$	Peak to peak magnetostriction
$\lambda_{t.d.}$	Magnetostriction in the transverse direction
λ	Sound wave length in air
$\hbar$	Wave length of light
μ_0	Permeability of the free space
υ	Vibration velocity
ω	Angular frequency
ϕ	Phase constant
σ	Stress
τ	Acceleration
ζ	Sound wave

List of Contents

Chapter 1

Background and Aim of Investigation

1.1 Introduction

There is continuous worldwide increase in electricity consumption due to growth of requirements of industry and facilities in households [1]. Transformers are essential components in electrical power systems which transfer electrical energy from the power plants to the loads. Step up transformers are used for increasing the voltage levels in order to reduce the losses in the transmission system and step down transformers are used for decreasing the voltage from transmission line to the required level of the loads. Although transformer efficiency during operation at full load is very high, core noise and core loss, are always present even on no load. To classify the class of a transformer, European standard categories on transformer no load losses and sound power level [2] are in place. Transformer noise is mainly caused by core vibration, winding vibration due to load currents and ancillary equipment such as the cooling pumps [3], [4]. Although transformer core vibration and noise have been widely studied [5], [6], a greater understanding is needed so that steps can be proposed to reduce them further. This work focuses on the acoustic noise emitted from the transformer core.

1.2 Objectives

It is widely accepted that magnetostriction of grain oriented silicon steel laminations and inter lamination magnetic forces are the main causes of transformer core noise. However, no conclusive agreement has been reached on how each contributes to the noise and vibration. Various ways of quantifying sound have been used. A-weighted sound power level has been introduced for comparison of output noise from transformer cores. It is independent of frequency of the sound, the distance of the measurement and the dimensions of the sound source. However, it is not easy to directly relate it to core vibration.

Core configuration and build have a large impact on transformer core noise because magnetic forces depend on the gaps at the core joints. Also the T-joints in the three phase transformer core are highly strained due to the presence of rotational magnetisation which is the flux remains constant in magnitude, but rotates with uniform angular velocity in the plane of the lamination. There is no explanation of how it is related to the core noise and vibration. To produce low noise cores, clamping and bonding the core laminations are investigated.

The following are the aims of this research:

1. To quantify the causes of transformer core vibration and noise.
2. To develop a model for separating the effect of magnetostriction and magnetic forces on transformer core vibration.
3. To identify the appropriate parameters for studying the relationship between transformer core vibration and noise.
4. To investigate the effect of transformer core building and bonding on transformer core noise and vibration.

In order to achieve the aims three phase, three limb and single phase core type transformer cores were designed and assembled from three types of grain-oriented electrical steel in multistep lap and single step lap configurations. The three phase and single phase cores had the same window size and cross sectional area per phase. A sound measurement system was developed to measure sound pressure generated from the cores under clamping torques from 2 Nm to 6 Nm and magnetic flux densities up to 1.8 T at a magnetisation frequency of 50 Hz. A scanning laser vibrometer was used for measuring core surface vibrations. Noise and vibration experimental results from the cores were compared. The following influential transformer core parameters were investigated in order to study the relationship between core noise and vibration: electrical steel grade, step lap configuration and, clamping torque. In addition, the effect of core bonding was investigated.

Chapter 2

Literature review

The aim of this chapter is to introduce previous related work on transformer core noise and vibration. The effect of step lap configurations, material grades, overlap length, number of step laps, length of overlap shift, clamping torques and number of laminations per stacking layer are described.

2.1 Transformer cores

Transformer cores are usually built up from a stack of grain oriented electrical steel laminations. To minimise the core losses due to magnetic flux flow across the lamination grain orientation direction (rolling direction) at the joints, the ends of the lamination are cut at 45° to the rolling direction. The jointing is known as a mitred joint [7]. To stack the laminations, an overlap is needed. If the stack has only one step overlap (two different shapes of laminations), it is called a single step lap (SSL). If the stack has more than one step overlap (three or more different shapes of laminations), it is termed a multistep lap (MSL). There are two constructions of step overlap: cross-step and longitudinal-step as shown in Fig.2-1.

Mitred joints can have single step lap or multistep lap. Each step can be assembled with one or more laminations depending on the size and cost of the cores [4]. Fig 2-2 shows both single step lap and multistep lap assemblies, (Fig. 2-2 a,c) also shows the dimension of the overlap length, a, length of overlap shift, s and number of step, N.

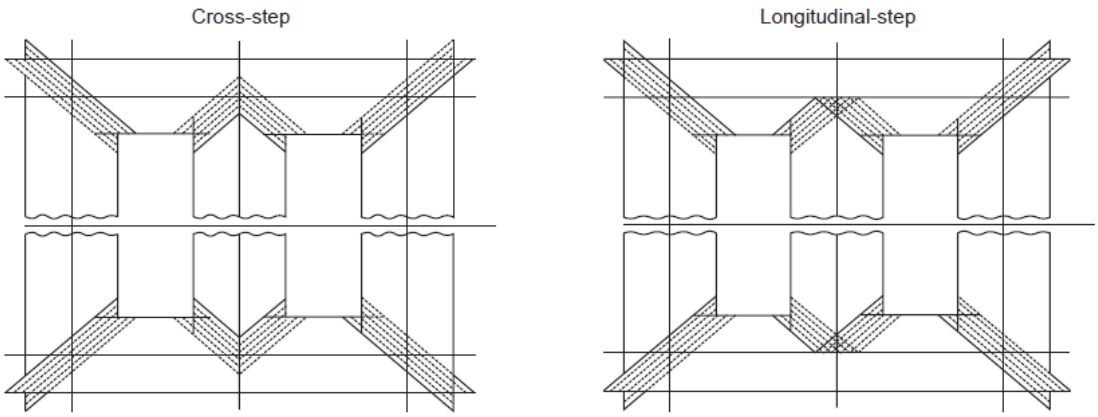

a) b)

Fig.2-1: The mitred joint constructions [8]
a) Cross-step construction
b) Longitudinal step construction

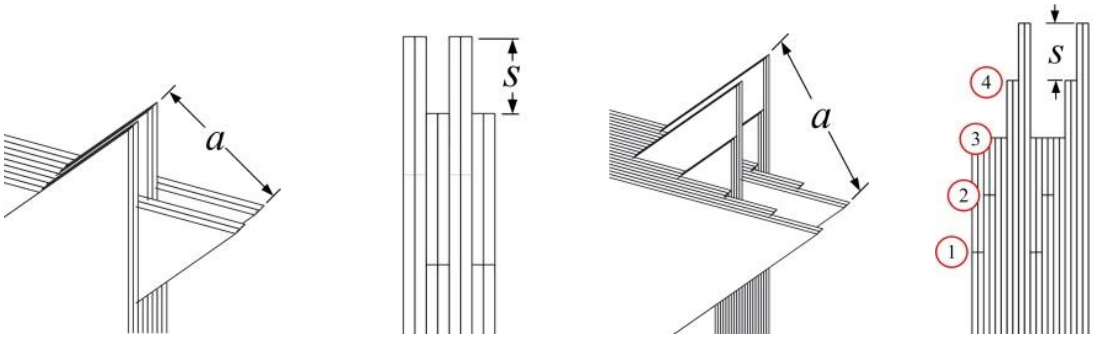

a) b) c) d)

Fig.2-2: Mitred joint corner
a) Single step lap
b) Side view of single step lap with two laminations per step
c) Multistep lap (four steps)
d) Side view of multi-step lap with two laminations per step

2.2 Study of transformer core noise

It is generally accepted that magnetostriction is a cause of transformer core vibration and noise. Magnetostriction (λ) is a deformation of magnetic materials due to magnetisation [9]. It is defined in Eq. 2.1 as follows

$$\lambda = \frac{\Delta l}{l} \tag{2-1}$$

where Δl is the change in length, l is the length of the material.

Magnetostriction is caused by rearrangements of domain structure especially the movements of non 180° domain walls. This phenomenon affects transformer core vibration; the other cause is magnetic force between the laminations. A review of the related works about transformer core noise and vibration follows.

In 1980, Reiplinger [10] mentioned that "transformers with cores made from low magnetostriction sheets often produced higher noise levels than transformer with cores made from high magnetostriction sheets" and proposed A-weighted vibration velocity in term of logarithmic ratio of velocity and reference velocity in the same way as sound pressure level for assessment of grain oriented laminations with respect to transformer noise. The suitable value of reference velocity for core weight 10000 kg was 10^{-6} m/s per m.

One year later, Foster and Reiplinger [11] presented the effects of different electrical steel lamination properties due to the production process and magnetostriction frequency components on the transformer noise. A different peak to peak magnetostriction, $\lambda_{p\text{-}p}$ of grain oriented silicon steel laminations (M5 grade) was found when annealed with different temperatures. The $\lambda_{p\text{-}p}$ at 780°C was positive and became negative when annealed at 850°C.

To compare the effect of $\lambda_{p\text{-}p}$ on noise level, three different $\lambda_{p\text{-}p}$ characteristics from M5 grade laminations produced by different manufacturers were used. Fig 2-3 shows the $\lambda_{p\text{-}p}$ characteristics in a DC and AC magnetic field. At 1.8 T, lamination I shows positive magnetostriction and lamination III shows negative magnetostriction. Magnetostriction components at 100 to 600 Hz were used for calculating the sound pressure level. The calculated results show lamination II had lowest sound pressure level both quantified in dB and dBA while lamination I had highest sound pressure

level in dB but lamination III presented the highest sound pressure level in dBA. These are due to their different harmonic characteristics of the magnetostriction because they have different coatings.

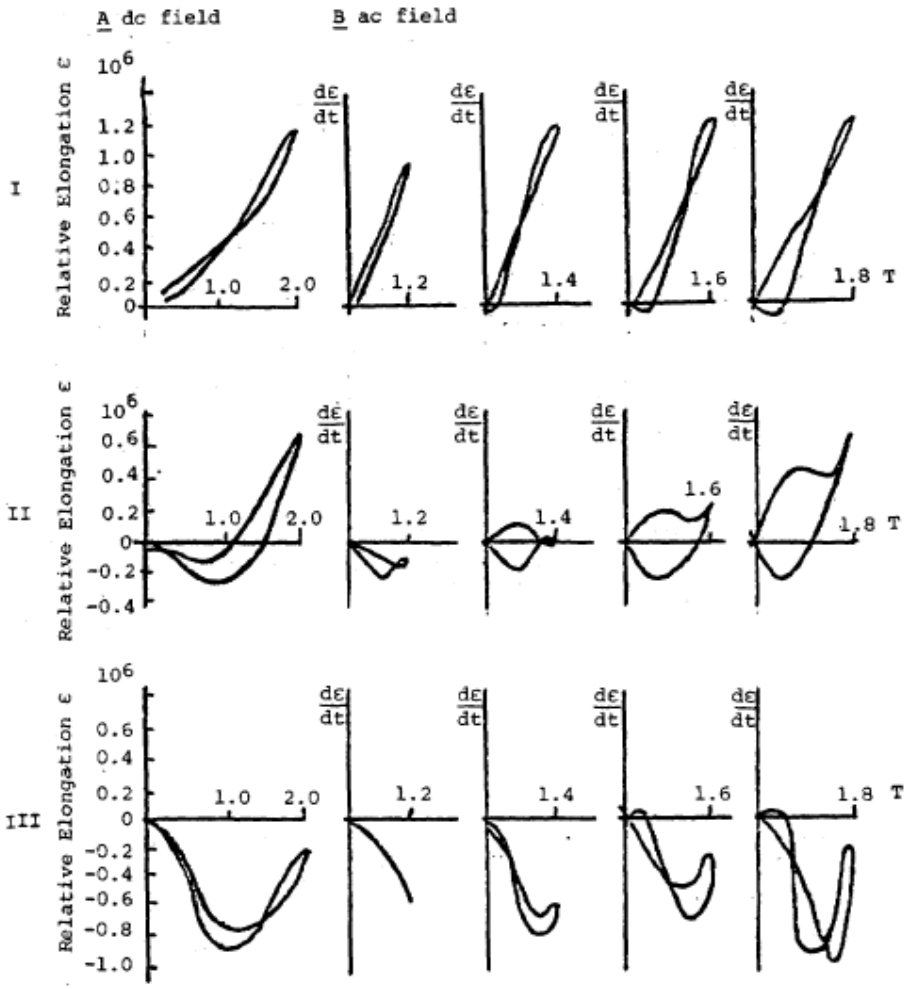

Fig.2-3: Comparison of magnetostriction characteristics after annealing of the same grade of material but used by different manufacturers [11]

In 1984, Mapp and White [12] studied characteristic of magnetostriction harmonics of both longitudinal and transverse to the rolling direction of single grains of grain-oriented (GO) 3.25% silicon-iron under compressive stresses in the [001] direction. This material was usually used in the transformer cores. The results showed the

components of the first three harmonics had an approximate 2:1 relationship between longitudinal and transverse direction.

In 1994, Valkovic [13] investigated the effect of electrical steel grades with regards to transformer core noise. Single phase cores, each with a mass of 105 kg and dimensions as shown in Fig.2-4, were used in the experiments. Cores were built from three 0.27 mm thick lamination grades, conventional grain oriented (commercial code M4), high permeability grain oriented (commercial code MOH) and domain refined (commercial code ZDKH). Single step lap core configuration with a length of overlap shift of 10 mm and two laminations per stagger layer were compared with five multistep laps core configuration with a length of overlap shift 2 mm and single laminations per stacking layer. The transformers were tested in an anechoic chamber. The results at magnetic flux densities (B), 1.4 T, 1.6 T and 1.8 T showed approximately the same noise level for MOH and ZDKH both on MSL and SSL configurations. The highest noise level was found from the M4 core. The cores had the same dimensions but different step lap configurations and materials, therefore, the author concluded that the variation of the noise between each of them had to be the operating magnetic flux density and step lap configuration.

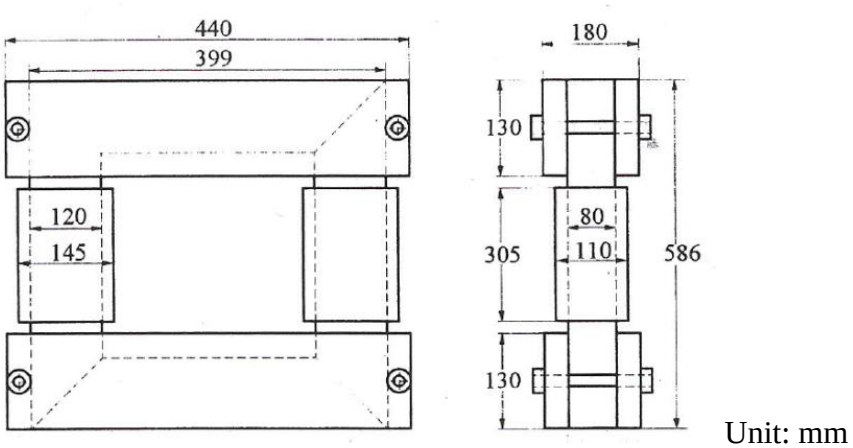

Fig.2-4: Structure and dimensions of single phase transformer core models [13]

In 1996, Valkovic [14] studied the effect of overlap length on transformer core noise. M4 laminations, 0.27 mm thick, was used. The SSL joint structure as shown in Fig.2-4 were built with overlap shifts of 2 mm to 14 mm. The experimental results at magnetic flux density 1.4 T to 1.75 T showed lowest noise at 2 mm overlap length and the highest at 14 mm. The reason for this is the longer overlap shift had more lamination protruding out from the core than the short one and this protrusion is allowed to freely vibrate.

Ilo et al. [15] studied relevance of length of overlap shifts and number of step laps. To eliminate the effect of rotational magnetisation, the linearisation core models as shown in Fig.2.5 (a) were used by assembling the laminations with overlap shift on the limb. The core was built with domain refined of high permeability grain oriented material (ZDKH-LS) with Epstein size. Fig 2.5 (b) shows detail of the overlap area.

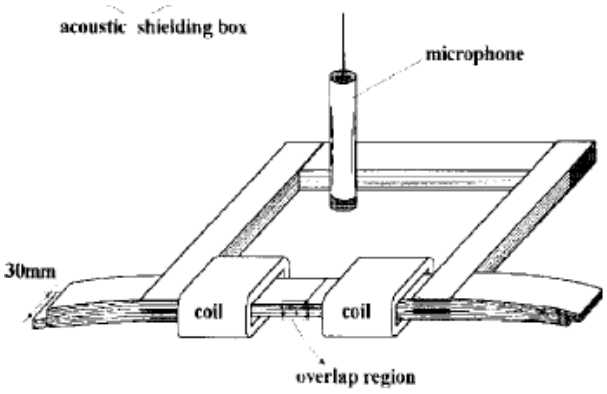

a)

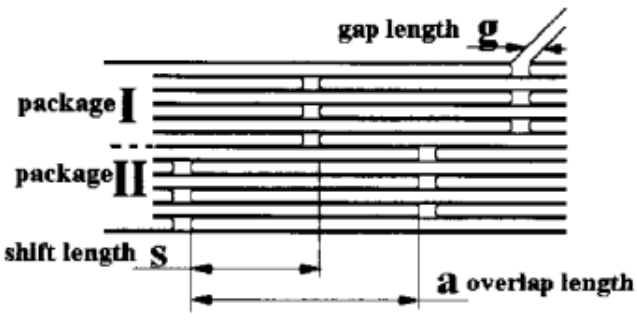

b)

Fig.2-5: Configuration of the core and linearisation overlap area [15]

a) Linearisation overlap model with microphone fixed at 30 cm above the core window

b) Detail of the overlap area

The limb with the overlap region was assembled from 0.23 mm thick laminations and the other limbs were assembled with 0.27 mm thick laminations. In the experiments, the cores were located in a bottomless 9 cm thick acoustic shielding test box with a Brüel&Kjær condenser microphone fixed at 30 cm above the core window. In this position, the microphone detected an average noise generated from all joints. The noise variation results were only from the changing of configuration of the overstep lap because the configuration of the butt joints were fixed. To compare the effect of number of step laps on noise level, overlap length and air gap length were fixed at 10 mm and 1 mm, respectively. The number of step laps influences the magnetic flux density of the laminations near the gaps. Magnetic flux densities in the laminations above and below the gap are higher than the operating magnetic flux due to magnetic flux flowing from the end of the lamination next to the gap to neighbouring laminations because the gap has higher reluctance. The operating magnetic flux density which causes the laminations above and below the gap to reach saturation is termed the critical induction, B_c, and can be approximated by Eq. 2-2 [16].

$$B_c \approx \frac{N}{N+1} \times B_{sat} \tag{2-2}$$

when B_{sat} is the saturation induction of the material.

There was no significant difference in experimental results with B lower than the B_c in the SSL core length of the overlap shift was varied. The critical induction was the saturation induction of the ends of laminations near the gap.

However, the noise increased rapidly when B was higher than B_c and the same for two MSL configurations with $B_c \approx 1.3$ T. The noise generated from MSL cores was lower than SSL cores at any operating B because of the effect of interlaminar forces at the end of the laminations at the joint.

To compare the effect of overlap length on noise level, an SSL configuration was used and the air gap lengths were fixed at 10 mm. The results showed comparison of noise between two overlap lengths. The first one was a half-length of the second one (the author did not mention the length in mm of the overlap). There was no significant difference on noise between them when they were operated at B lower than the critical induction, $B_c \approx 1.0$ T. However, the noise of the shorter overlap lengths was higher when $B > B_c$. This result is in conflict with a previous paper [14] due to the linearisation the core did not have the lamination protruding out from the core.

In 1998, Valkovic [17] presented the effect of transformer core design on noise level. The effect of number of step laps and number of laminations per stacking layer in single phase cores identical in dimensions to [13] and [14] built with 0.27 mm thick M4 grade laminations were investigated. The cores were tested at 1.4 T to 1.7 T. The result was similar to that in [15] which was that SSL showed higher noise than MSL and there was no significant difference between step lap 2 to 5. Changing the number of lamination per stacking layer from 1 to 3 laminations had little effect in the SSL core. However, two laminations per stacking layer showed approximately 2 dB lower noise than the others. However, there was no mention of a repeatability of the measurements so 2 dB may be in this range.

Ishida et al. [18] investigated the effect of core models, lamination materials and clamping pressures on three phase transformer cores. Four different B_8 electrical steels were used for building the cores. B_8 is used for specifying magnetic flux density at a magnetic field, H=800 A/m, 50 Hz. This number was used for comparing the material grades. The higher B_8 was better because the magnetic material had more magnetic flux when applied with the same amount of magnetic field and had less domain misorientation which affected magnetostriction. Eight, three phase three limbs cores were built with laminations whose characteristics are shown in Table 2-1. Two step lap configurations, a single step lap with overlap length 14 mm and 4 multistep laps with 2 mm overlap length, were compared. Fig. 2-6 shows single step three phase

core structures and five longitudinal multistep lap three phase core structures. Comparing the noise level between step lap designs, multistep lap showed lower noise both with 0.23 mm and 0.3 mm thick laminations. The noise decreased by roughly 2 dB for each increase of 0.01 T in B_8. The 0.23 mm thick laminations had lower noise than the 0.3 mm material because they had a higher B_8.

Table 2-1: Properties of electrical steel laminations and commercial code [18]

No.	Material name	Thickness [mm]	B_8 [T]
1	23RGH090N	0.23	1.931
2	23RGH090		1.898
3	30GRH105N	0.30	1.930
4	30GRH105		1.896

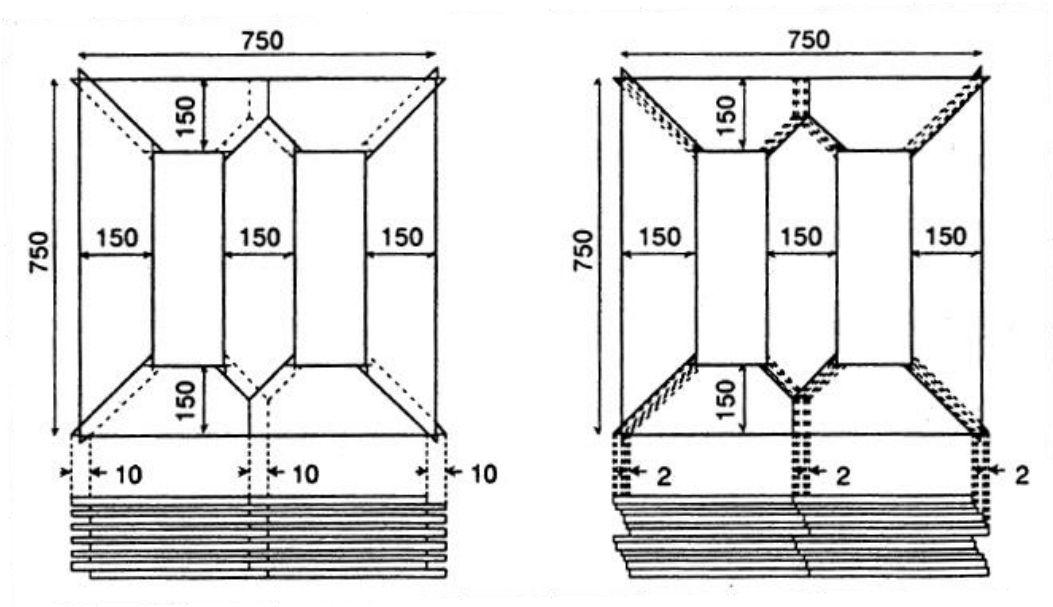

a) b) Unit: mm

Fig.2-6: Three phase three limb core structure and dimensions [18]
a) Three phase core with single step lap configuration
b) Three phase core with longitudinal multistep lap configuration

The effect of clamping pressure was investigated with the cores built with 0.3 mm thick lamination both MSL and SSL configuration. Pressure up to 0.25 MPa was

applied at peak magnetic flux densities from 1.5 T to 1.8 T. The noise from the MSL cores was least between 0.075 MPa and 0.1 MPa at B = 1.5 T. The clamping pressure decreased to 0.025 MPa for the lowest noise at 1.8 T. In the case of single step lap cores, the lowest noise at the whole range of the magnetic flux density was found at 0.05 MPa. Multistep lap and single step lap cores displayed similar trends, the noise decreased when clamping pressure increased from zero to the optimum value and then increased as the clamping pressure was increased further. It can be seen that a certain pressure was needed to prevent the laminations from flapping. Increasing the pressure beyond this was likely to produce regions of non-uniform stress leading to an increase in magnetostriction [19] and hence transformer core noise. Moreover, the authors described the relationship between noise and magnetostriction vibration characteristic and the harmonic components, p_n, of magnetostrictive vibration acceleration as shown in Eq. 2-3.

$$p_n = (2\pi f_n)^2 \lambda_n A_{wn} \quad \text{m/s}^2 \qquad (2\text{-}3)$$

when f_n is the nth harmonic frequency, λ_n is the magnetostriction harmonic component and A_{wn} is the coefficient for the A-weighting scale. Then the A-weighted magnetostrictive vibration acceleration level P can be calculated from the harmonic components as shown in Eq. 2-4.

$$P = 20\log\left(\frac{\sqrt{\sum_n p_n^2}}{p_o}\right) \quad \text{dB} \qquad (2\text{-}4)$$

when $p_o = (2\pi)^2 \times 10^{-5}$, the magnetostriction vibration acceleration reference level.

In 2000, Weiser et al. [6] presented the effect of transformer core design on transformer core noise. ZDKH material with 0.27 mm thick was used. Table 2-2 shows core configurations used in the experiments. The effect of step lap design and gap length between the lamination joints (g) on core noise was investigated. The experimental results are shown in Fig.2-7 and 2-8.

Table 2-2: Dimensions of single phase cores used in [6]

Core No.	Lamination width [mm]	Window area [mm^2]	Stacking height, k, [laminations]
1	50	300×110	110, 160
2	80	300×110	180

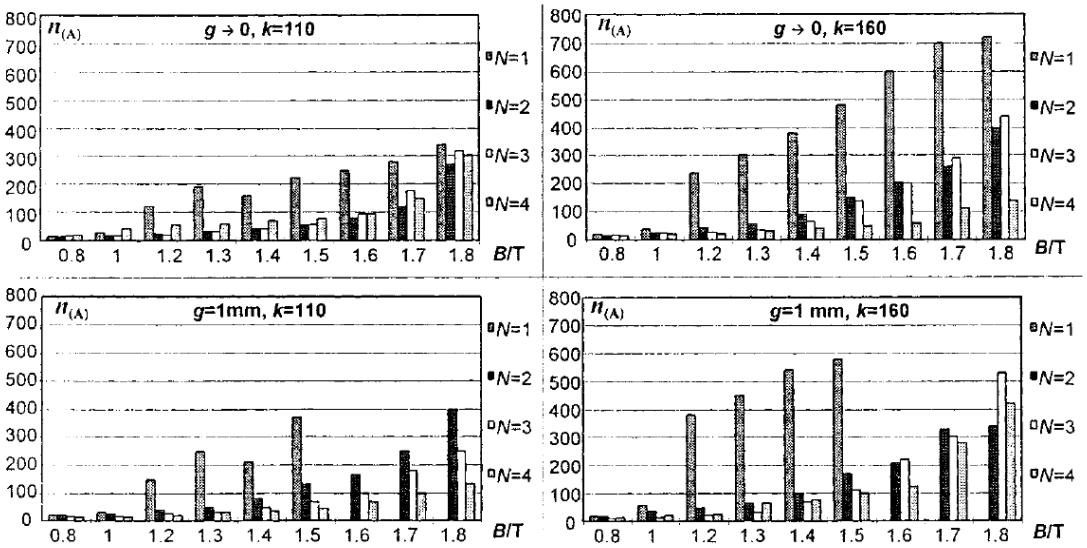

Fig.2-7: Noise experimental results of single phase transformer core built with 50 mm lamination width at various number of laminations 110 to 160 and gaps close to zero to 1 mm and magnetic flux density 0.8 T to 1.8 T. [6]

From the results in Fig.2-7, the lowest noise was found on cores built with 110 laminations with the gap close to zero. The noise was found to be inversely proportional to the number of step laps. Similar trends were found with a gap of 1 mm. The noise on the core built with 160 laminations was higher than built with 110 laminations. Comparing the number of step laps, it can be seen that noise

increased dramatically at an operating flux density, $B > B_c$ for the SSL while there was slightly increases for the MSL configuration.

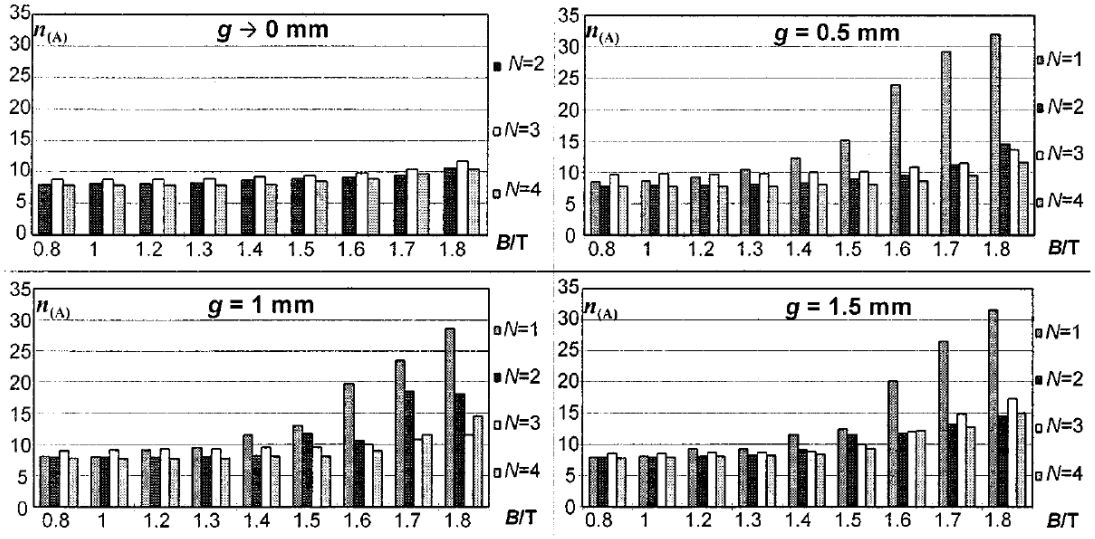

Fig.2-8: Noise experimental results of single phase transformer core built with 80 mm lamination width and number of lamination 180 laminations at various gaps close to zero to 1.5 mm and magnetic flux density 0.8 T to 1.8 T. [6]

From the results in Fig. 2-8, the lowest noise was found for gaps close to zero as with the results of the core built with 50 mm lamination width in Fig. 2-7. At gap close to zero, three step laps shows the highest noise. In the case where the gap was not equal to 0, SSL at gap equal to 1 mm had the lowest noise. There was no significant difference when the number of step laps in the MSL cores was changed.

Ishida et al. [20] extended their work [18] to investigate the noise using 0.23 mm thick laminations with different B_8 values. Four, three phase three limb cores with the same dimensions as in their previous work were used. Table 2-3 shows the material properties and noise level under test with 0.2 MPa clamping pressure at 1.7 T, 50 Hz. These results confirm their conclusion in their previous work that the noise decreased by roughly 2 dB for each increase of 0.01 T in B_8. In addition, the authors investigated the effect of primary voltage waveform with a superimposed 5^{th} harmonic shifted, δ,

between 0° and 180° with respect to the fundamental voltage on the noise. δ was zero when both component's zero crossings from negative to positive were simultaneous. It was measured on the harmonic angular scale. Fig. 2-9 shows the noise level change versus percentage of 5th harmonic relative to the fundamental voltage on the cores with clamping pressure 0.2 MPa operated at 1.7 T, 50 Hz.

Table 2-3: Specifications and noise output of the three phase three limb transformer cores [20]

Core No.	Material	Step lap design	B_8 [T]	Noise level [dB]
1	A	MSL	1.89	52
2	B	MSL	1.88	54
3	A	SSL	1.89	55
4	B	SSL	1.88	56

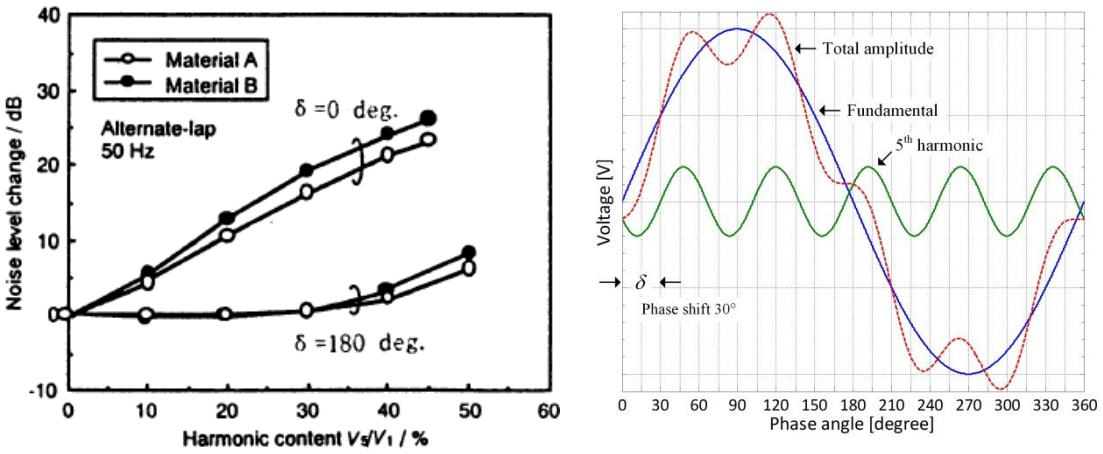

a) b)

Fig.2-9: Effect of harmonic component of magnetic flux density on transformer core noise

a) Variation of noise output of single step lap configuration three phase three limb transformer core built with different materials as shown in Table 2-3 at various percentage of 5th harmonic component and phase shift δ at 1.7 T, 50 Hz. [20]

b) Variation of total amplitude of magnetic flux density due to phase shift of 5th harmonic component

With zero phase shift δ=0, the noise level increased when the amplitude of the magnetic flux was increased due to the harmonic component. While for the phase shift δ=180°, the noise level decreased slightly at 10% and then increased at a lower rate than when the phase shift was zero. This was due to the change of the amplitude of the magnetic flux density signals with different harmonics present. Table 2-4 shows the percentage changes of the voltage amplitude supplied to the winding due to the harmonic component.

Table 2-4: Percentage variations of voltage amplitude supplied to the primary winding of the transformer core with single step lap configuration due to 5^{th} harmonic component and phase shift at 1.7 T, 50 Hz.

5^{th} harmonic	10%	20%	30%	40%	50%
Phase shift 0°	+10	+20	+30	+40	+50
Phase shift 180°	-4	+4	+13	+23	+32

In 2008, Snell [21], [22] studied the effect of six core design parameters i.e. clamping torque (0, 13.6 and 27.2 Nm), core re-build, number of laminations per stacking layer (one and two laminations), number of step lap (two, four and six steps), length of overlap shift (two, four and six mm) using three materials (conventional grain oriented (27M3), high permeability (27M0H) and ball unit domain refined high permeability grain oriented electrical steel (BUDR)) on transformer core noise. Refinement of magnetic domains in the laminations is the technique for reducing the width of magnetic domain in order to reduce the core loss. In this experiment, BUDR is 27M0H with domain refined using ball unit system, 6 mm line spacing perpendicular with the rolling direction. Three phase, three limb transformer models with outside core dimensions of 600 mm × 500 mm were used for the investigation.

A core with N=5, s=6 mm, built with 27M3 material tested at 1.7 T, had noise of 56 dBA, 56.2 dBA and 59 dBA when changing clamping torque 0, 13.6 and 27.2 Nm, respectively. It was found that at low clamping torque there was no

significant difference in noise, however, the noise increased when clamping torque was increased. Each core was rebuilt three times and tested at magnetic flux density 1.5, 1.7 and 1.75 T. The results showed the variation of measurements between each build was up to ±6 dB.

To investigate the effect of number of laminations per stacking layer, cores assembled from, 27M0H and 27M3 were built twice with one and two laminations per stacking layer. Less noise was found from one lamination per layer for the over range of magnetic flux density 1.5 T to 1.8 T.

To compare the effect of number of step lap and length of overlap shift, cores of 27M0H and 27M3 were built with three, five and seven step lap and two, four and six mm length of overlap shift. Each model was built twice. The average noise from three trials on each core is shown in Table 2-5. The results show noise was significantly dependent on operating *B*, number of step lap and length of overlap shift. Finally, the author presented a comparison of the application of ball unit domain refinement (6 mm line spacing) with standard 27M0H on core noise as shown in Table 2-6. The cores were built with N=5, s=6 mm, one lamination per stacking layer. Results were not significantly material dependent.

Table 2-5: Comparison of noise output on three phase transformer core built with different number of step laps, overlap length and materials at flux density 1.5 to 1.8 T, 50 Hz. [22]

		27M0H			27M3		
Step lap	Overlap [mm]	1.5 T	1.7 T	1.8 T	1.5 T	1.7 T	1.8 T
3	2	49.8	55.4	59.7	55.2	61.3	64.0
	4	52.0	61.7	66.7	50.2	56.6	59.1
	6	50.3	60.3	64.6			
5	2	51.9	56.4	62.5	51.8	57.2	60.1
	4	46.5	53.9	59.8	48.3	55.4	59.1
	6	45.2	52.8	59.4	48.2	56.7	60.1
7	2	51.9	56.7	60.4	52.6	57.3	59.4
	4	46.7	52.1	59.4	49.3	56.6	59.9

Table 2-6: Comparison of noise output on three phase transformer core built with different materials at flux density 1.5 to 1.8 T, 50 Hz. [22]

Magnetic flux density [T]	1.5	1.7	1.8
Non-domain refined [dBA]	45.5	52.8	59.3
Ball unit domain refined [dBA]	45.1	53.1	59.0

In 2011, Girgis et al. [23] presented the method for minimising the transformer core noise. By extensive investigation, the authors found that transformer core and load noise were affected by the mounting methods. Therefore, the tank was designed for reducing the noise generated from the transformer. In tank designing process, (a) accurate calculation of resonance frequency of the core, (b) accurate calculation of frequency spectrum of core noise, (c) accurate calculation of load noise, (d) decoupling active parts vibration from the tank, (e) proper design of tank plate field and tank bracing and (f) proper transformer mounting techniques were carefully considered. The results showed that the core noise was reduced 3.7 dB for transformer 93 MVA and 6.5 dB for transformer 65 MVA. In 2012, Lahn et al. improved transformer core noise by using optimised laser domain refinement [24].

2.3 Study of transformer core vibration

In 1996, Weiser et al. [25] studied the mechanism of vibration on no load single phase transformer cores. Two, single phase cores with four multi step laps and single step lap configuration were assembled from 0.27 mm thick M0H grade laminations, 170 mm width with window 400 mm × 400 mm were studied. Fig. 2-10 shows the position of the measurements, clamping regions and displacement experimental results obtained by means of a miniature triaxial accelerometer (Brüel & Kjær 4326) at magnetic flux density 1.0 T to 1.4 T.

The results did not show symmetry with the middle point (point 16) because of the lack of a reference point. Low and high vibration was found at the centre and corners respectively of each core. Displacements along the rolling direction (χ_x) and transverse direction (χ_y) had different values with the magnetostriction characteristics. The authors proposed a Maxwell stress vector based on displacements in the normal direction (χ_z), to explain the vibration. The stress strongly depended on the magnetic flux distribution.

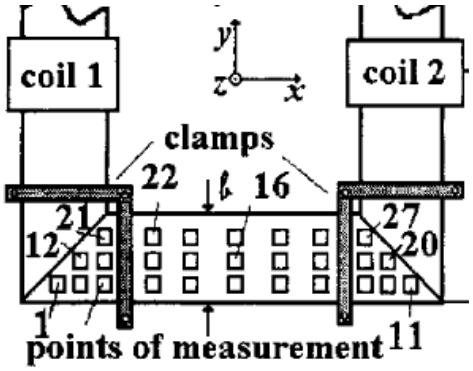

a)

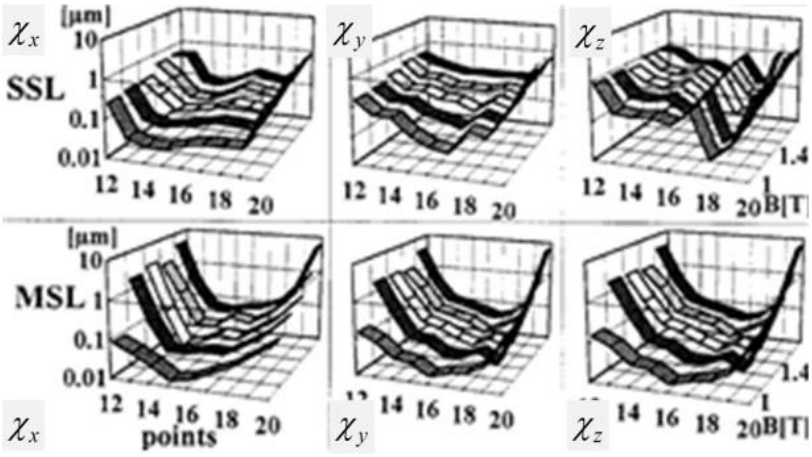

b)

Fig.2-10: Single phase core model with clamping position [25]
a) Displacement measurement points
b) Displacement experimental results

To investigate the stress, the core was separated into three regions with regard to the characteristic of magnetic flux distribution. The first region was the overlap region where in-plane magnetic flux flows through the gaps from one lamination to another in-plane lamination. An attractive stress between the lamination in in-plane direction, p_g, can be calculated from Eq. 2-5.

$$p_g = \frac{B_g^2}{2\mu_0} \qquad \text{N/m}^2 \qquad (2\text{-}5)$$

where B_g is in-plane magnetic flux flow through the gap and μ_0 is the permeability of the free space.

The second was the overlap region where normal magnetic flux exists. An attractive interlaminar stress between the lamination in the normal direction, p_z, can be calculated from Eq. 2-6.

$$p_z = \frac{B_z^2}{2\mu_0} \qquad \text{N/m}^2 \qquad (2\text{-}6)$$

where B_z is magnetic flux flow through the gap in normal direction.

The third region was the homogeneous area of the limb and yoke which exhibited repelling interlaminar stress. However, it can be assumed that only in-plane magnetic flux occurs therefore stress in this region can be neglected.

The averaged displacement χ_z of the MSL configuration was higher than that of the SSL core but this was not compatible with the A-weighted sound pressure level. The core with MSL joint had lower noise. The authors explained that the MSL core had higher χ_z amplitude but less distortion. However, the frequency distribution of χ_z was not shown in the paper. In addition, the χ_z was found not to be independent of core stacking height. The experiments were carried out by increasing core stacking height from 45 to 180 laminations.

In 1997, Mizokami et al. [5] presented three phase, three limb transformer core vibration measurements obtained using a laser Doppler system. The core was built with high permeability grain oriented, 0.23 mm thick, single step lap configuration with two laminations per stacking layer. The core cross sectional area was square. Fig. 2-11 shows the core dimensions and magnetostriction properties whilst Fig. 2-12 shows measuring surfaces and positions.

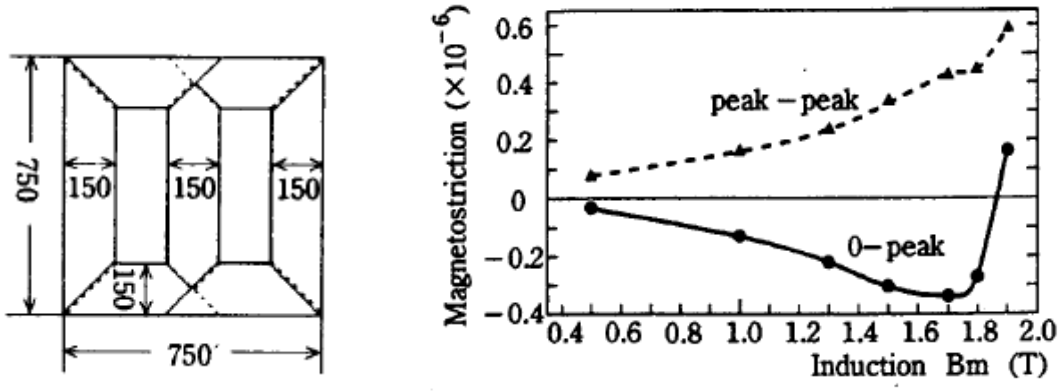

a) b)

Fig.2-11: Three phase three limb transformer core model and magnetostriction properties [5]

a) Core dimensions (mm)

b) Magnetostriction properties of material prior to being built into the core

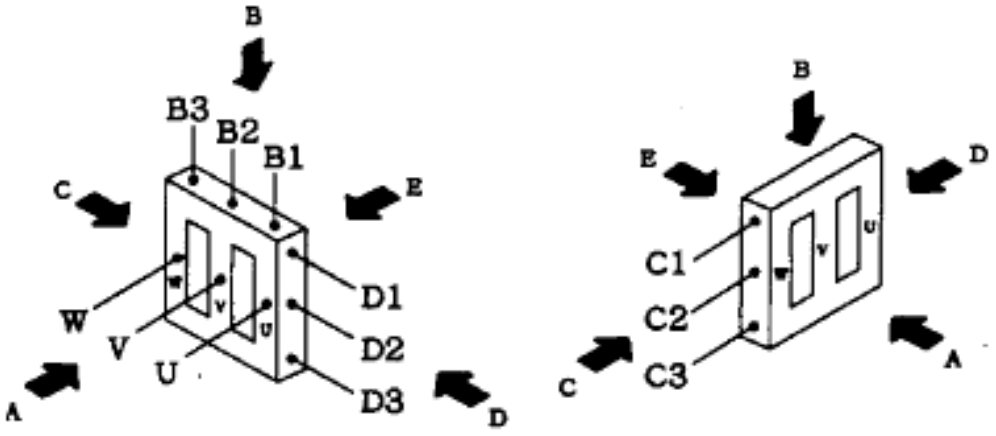

Fig.2-12: Measuring positions on the core surfaces [5]

It can be seen from Fig. 2-13 that the vibration of surface E was higher than surface B, C and D. The vibration of the limbs was higher than the yokes while the middle limb was higher than the outer limbs. On the top surface (surface B), the area above the limb had vibration higher than at the middle. Fig. 2-14 shows that the middle limb vibration phase was shifted approximately 180° compared to the outer limbs. In addition, the effect of excitation frequency was compared; there was no significant vibration on the surfaces B, C and D.

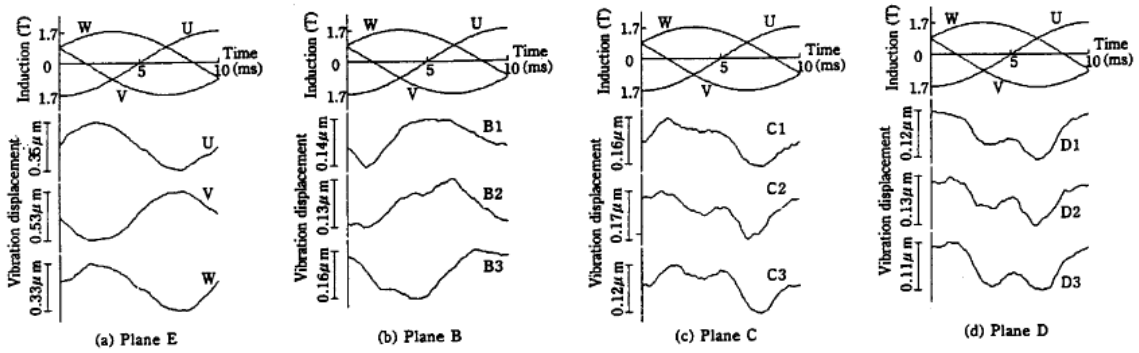

Fig.2-13: Vibration displacement signals of the core at 1.7 T, 50 Hz. [5]

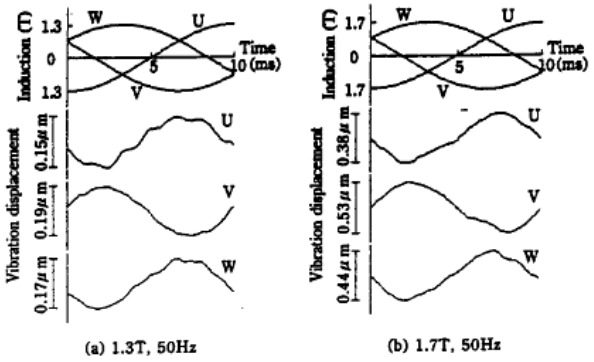

Fig.2-14: Comparison of vibration displacement signals on surface A at magnetic flux densities of 1.3 T and 1.7 T, frequency 50 Hz. [5]

In 1998, Ishida, et al.[18] reported the vibration distribution normal to the surface of three phase three limb transformer cores. The experiments compared four cores. The cores were constructed with material grades 30RGH110 (RGH) and 30RGH105N

(NewRGH), 0.3 mm thick in five multi step lap and single step lap designs as shown in Fig. 2-6. Fig. 2-15 shows vibration acceleration level of the core surface in $\mu m/s^2$ at 1.7 T. It can be seen that vibration is high at the joints between yokes and limbs. There is a variation of approximately 10 dB between the middle of the lamination and the joints. The multistep lap core had lower vibration for both materials. It can be seen that New RGH material vibrates less than RGH material for both step lap designs.

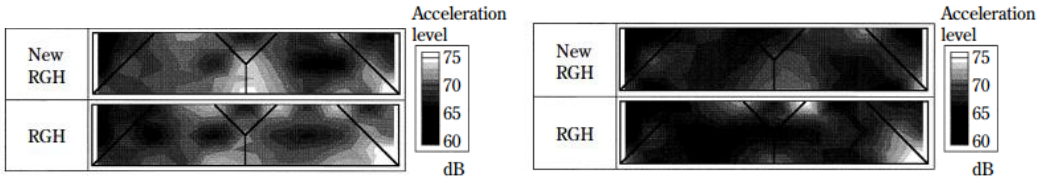

a) b)

Fig.2-15: Comparison of vibration distribution of single step lap and multistep lap cores [18]

a) Vibration distribution of single step lap core

b) Vibration distribution of multistep step lap core

Weiser and Pfützner [26] investigated the relationship between magnetic forces and vibration in a single phase transformer core. Different cores to those used in the previous work [25] were investigated. The core built with ZDKH material, 0.27 mm thick, 50 mm width with window 300 mm×110 mm and also a different clamping area is shown in Fig. 2-16. Vibration was measured with miniature triaxial accelerometers (Brüel&Kjær 4326) as in the previous work [25]. The results showed vibration displacement, vibration velocity and A-weighted velocity without the relevance of phase differences. Fig. 2-17 shows experimental vibration results of the multistep lap core at 1.6 T, 50 Hz.

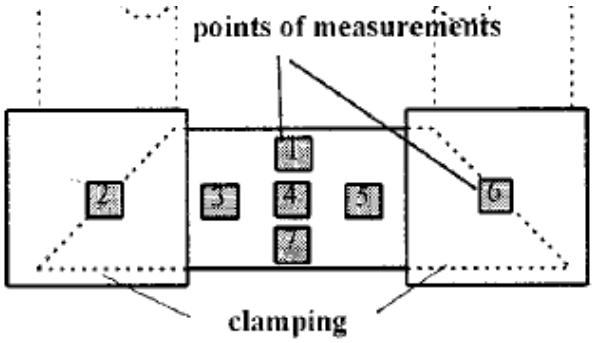

Fig.2-16: Position of vibration measurements and clamping area of the core model [26]

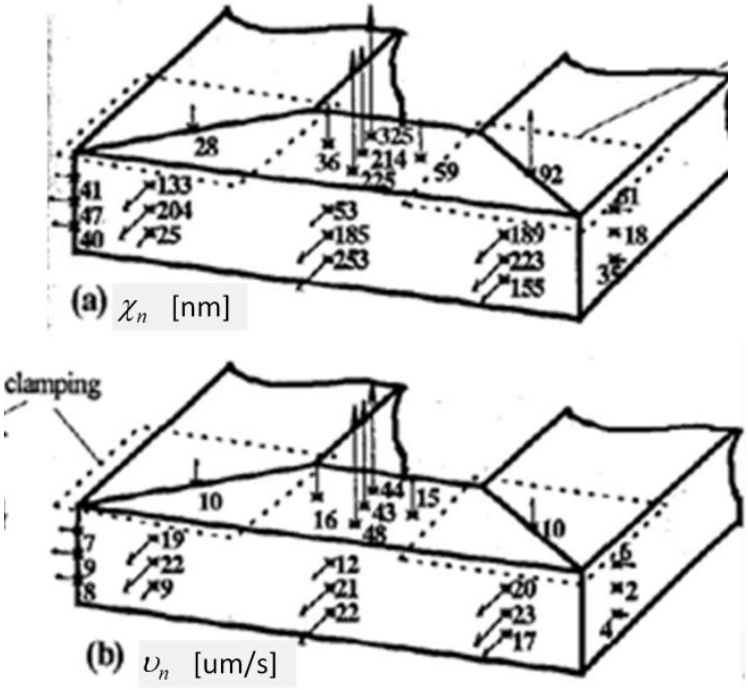

Fig.2-17: Vibration experimental results from triaxial accelerometer at the position as shown in Fig. 2-16 [26]

a) Vibration displacement, nm

b) Vibration velocity, μm/s

The results show a difference with their previous work [25]. The highest vibration did not appear at the joints because they were completely clamped. The results at points 2 and 6 were the average vibration of the clamps. Fig. 2-18 shows averaged A-weighted velocities of the core at 1.4 T and 1.8 T with number of step laps from one to four and

core stacking height 110 laminations and 160 laminations. The results showed vibration velocity in the normal direction (υ_z) was higher than the in-plane vibration. For the SSL configuration, it can be seen that the core stacking height strongly affected with υ_z but the effect was less with MSL. The υ_z appeared to have a random variation when the number of step laps were increased.

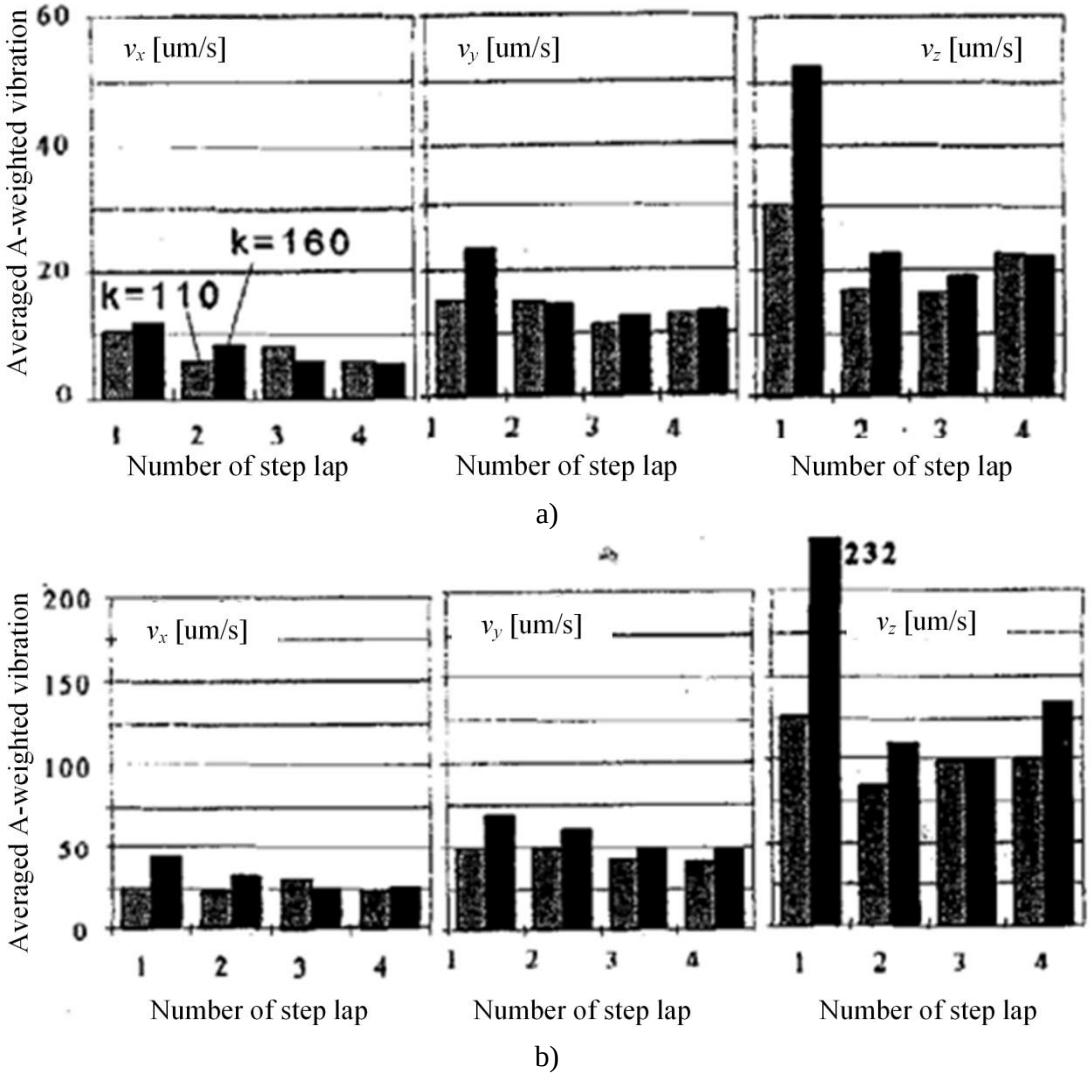

Fig.2-18: Averaged A-weighted vibration velocities [26]

a) The averaged A-weighted vibration velocities at 1.4 T, 50 Hz.

b) The averaged A-weighted vibration velocities at 1.8 T, 50 Hz.

In 2002, Vandevelde et al. [27] presented a modelling for magnetoelastic material. This work was based on the virtual work principle by considering the component of magnetostriction and Maxwell forces simultaneously. One year later, they applied the modelling to rotating machine and transformer core. Calculation of core deformation and vibration was carried on the measured magnetostriction on the electrical steel lamination and finite element method (FEM) [28], [29]. The modelling work have been developed continuously by improving an algorithm and input parameters [30], [31], [32], [33].

2.4 Summary

Based on the reviews in Section 2.2 to 2.3, it can be summarised that:

1. Causes of core vibration, which is the main cause of transformer noise, are deformation of core laminations due to magnetostriction and magnetic forces at overlap regions.
2. Variation of transformer core noise depends on lamination grades, overlap length, number of step lap, length of overlap shift, clamping stress and number of laminations per stacking layer. The optimum values for each parameter depends on core structure.
3. Magnetic forces depend on in-plane and interlaminar magnetic flux through air gap at core overlap region, core structures and clamping force.
4. Transformer core noise varies with lamination grades but no definite correlation between them has been found. There is no agreement on which parameter of material properties is the most significant. Some researchers refer to level of magnetic flux density at a magnetic field equal to 800 A/m but some researches refer to magnetostriction.
5. Although magnetostriction is generally accepted that it is the one of main causes of transformer core vibration and noise, there is no agreement on which

magnetostriction parameter is the most relevant to transformer core vibration and noise.

6. There is significant increase in transformer core noise when the core is operated over the core critical induction.
7. Multi step lap configuration has lower noise values than a single step lap configuration.
8. There is no conclusion of the optimum value of clamping pressure applied to the core and the configuration of the clamp.

According to the summary above, the following questions arise:

1. How does the magnetostriction relate to core vibration?
2. How does the core vibration relate to core noise?
3. Is there any quantitative correlation between vibration magnitude and core noise?
4. What are the most significant factors affecting transformer core noise?
    - Materials (magnetostriction, B_8, thickness, coating effect)
    - Core configurations (B_c ,MSL, SSL)
    - Clamping torques (lamination residual stresses)
    - Magnetic forces

Table 2-7 to 2-9 summarises previous work on transformer core noise and vibration measurements. There are blanks in some boxes in the table since the data were not provided. A gap in time is due to the research focus on transformer core losses and modelling.

Table 2-7: Summary of previous work on transformer core noise and vibration (1981-1996)

Year	1981	1994	1996	
Authors	Foster et al.	Valkovic	Ilo et al.	Valkovic
phase		Single phase core type	Single phase core type with linearisation overlap	Single phase core type
Power rating [VA]	200M			
Weight [kg]		105		105
material	M5	Parameter (M4, M0H, ZDKH)	ZDKH-LS	M4
B_8				
thickness [mm]		0.27	0.23 for overlap, 0.27 for yokes	
Core outside dimension [mm×mm]		399×586	300×300	399×586
window [mm×mm]		159×346	240×240	159×346
lamination width [mm]		120	30	120
No. lamination		296	20	296
Core stacking height [mm]		80		80
No step		5	Parameter (1, 2)	1
Overlap length [mm]		14	10 and parameter (1, 2)	Parameter (2, 6, 10, 14)
overlap shift [mm]		2	Parameter (0, 3, 5, 7)	
No lamination / stacking layer		1		
Gap [mm]			1	
Core position			H	
Microphone position				
Core build				
Measurement parameter	noise	A-weighted, Noise spectra	Noise, Loss	Noise
Instrument			B&K condenser mic	
Measurement Environment		Anechoic chamber	A bottomless acoustic shielding test box 9 cm thick	Anechoic chamber
Standard		IEC 179		IEC 60551/1987

Table 2-8: Summary of previous work on transformer core noise and vibration (1998)

Year	1998				
Authors	Valkovic	Ishida, et al.			
phase	Single phase core type	Three phase three limb			
Power rating [VA]					
Weight [kg]	105	100			
material	M4	23RGH090N	23RGH090	30RGH105N	30RGH110
B_8		1.931	1.898	1.930	1.896
thickness [mm]	0.27	0.23		0.3	
Core outside dimension [mm×mm]	399×399	750×750			
window [mm×mm]	159×159	150×450			
lamination width [mm]	120	150			
No. lamination	300	144		108	
Core stacking height [mm]	80				
No step	Parameter (1, 2, 3, 4)	Parameter (1, 5)			
Overlap length [mm]					
overlap shift [mm]		Parameter (2 , 10)			
No lamination / stacking layer	Parameter (1, 2, 3)				
Gap [mm]					
Clamping				Parameter (0, 0.05, 0.10, 0.15, 0.20 MPa)	
Microphone position					
Core build					
Measurement parameter	Noise	λ, Noise		λ, Noise, Vibration	
Instrument	[B&K Analyser 2121 & Mic 4190], [HP Analyzer & B&k Mic 4145]				
Measurement Environment	Anechoic chamber				
Standard	IEC 60551/1988	Noise, JIS C 1505/1988			

Table 2-9: Summary of previous work on transformer core noise and vibration (2000-2008)

Year	2000								2008	
Authors	Weiser et al.				Ishida et al.				Snell	Snell
phase	Single phase core type				Three phase three limb				Three phase three limb	Three phase three limb
Power rating [VA]										
Weight [kg]					100					
material	ZDKH				LDR-A		LDR-B		Parameter (27M3, 27M0H)	Parameter (27M3, 27M0H+BUDR)
B_8					1.890		1.880			
thickness [mm]	0.27				0.23					
Core outside dimension [mm×mm]	400×210	460×270			750×750				600×550	600×550
window [mm×mm]	300×110	300×111			150×450					
lamination width [mm]	50	80			150					
No. lamination	Parameter (110, 160)	180			144					
No step	Parameter (1, 2, 3, 4)				1	4	1	4	4	Parameter (2, 4, 6)
Overlap length [mm]					10		10			Parameter (2, 4, 6)
overlap shift [mm]					10	2	10	2	6	
No lamination / stacking layer									Parameter (1, 2)	
Gap [mm]	Parameter (0, 1 mm)	Parameter (0, 0.5, 1, 1.5 mm)								
Clamping					0.2 MPa				Parameter (0, 13.6, 27.2 Nm)	
Core position	H								H	H
Microphone position									parameter (11 points)	
Core build									parameter (3 trials)	
Measurement parameter	Vibration (N=2), Noise	Noise							Noise	Noise
Instrument									Cirrus CR:831A Type 1	Cirrus CR:831A Type 1
Measurement Environment	A bottomless acoustic shielding test box 9 cm thick								Fabricated sound booth	
Standard									IEC 60651	

Chapter 3

Development of the Measurement System

This chapter provides basic theories of sound and vibration and describe the measurement system used for investigating sound and vibration in transformer cores. The sound measurement system was used for determining sound pressure level and calculating sound power level. The vibration measurement system using a scanning laser vibrometer and a localised magnetic flux density measurement system is also presented. Finally, uncertainties of all the measurements are quantified.

3.1 Instrumentation for Sound Measurement

Sound, by definition is a variation of pressure generated by the vibration of a medium where power from the medium is radiated away by progressive sound wave [34]. A sound wave, ζ , can be mathematically expressed by Eq. 3-1.

$$\zeta(x,t) = A\sin(mx - \omega t + \phi) \quad \text{Pa} \quad (3\text{-}1)$$

where A is the maximum amplitude of the wave, x is space coordinate, t is time coordinate, m is wave number, ω is angular frequency and ϕ is a phase constant.

Sound sometimes is satisfying but sometimes is annoying; unwanted sound is called noise. In this work, sound and noise are synonymous. The sound levels in factories are used for analysis and comparing annoying sound emitted from machines or production line processes. Sound can be expressed as sound pressure, sound pressure level, sound power level and sound intensity.

3.1.1 Basic Terms in Sound

Sound power, S_w, is the overall acoustic power emitted by a sound source. It is independent of the environment. Sound power of a human whisper is very low, approximately 10^{-9} W, while sound power of a jet airliner is approximately 50 kW [34] at source. Fig. 3-1 shows sound power output of some typical sources. It is usual to quantify sound power in term of sound power level, L_w as Eq.3.2.

$$L_w = 10\log\left(\frac{S_w}{S_{w,ref}}\right) \quad \text{dB} \quad (3\text{-}2)$$

where $S_{w,ref}$ is a reference sound power, 1×10^{-12} W.

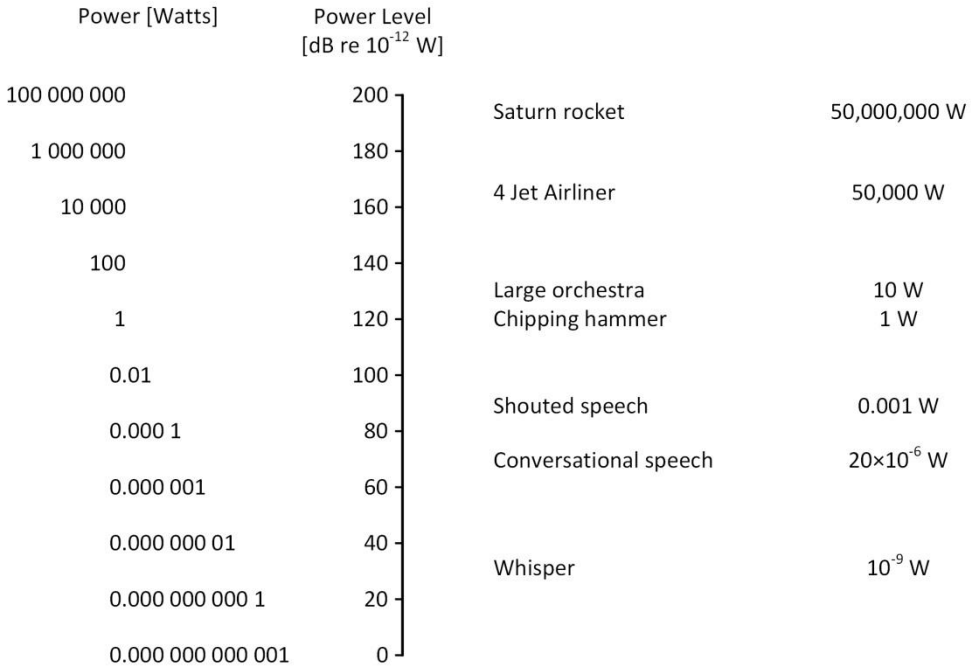

Fig.3-1: Sound power output of some common noise sources [34]

The human ear can detect sound pressure, p, from approximately 20×10^{-6} Pa to 100 Pa and in frequency range 20 Hz to 20 kHz, the audible sound range. It is simpler to compare the sound pressure level when expressed in decibels. Sound pressure is

proportional to the square root of sound power [34], therefore sound pressure level can be expressed as Eq.3-3.

$$L_{\mathrm{p}} = 10\log\left(\frac{p_{\mathrm{rms}}^2}{p_{\mathrm{ref}}^2}\right) = 20\log\left(\frac{p_{\mathrm{rms}}}{p_{\mathrm{ref}}}\right) \quad \text{dB} \qquad (3\text{-}3)$$

where p_{rms} is the measured root mean square sound pressure in Pa and p_{ref} is a reference pressure. The reference pressure was selected to be approximately equal to the threshold of human hearing at 1000 Hz, i.e., 20×10^{-6} Pa. The difference between sound power and sound pressure can be described simply as sound power is the cause whereas sound pressure is the effect.

The human ear does not equally respond to sound pressure at all frequencies, therefore the A-weighting scale was introduced. It used 1 kHz as a reference frequency because the sound pressure at this level is equivalent to the loudness in Phon [34]. The A-weighting curve is shown in Fig. 3-2 and the coefficient for the A-weighting scale, A_w, at any frequency can be calculated from [35] using Eq. 3-4.

$$A_w(f) = 2 + 20\log\left[\frac{12194^2 f^4}{\left(f^2+20.6^2\right)\left(f^2+107.7^2\right)^{\frac{1}{2}}\left(f^2+737.9^2\right)^{\frac{1}{2}}\left(f^2+12194^2\right)}\right] \qquad (3\text{-}4)$$

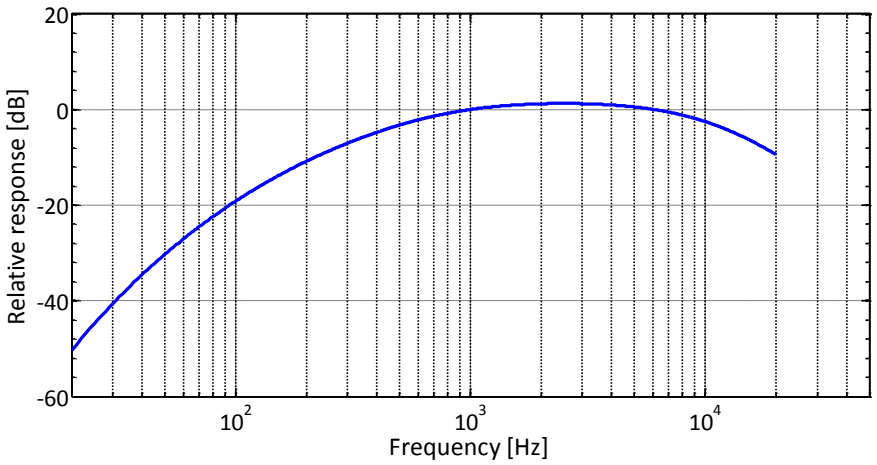

Fig.3-2: A-weighting curve

3.1.2 Measuring Microphones

Microphones are transducers used for converting sound signals to electrical signals. Measuring microphones are carefully calibrated microphones in order to have uniform frequency response. They are different from microphones used in studios which do not have uniform frequency response. There are two types of measuring microphones: the condenser microphone and dynamic microphone.

The condenser microphone uses a capacitor as a sensor with a diaphragm which deflects with variation of pressure difference across it. Fig. 3-3 shows the principle structure of a condenser microphone. The dynamic microphone uses a moving coil, which is mounted in a magnetic field, connected with a diaphragm. When the sound wave travels through the diaphragm, the moving coil is moved and this generates a voltage output signal. Condenser microphones are more stable, have a wider range of frequency, and are very insensitive to vibration. However, they are more expensive and sensitive to humidity and moisture.

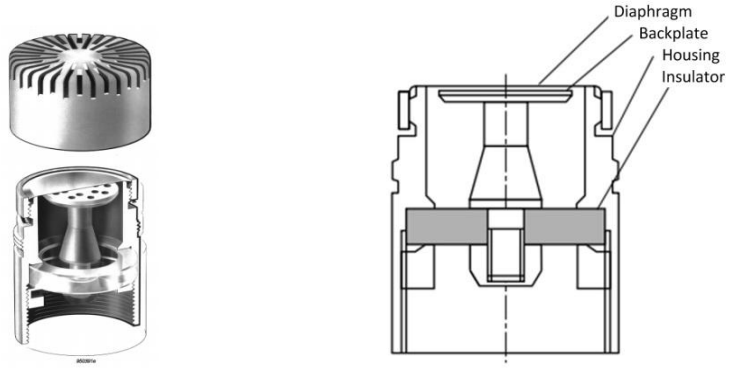

Fig.3-3: Schematic of condenser microphone [36]

Condenser microphones are separated into three types dependent on response characteristics: free-field response microphone, pressure response microphone and random-response microphone. The free-field response microphone is used for measuring sound pressure coming directly in front of the microphone's diaphragm.

The frequency response characteristic of this microphone is designed to compensate for disturbance due to interference and diffraction in front of the diaphragm. The pressure response is used for measuring noise on the surface such as noise on the floor. Random response microphones can measure sound that arrives from any direction in a diffuse sound field. Fig. 3-4 shows different microphones in the sound field.

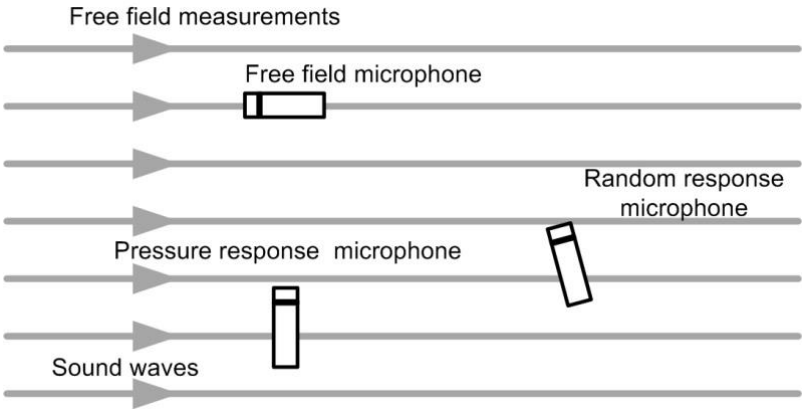

Fig.3-4: Different type of condenser microphones in the sound field [37]

All commercially measuring microphones are supplied with individual calibration charts as show in Fig. 3-5. Information provided includes: size, frequency response, open circuit sensitivity, dynamic range and correction factor.

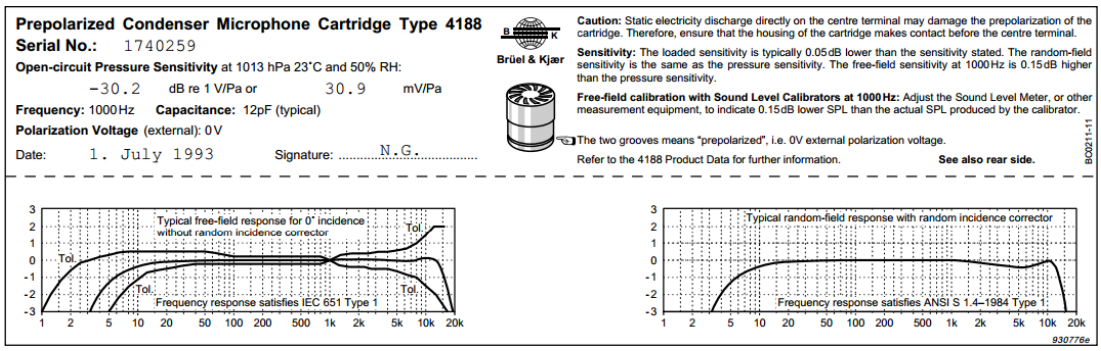

Fig.3-5: Calibration chart supplied with a Brüel & Kjær Prepolarised Condenser Microphone Type 4188 [38]

The size of a microphone influences its frequency sensitivity. The smaller it is the higher the frequency response. The relationship between sound frequency, f, and sound wave length in air, λ, can be expressed by Eq.3-5.

$$\lambda = \frac{c}{f} \quad \text{m} \qquad (3\text{-}5)$$

where c is the sound velocity in air (approximately 344 m/s).

It can be seen that high frequency has a low wave length. Then, a small microphone, for example 6.35 mm (¼ inch) diameter, will not disturb the sound frequency lower than 54 kHz while a microphone size 25.4 mm (1 inch) diameter has a limitation at 13.5 kHz. Open circuit sensitivity represents the expected output voltage from a microphone. Dynamic range presents the lowest and highest sound pressure level which can be measured by the microphone. To amplify the output signal from the microphone and provide suitable matching impedance for the instrument, a microphone is always connected to a preamplifier. The preamplifier's input impedance is high but not infinite. Therefore, a correction factor is needed in order to correct the open circuit sensitivity characteristic of the microphone.

3.2 Instrumentation for Vibration Measurement

3.2.1 Vibration

Vibration by definition is the motion of particles. When vibration occurs, sound waves are formed [39]. Vibration signals can be measured in term of displacement, χ (m), velocity, υ (m/s) and acceleration, τ (m/s^2). Fig. 3-6 shows phase correlation between the three parameters.

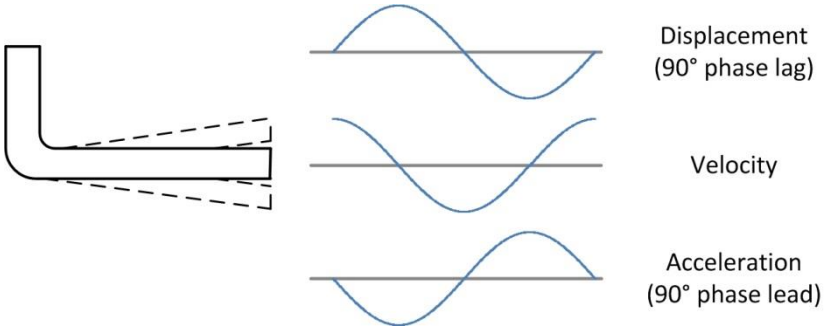

Fig.3-6: Phase difference between displacement, velocity and acceleration

In practice high displacements only arise at low frequencies, while large accelerations only occur at high frequencies [40]. Thus, it is necessary to select the instrument that has a dynamic range to cover the frequencies of interest.

3.2.2 Piezoelectric Accelerometers

An accelerometer is an instrument used for measuring the vibration of an object that it is mounted upon. Piezoelectric accelerometers are generally used for vibration measurement. They can be single or tri-axial. The most importance component of piezoelectric accelerometer is the slice of piezoelectric material. Generally, an artificial polarized ferroelectric ceramic, which exhibits the unique piezoelectric effect, is used. Fig. 3-7 shows the basic structure of a compression type accelerometer. When subjected to vibration, the accelerometer experiences a force. The sensor, which is a piezoelectric crystal, generates an electrical signal proportional to applied force. The acceleration can be calculated from, Force = Mass × Acceleration.

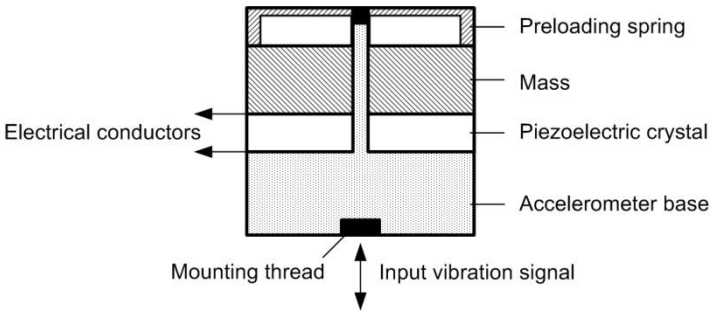

Fig.3-7: Basic structure of an accelerometer [41]

Techniques for attaching an accelerometer to the target include connecting thread stud, cementing stud, wax, magnet and hand held probes. The last two techniques affect the frequency response of the sensor. When using the magnet technique the frequency response is limited to around 6 kHz. The hand held probe is very flexible to use but the frequency response is limited to approximately 1 kHz [41].

To select an accelerometer, the range of acceleration, frequency and sensitivity of the output voltage signal needs to be specified. Commercially, the range of acceleration is defined in terms of the acceleration due to gravity (1 gravity = 9.80665 m/s^2). There is a trade-off between frequency range and sensitivity whereby a wider frequency range results in lower sensitivity [41].

3.2.3 Laser Doppler Vibrometer

The Laser Doppler Vibrometer (LDV) is used for non-contact measurement of a vibrating surface. The LDV uses the Doppler Effect to calculate the vibration frequencies [42]. A simple diagram of an LDV is shown in Fig.3-8.

A coherent light source, of which a helium-neon laser is the most common type [43], with frequency f_1 shines on to a semi-transparent prizm (Z) and splits into a test beam and reference beam. The test beam illuminates the desired measurement object and is reflected with modulated frequencies $f_1 \pm f_D$, which results from the Doppler Effect. The reference beam illuminates the reflector (Z_1) and interferes with $f_1 \pm f_D$ signal at

the detector. The frequency difference is detected and the vibration is calculated from Eq. 3-6.

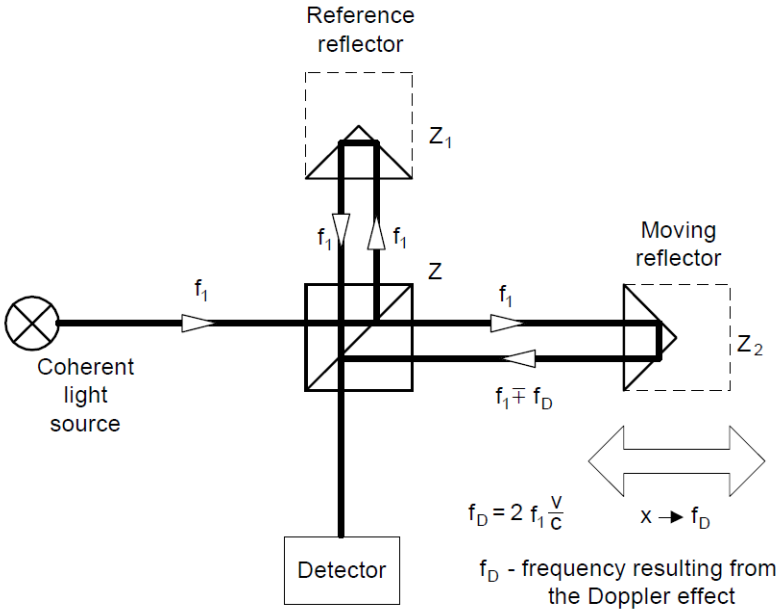

Fig.3-8: Principle diagram of Laser Doppler Vibrometer

$$\text{vibration} = f_D \times \frac{\hbar}{2} \qquad \text{m/s} \qquad (3\text{-}6)$$

where $\hbar$ is the wave length of light

Although the LDV technique is very expensive, it has many advantages over using accelerometers. The LDV can measure on surfaces that are difficult to access such as close to the lamination joints where it is not only difficult to attach the accelerometer but also there is an error due to mass loading. Therefore the LDV was chosen for this work.

3.3 Technique for Localised Magnetic Flux Density Measurements

The two most common techniques for the measurement of localised magnetic flux density are the search coil (also termed as a B coil) technique and the needle technique. Fig. 3-9 shows a schematic diagram of search coil and needle probe techniques. In the figure, if W>>d, the distance between the needle probes is equal to the search coil width.

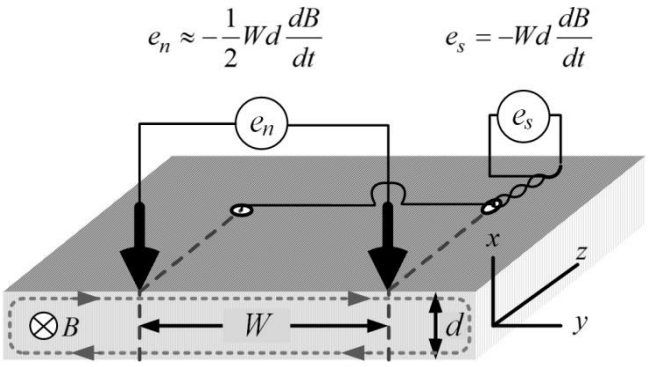

Fig.3-9: Schematic illustration of flux density measurement techniques

3.3.1 Search Coil Technique

The search coil technique is a classical method based on Faraday's law. Magnetic flux density can be calculated from the induced voltage in the search coil. A wire is threaded through holes drilled through a lamination to form the search coil. Under magnetisation, the induced voltage in the search coil is proportional to the rate of change of the magnetic flux density across a 1-turn search coil loop in the *z* direction and can be written as shown in Eq. 3-7.

$$e_s = -Wd\frac{dB}{dt} \quad \text{V} \qquad (3\text{-}7)$$

where e_s is the induced voltage in the search coil wound around the investigated cross sectional area $W \times d$, W is search coil width and d is the lamination thickness.

3.3.2 Needle Probe Technique

The needle probe technique is a non-destructive technique. This technique requires two sharp contact needles to press through the lamination insulation coating into the lamination itself. If the magnetic flux is distributed uniformly in the laminations and the distance between the needle probes is large enough, the magnetic flux density can be approximated by the induced voltage due to the eddy currents between the needle probes as [44] shown in Eq. 3-8.

$$e_n \approx -\frac{1}{2} Wd \frac{dB}{dt} \quad \text{V} \qquad (3\text{-}8)$$

The accuracy of the measurement is dependent on the uniformity and symmetry of the flux due to the ratio of the needle distance and the lamination thickness, the magnetic domain structure and the homogeneity in microscopic structures of the measurement area. The relative merits of the search coil technique and needle probe technique are shown in Table 3-1. Because the needle probe technique cannot measure localised magnetic flux density in the stack of laminations, the search coil technique was chosen for this work.

An array of single turn search coils was arranged to detect components of flux density along the rolling and transverse directions on the core laminations by threading 0.19 mm diameter (SWG-36) enamelled copper wire through holes 0.5 mm diameter.

Table 3-1: Comparison of advantage and disadvantage between search coil and needle probe techniques [44], [45]

	Search Coil Technique	Needle Probe Technique
Advantages	• Simpler • More accuracy • Able to measure in stack of laminations	• Complex • Non-destructive (do not need to drill the lamination) • Fast
Disadvantages	• Drilling induces stress in the material • Destructive • Time consuming for preparing the search coil	• Error due to vertical electric field component • Sensitive to noise interference • Coated samples need care

3.4 Development of the Measurement System

To develop the measurement system for studying the relationship between transformer core vibration and noise, a measurement system was developed [46].

Fig. 3-10 shows a schematic diagram of the measurement system. A three phase variable transformer was used as a power supply which was able to adjust the primary voltage. An exciting current was controlled by a primary voltage and then a magnetic flux was produced in the cores. Primary and secondary voltage, exciting current, power loss and exciting power were measured by a power analyser. A condenser microphone with matching amplifier was used for acquiring the acoustic signals. A laser scanning vibrometer was selected for the vibration measurements. The last system is for data acquisition and signal processing, LabVIEW, Matlab, PolyTec PSV 8.8 and ScanViewer 2.0 were used.

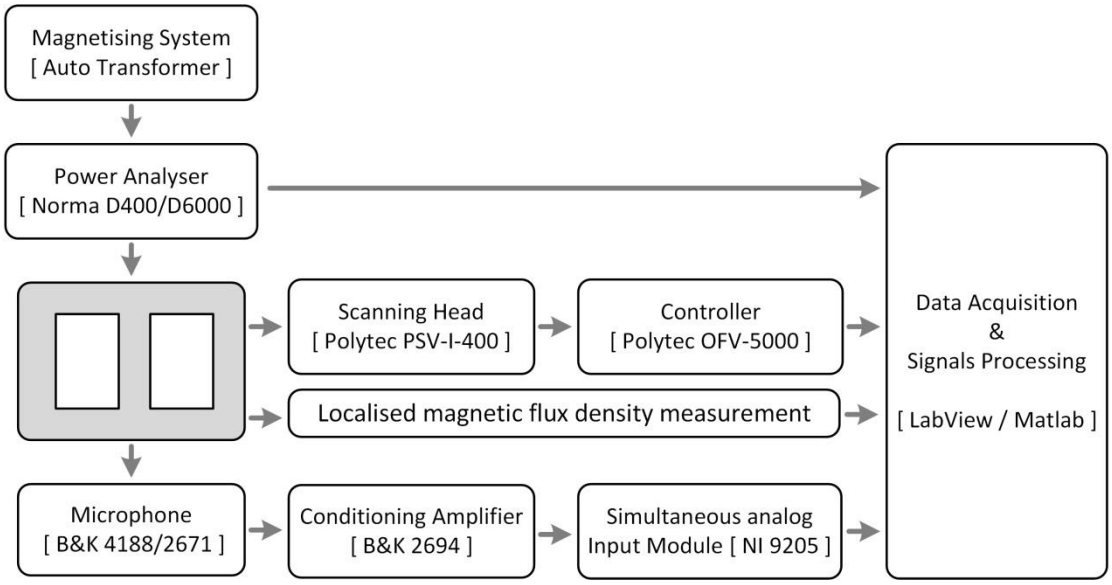

Fig.3-10: Schematic diagram of the transformer magnetising method, noise, vibration and localised magnetic flux density measurement system

3.4.1 Sound Measurement System

To investigate the noise emitted from the transformer core, a sound measurement system was developed. The standard used in the literature review for determination of sound level, IEC 60551:1993, has recently been withdrawn and replaced by IEC 60076-10 [47]. Thus, the newer version was used as a guide for determination of sound level.

The most important component in the sound measurement system is the measuring microphone. To select the appropriate measurement microphone for these experiments, the frequency response range must be considered. The causes of transformer core noise are magnetostriction and magnetic forces. The fundamental frequency of magnetostriction and magnetic forces are double the magnetising frequency [25] with harmonics potentially occurring at integer multiples of the fundamental frequency. Therefore the frequency range of the microphone should cover the fundamental and its harmonics. A condenser microphone B&K 4188 with a frequency response 8 Hz to 12.5 kHz was selected. This frequency range covers the

fundamental frequency of magnetostriction, magnetic forces and up to the 100th harmonic of them.

The measurement system comprises nine B&K 4188-A-021 microphones with preamplifiers with a frequency range 20 Hz-12.5 kHz [48], a B&K 2694 conditioning amplifier with a frequency range 0.1 Hz-50 kHz, an NI 9215 analog input module, ± 10 V, 100 kS/s/Ch [49], and a computer, in which LabVIEW version 2010 from National Instruments was already installed. The specifications of the microphone and analog input module are shown in Table 3-2 and Table 3-3. The microphones were connected to the conditioning amplifier. The signals from the conditioning amplifier were acquired with the analogue input module. LabVIEW was used for data processing and controlling the sound measurement system. Finally, Matlab was used for analysing the measurement data.

Table 3-2: Specifications of the B&K 4188-A-021 (Microphone with pre amplifier)

Sensitivity :	31.6 mV/Pa
Frequency :	20 Hz – 12.5 kHz
Dynamic range :	15.8 – 146 dB
Temperature :	– 30 to +125°C
Polarization :	Prepolarized

Table 3-3: Specification of the NI 9215 (Simultaneous Analogue Input Module)

Resolution :	16 bits
Sample Rate :	100 kS/s/Ch
Max Voltage :	10 V
Maximum Voltage Range :	-10 V - 10 V
Maximum Voltage Range Accuracy :	0.003 V
Simultaneous Sampling :	Yes

Fig. 3-11 shows a schematic diagram of the sound measurement system, microphone positions and the height of transformer core, *h*, for measurement of sound pressure. Eight microphones were located at half the height of the core at approximately

equally spacing of 0.3 m from the core surface while one microphone was fixed 0.3 m above the top surface.

Using the distance 0.3 m with the principal noise radiating surface 1 m^2 as a reference, the sound power levels from transformer cores with different dimensions can be compared since the sound power level is independent of the environment and measuring distance. Hence sound power level can be compared between investigations. Comparing the amount of noise emitted by transformer cores with identical dimensions, sound pressure level can be accepted. The procedure of the determination of sound power level is described in Chapter 4. The output of the measurement system yields the sound pressure and sound pressure level from each microphone, the corrected average A-weighted sound pressure level and sound power level.

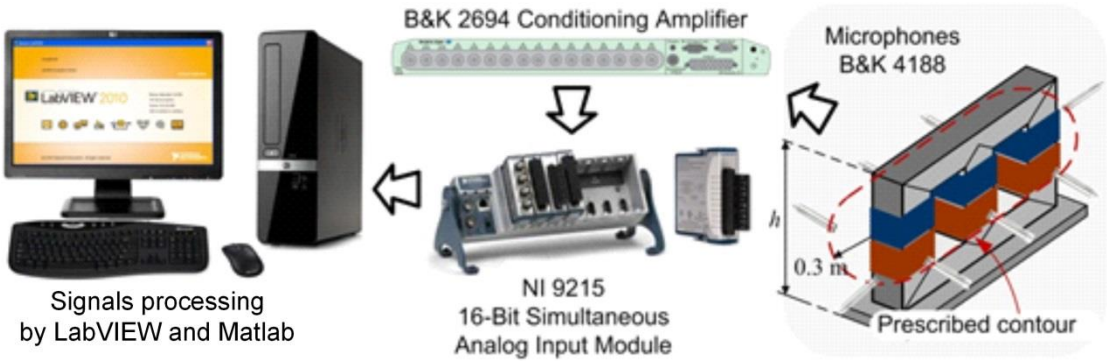

Fig.3-11: Schematic diagram of sound pressure level measurement system for transformer core

A Virtual Instrument (VI) for determining the sound pressure level was developed. The front panel of the VI is shown in Fig. 3-12.

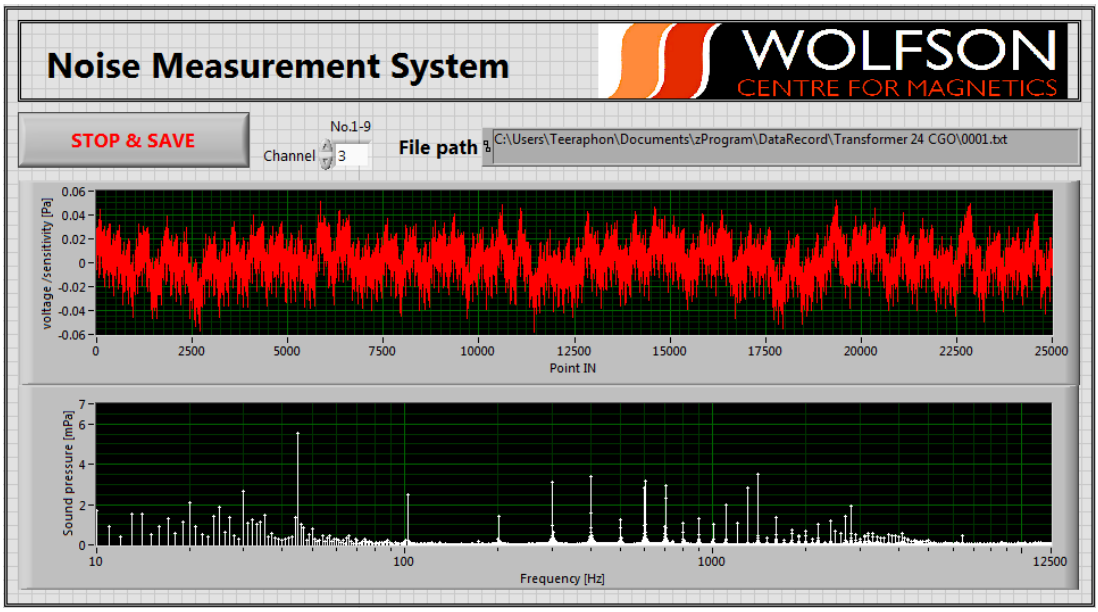

Fig. 3-12: Front panel of noise measurement system

Fig. 3-13 shows a simple box diagram of the VI. A 1D analogue input VI reads sound pressure signals from the voltage module (NI9215). The signal was divided by the microphone sensitivity and then sound pressure levels were calculated by Eq. 3-3. The outputs both in time domain and frequency domain were saved in spread sheet format. Matlab was used for calculating A-weighted sound pressure level, the averaged A-weighted sound pressure level, the collected average A-weighted sound pressure level and the A-weighted sound power level as described in Chapter 4.

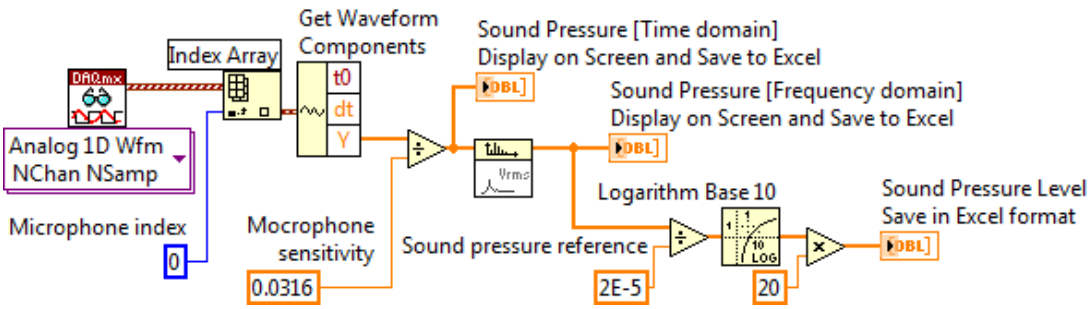

Fig.3-13: Schematic diagram of sound pressure level measurement system for a transformer core

In order to make measurements without reflecting objects, the measurements were made in a hemi-anechoic chamber whose ceiling and walls were covered by a highly absorptive material to eliminate reflections. Fig. 3-14 shows the hemi-anechoic chamber which has a dimension 2 m×3.5 m×2.2 m (W×L×H) and shows a photograph of microphones positioned on the prescribed contour. The average acoustic absorption coefficient of the chamber was 0.5 and the total area of the surface was 38.2 m^2.

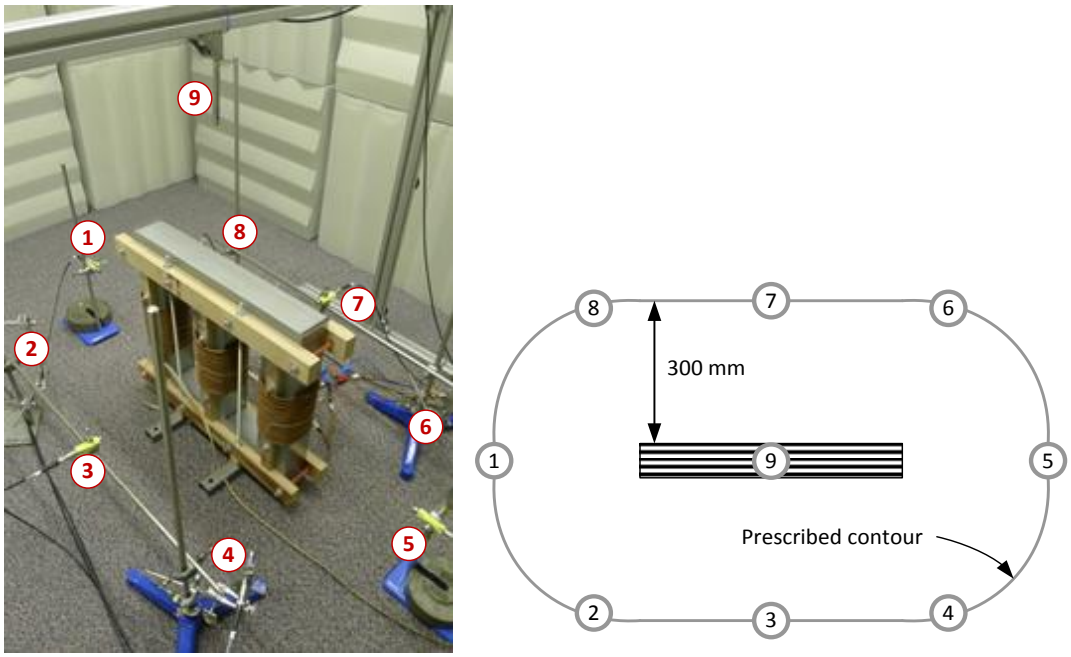

a) b)

Fig.3-14: Microphone positions and the prescribed contour
a) Microphone positions
b) The prescribed contour

3.4.2 Vibration Measurement System

To investigate the correlation between vibration and noise of the transformer cores, a non-contact PSV-400 Scanning Vibrometer, was used. It is a full-field vibrometer measurement and visualization system. Also, a PSV Software Package provided detailed vibration data analysis including graphing, animation of 2-D colour maps

[43]. The vibration system consists of scanning head (PSV-I-400), Junction box (PSV-E-401), Controller (OFV-5000) and PC (PSV-W-401) as shown in Fig. 3-15. Outputs from the system yielded vibration velocity in average rms, and the frequency domain and a 2-D animation of vibration.

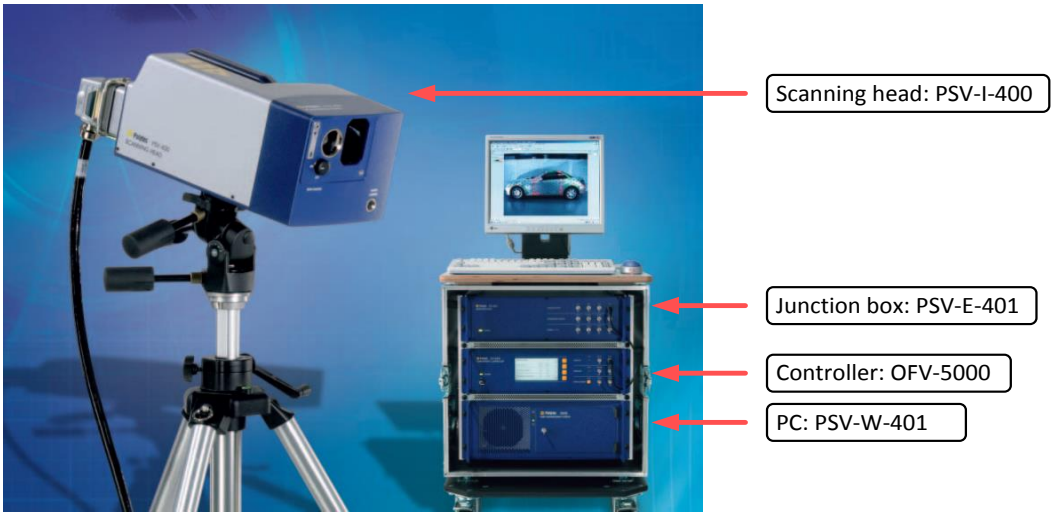

Fig.3-15: Photograph of the vibration measurement system [43]

The scanning head measures the vibration component of every defined measurement point. The system has a velocity range 0.01 µm/s – 10 m/s and frequency bandwidth 0 – 80 kHz. Table 3-4 shows the specification of the scanning head. A junction box is used for interfacing between the scanning head and controller.

The controller is used for controlling the velocity range of the laser head and there is an analogue (hardware) low pass filter with frequency a limit of 5 kHz. The PSV 8.8 scanning vibrometer software was installed in the PC. It controls all measurement tasks, setting measurement parameters, acquiring, displaying, processing and exporting measurement data. The procedure of the measurement of the cores vibration surfaces is described in Chapter 4.

Table 3-4: Specification of scanning laser vibrometer PolyTec PSV-400 [43]

Dimensions [W×L×H]	190 mm × 376 mm × 163 mm
Weight	7 kg
Laser type	HeNe laser (633 nm)
Laser safety class	Class 2 (< 1 mW visible output)
Working distance	LR lens: 0.35 m – 100 m
Sample size	From few mm^2 up to several m^2
Camera	Colour video camera, CCD ¼" , 752×582 pixels, with Auto focus and 72X zoom
Bandwidth	0 – 80 kHz
Velocity range	0.01 µm/s – 10 m/s
Scanner	High precision scan unit (scanning range ± 20° about X,Y)
Scan speed	Up to 30 points/s (typical)

3.4.3 Localised Magnetic Flux Density Measurement System

An array of single turn search coils both in the rolling and the transverse directions were prepared by threading 0.19 mm diameter enamelled copper wire through 0.5 mm diameter holes. To measure the localised magnetic flux density, the instantaneous induced voltage of each search coil was acquired by a data acquisition module NI-9215 with a sampling rate of 1 kS/s while the core was magnetised. The localised magnetic flux density was obtained by integrating the instantaneous induced voltage signal. Fig. 3-16 shows a block diagram of the method for implementation of magnetic flux density. The array of voltage signals were integrated and divided the lamination cross section area.

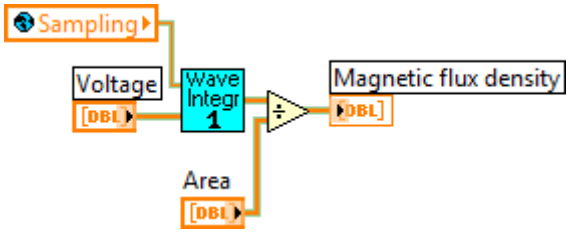

Fig.3-16: Block diagram showing Virtual Instrument for calculating magnetic flux density

3.5 Uncertainty in the Measurement

Uncertainty in the measurements is not an error of the measurements. The error of the measurement is the difference between the measured value and the true value but the uncertainty is the range of possible true values.

To present the uncertainty in measurement, the measured value y which is the function of the input quantities of $x_1, x_2, x_3, ..., x_n$ are applied by the uncertainty, U as $y \pm U$. It presents an expect true value of y is between $y-U$ and $y+U$.

The uncertainties of the measurement system were considered according to the recommendations given in UKAS M3003 "The Expression of Uncertainty and Confidence in Measurement" [50]. Sources of uncertainty comprise random and systematic uncertainties. The random uncertainty or repeatability of the measurement was called Type A uncertainty, u_A, which was evaluated by statistic methods. The systematic uncertainty was called Type B uncertainty, u_B, which was derived by the agglomeration of the individual reference calibration of the instruments taken from the manufacturers specifications. In addition, systematic uncertainties dealt with drift in the calibrated instruments, measurement process, operator skill and environmental effects [51]. To estimate the uncertainty in the measurement, UKAS M3003 [50] and A beginner's guide to uncertainty in measurement [51] were used as a guide.

The following steps show details of how the uncertainty in measurement was estimated. The root sum of the squares of u_A and u_B was called combined standard uncertainty, u_C . It was calculated from Eq. 3-9.

$$u_C(y) = \sqrt{u_A^2(y) + u_B^2(y)} \tag{3-9}$$

The u_A can be calculated from the standard deviation (stdev) of the mean of a set of several repeated measurements, divided by square root of the number of measurements, n, as in Eq. 3-10.

$$u_A(y) = \frac{\text{stdev}}{\sqrt{n}} \tag{3-10}$$

The u_B can be calculated from Eq. 3-11.

$$u_B^2(y) = c_1^2 u^2(x_1) + c_2^2 u^2(x_2) + \ldots + c_n^2 u^2(x_n) \tag{3-11}$$

where c_i is sensitivity coefficient. It is the partial derivative of the *y* with respect to x_i as in Eq. 3-12.

$$c_i = \frac{\partial y}{\partial x_i} \tag{3-12}$$

Eq.3-12 is used if the mathematical relation between the measurements can be defined. If the mathematical equation cannot be found, c_i can be estimated by calculating the rate of change of y with x_i. The sources of uncertainty are usually provided with the instrument specifications. In this work, the calibration certificate of the Digitronic calliper was not available. Thus, estimation of the uncertainty is necessary. The source of uncertainty can be estimated by a half of their minimum scale divided by $\sqrt{3}$. To estimate the upper and lower limits at confidence 95 %, 2 is used as the divisor for the normal distribution components and $\sqrt{3}$ is used for rectangular distribution components. Normal distributions are assumed for calibrated references. Rectangular distributions are assumed for uncertainties where only the upper and lower limits are known such as scale reading. Finally, the combined standard uncertainty is multiplied by the coverage factor (k_{95} = 2) to give the final expanded uncertainty as in Eq. 3-13.

$$U = k_{95} \cdot u_C \tag{3-13}$$

Tables 3-5 to 3-9 show uncertainty budgets for the measurements made during this study.

Table 3-5: Uncertainty budget in the measurement of average magnetic flux density on the limbs of three phase transformer cores

Source of uncertainty	± %	Probability distribution	Divisor	C_i	U_i ± %
Voltage (reading)	0.050[(a)]	Normal	2.0000	1	0.02500
Voltage (range)	0.005[(b)]	Normal	2.0000	1	0.00250
Lamination width	0.010[(c)]	Rectangular	1.7321	1	0.00577
Stack thick	0.010[(d)]	Rectangular	1.7321	1	0.00577
Frequency	0.100[(e)]	Normal	2.0000	1	0.05000
Drift between calibrations	0.020[(f)]	Rectangular	1.7321	1	0.01155
Type A uncertainty, V_A	-[(g)]	Normal	2.0000	1	-
Type A uncertainty, V_B	-[(h)]	Normal	2.0000	1	-
Type A uncertainty, V_C	-[(i)]	Normal	2.0000	1	-
Combined uncertainty					-
Expanded uncertainty at a confidence level of 95 %					-

The values in Table 3-5 can be determined in the following way:

a) Voltage (reading): The accuracy of the voltage measurement in power analyser Norma D6000 (reading) is ±0.05 % [52].
b) Voltage (range): The accuracy of the voltage measurement in power analyser Norma D6000 (range) is ±0.005 % [52].
c) Lamination width measured by Digitronic Calliper: The resolution of the calliper is 0.01 mm.
d) Stack thick measured by Digitronic Calliper: The resolution of the calliper is 0.01 mm.
e) Frequency: The accuracy of the frequency measurement in power analyser Norma D6000 is ±0.01 % [3-52].
f) Drift between calibrations: Drift error occur after the measuring instrument calibration, approximately 0.02 % [53]

g) Type A uncertainty, V_A: The repeatability of magnetising voltage on the core limb A can be calculated by Eq. 3-10.

h) Type A uncertainty, V_B: The repeatability of magnetising voltage on the core limb B can be calculated by Eq. 3-10.

i) Type A uncertainty, V_C: The repeatability of magnetising voltage on the core limb C can be calculated by Eq. 3-10.

Table 3-6: Uncertainty budget in the measurement of average magnetic flux density on limbs of single phase transformer cores

Source of uncertainty	± %	Probability distribution	Divisor	C_i	U_i ± %
Voltage (reading)	0.100[(a)]	Normal	2.0000	1	0.05000
Voltage (range)	0.100[(b)]	Normal	2.0000	1	0.05000
Lamination width	0.010[(c)]	Rectangular	1.7321	1	0.00577
Stack depth	0.010[(d)]	Rectangular	1.7321	1	0.00577
Frequency	0.100[(e)]	Normal	2.0000	1	0.05000
Drift between calibrations	0.020[(f)]	Rectangular	1.7321	1	0.01155
Type A uncertainty, V	-[(g)]	Normal	2.0000	1	-
Combined uncertainty					-
Expanded uncertainty at a confidence level of 95 %					-

The values in Table 3-6 can be determined in the following way:

a) Voltage (reading): The accuracy of the voltage measurement in power analyser Norma D4000 (reading) is ±0.1 % [54].

b) Voltage (range): The accuracy of the voltage measurement in power analyser Norma D4000 (range) is ±0.1 % [54].

c) Lamination width measured by Digitronic Calliper: The resolution of the calliper is 0.01 mm.

d) Stack thick measured by Digitronic Calliper: The resolution of the calliper is 0.01 mm.

e) Frequency: The accuracy of the frequency measurement in power analyser Norma D6000 is ±0.01 % [54].

f) Drift between calibrations: Drift error occur after the measuring instrument calibration, approximately 0.02 % [53]

g) Type A uncertainty, V: The repeatability of magnetising voltage on the core can be calculated by Eq. 3-10.

Table 3-7: Uncertainty budget in the measurement of noise

Source of uncertainty	± %	Probability distribution	Divisor	C_i	U_i ± %
Accuracy of B&K 4188-A-021	-[(a)]	Normal	2.0000	1	-
Accuracy of B&K 2694	-[(b)]	Normal	2.0000	1	-
Accuracy of NI 9215 (reading)	0.020[(c)]	Normal	2.0000	1	0.01000
Accuracy of NI 9215 (range)	0.014[(d)]	Normal	2.0000	1	0.00700
Drift between calibrations	0.020[(e)]	Rectangular	1.7321	1	0.01155
Type A uncertainty, noise	-[(f)]	Normal	2.0000	1	-
Combined uncertainty					-
Expanded uncertainty at a confidence level of 95 % (k_{95}=2)					-

The values in Table 3-7 can be determined in the following way:

a) Accuracy of B&K 4188-A-021: The accuracy of the microphone and preamplifier is ±0.2 dB. Thus relative accuracy is (0.2×100)÷measured value.

b) Accuracy of B&K 2694: The accuracy of the conditioning amplifier is ±0.05 dB [55]. Thus relative accuracy is (0.05×100)÷measured value.

c) Accuracy of NI 9215 (reading): The accuracy of the voltage measurement (reading) is ±0.02 % [56].

d) Accuracy of NI 9215 (range): The accuracy of the voltage measurement (range) is ±0.014 % [56].

e) Drift between calibrations: Drift error occur after the measuring instrument calibration, approximately 0.02 % [53]

f) Type A uncertainty, noise: The repeatability of noise can be calculated by Eq. 3-10.

Table 3-8: Uncertainty budget in the measurement of vibration

Source of uncertainty	± %	Probability distribution	Divisor	C_i	U_i ± %
Accuracy of Vibrometer	1.300[(a)]	Normal	2.0000	1	0.65000
Drift between calibrations	0.020[(b)]	Rectangular	1.7321	1	0.01155
Type A uncertainty, V	0.000[(c)]	Normal	2.0000	1	0.00000
Combined uncertainty					0.65010
Expanded uncertainty at a confidence level of 95 %					2

The values in Table 3-8 can be determined in the following way:

a) Accuracy of Vibrometer: The accuracy of the scanning vibrometer is ±1.3 % [57].
b) Drift between calibrations: Drift error occur after the measuring instrument calibration, approximately 0.02 % [53]
c) Type A uncertainty, vibration velocity: The repeatability of vibration velocity can be calculated by Eq. 3-10.

Table 3-9: Uncertainty budget in the measurement of localised magnetic flux density

Source of uncertainty	± %	Probability distribution	Divisor	C_i	U_i ± %
Voltage (reading)	0.020[(a)]	Normal	2.0000	1	0.01000
Voltage (range)	0.014[(b)]	Normal	2.0000	1	0.00700
Lamination width	0.010[(c)]	Rectangular	1.7321	1	0.00577
Lamination thick	0.010[(d)]	Rectangular	1.7321	1	0.00577
Frequency	0.100[(e)]	Normal	2.0000	1	0.05000
Drift between calibrations	0.020[(f)]	Rectangular	1.7321	1	0.01155
Type A uncertainty, V	-[(g)]	Normal	2.0000	1	-
Combined uncertainty					-
Expanded uncertainty at a confidence level of 95 %					-

The values in Table 3-9 can be determined in the following way:

a) Voltage (reading): The accuracy of the NI9215 voltage measurement (reading) is ±0.02 % [56].

b) Voltage (range): The accuracy of the NI9215 voltage measurement (range) is ±0.014 % [56].
c) Lamination width was measured by Digitronic Calliper: The resolution of the calliper is 0.01 mm.
d) Stack thick was measured by Digitronic Calliper: The resolution of the calliper is 0.01 mm.
e) Frequency: The accuracy of NI9215 frequency measurement is ±0.01 % [56].
f) Drift between calibrations: Drift error occur after the measuring instrument calibration, approximately 0.02 % [53]
g) Type A uncertainty, localised magnetic flux density: It can be calculated by Eq. 3-7.

Chapter 4

Transformer Core Models and Measurement Procedures

This chapter describes the structures of transformer core models used in the investigation and describes the procedure for the measurement of noise and vibration. Also the detail of localised magnetic flux density measurement is presented. There are several parameters of the core structure which influence transformer core noise and vibration. Therefore some parameters have to be controlled. This work focuses on the effect of the core materials, step lap designs, effect of clamping torques and core bonding.

4.1 Transformer Core Models

To quantify the factors affecting transformer core noise and vibration, three phase, three limb transformer cores were designed for investigation of noise and vibration on surfaces. Single phase core types were used for comparing the effect of the noise and vibration at the T joints with the three phase core. The three phase cores were designed with multistep and single step configurations. Four overlap steps with single lamination per stacking layer with a length of overlap shift of 3 mm were used for multistep configuration and three laminations per stacking layer with length of overlap shift 6 mm were used for single step lap configuration.

All transformer core models were assembled from three grades of electrical steel: conventional grain oriented (CGO), high permeability grain oriented (HGO) and laser scribed domain refined (LDR), using a similar procedure to the manufacturers with laminations 100 mm wide, 0.3 mm thick and density of 7650 kg/m^3. The significant differences between these three materials are B_8 and core loss. They have the same

(011)[100] texture which known as Goss texture or cube-on-edge texture as shown in Fig.4-1. It was developed by Norman P Goss in 1933 [58]. The HGO material has a bigger grain size and lower core loss than the CGO. The LDR was developed by reduced core loss of the HGO by reducing the width of magnetic domains by means of laser irradiation [59]. The structures of magnetic domain before and after laser irradiation process are shown in Fig. 4-2. However, the laser irradiation produces stress in the lamination which then creates discontinuous domain structure. The closure domains are settled and this lead to increasing of magnetostriction.

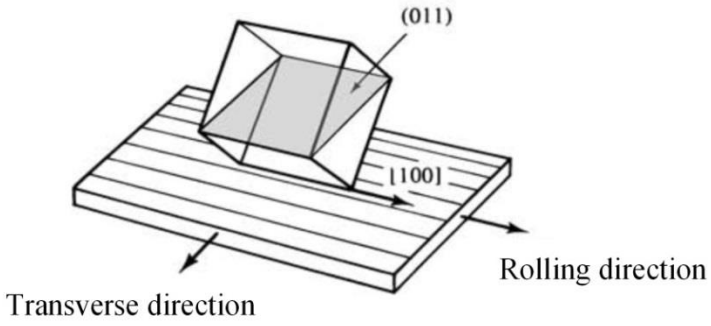

Fig. 4-1: (011)[100] texture of grain oriented electrical steel [58]

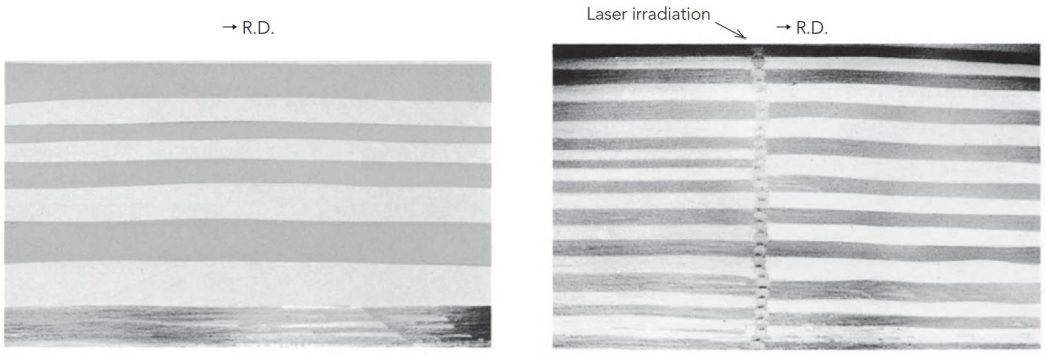

a) b)

Fig. 4-2: Domain structure of high permeability grain-oriented material [59]
a) Before laser irradiation
b) After laser irradiation

Table 4-1 shows relevant magnetic properties of the CGO, HGO and LDR material used. Figs. 4-3 to 4-5 show magnetostriction-stress characteristics along the rolling direction, $\lambda_{r.d.}$, of the materials at magnetic flux density 1.0 T to 1.7 T, 50 Hz [60]. A transverse magnetostriction, $\lambda_{t.d.}$, is approximately half of the magnetostriction along the rolling direction and opposite in sign [61].

The transformer cores have windows $320\text{ mm} \times 120\text{ mm}$ and 75 mm build up. Primary and secondary windings were evenly wound along the limbs with 30 turns of insulated copper wire, 1.5 mm^2. The numbers of turns were calculated from Faraday's induced voltage equation as shown in Eq.4.1.

$$\text{Number of turn} = \frac{V}{4.44\, f B A_c} \quad \text{turn} \qquad (4\text{-}1)$$

where V is induce voltage (V), f is frequency (Hz), A_c core cross sectional area (m^2)

The size of the conductor was calculated from the approximate apparent power per unit weight of the laminations, the core weight at a maximum magnetic flux density and approximate current density [62].

Figs. 4-6 to 4-8 show dimensions of yoke, outer limb and middle limb of three phase three limb transformer core with multistep lap configuration. Identical dimensions of the middle layer of yoke and outer limb of the multistep lap configuration were used for single step lap configuration. Typical dimensions of middle limb of the single step lap configuration are shown in Fig.4-9.

Fig. 4-10 shows yoke dimensions of single phase transformer cores with multistep lap configurations. The dimensions of the middle layer were also used for single step lap configuration. Limb dimensions of single phase transformer cores, both multistep and single step configurations, were identical in size to the middle layer of the multistep lap configuration of the three phase cores.

Table 4-1: Typical magnetic properties of CGO, HGO and LDR [63], [64], [65]

	CGO	HGO	LDR	
B_8	1.830	1.905	1.917	T
$W_{17/50}$	1.25	1.02	0.95	W/kg
B_{sat}	2.00	2.03	1.99	T
Stacking factor	0.965	0.965	0.973	
Density	7650	7650	7650	kg/m^3
Thickness	0.3	0.3	0.3	mm
Resistivity	0.48	0.48	0.50	μΩ-m
Modulus of Elasticity				
Rolling direction.	114	113	113.8	GPa
Transverse direction	196	195	203	GPa

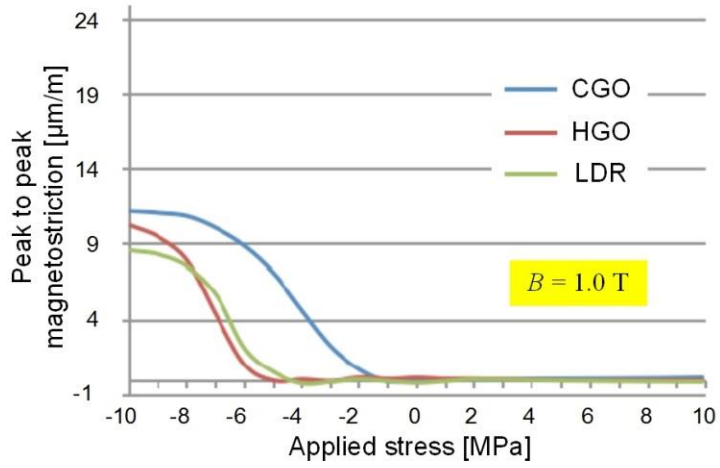

Fig.4-3: Magnetostriction-stress characteristics along the rolling direction of CGO, HGO and LDR materials at 1.0 T 50 Hz. [60].

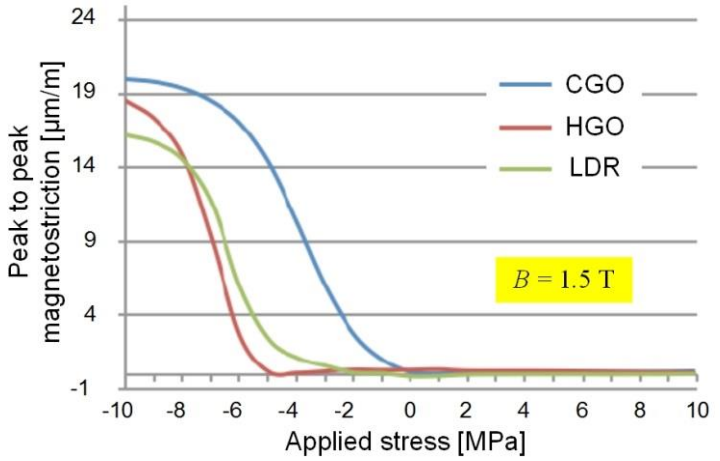

Fig.4-4: Magnetostriction-stress characteristics along the rolling direction of CGO, HGO and LDR materials at 1.5 T 50 Hz. [60].

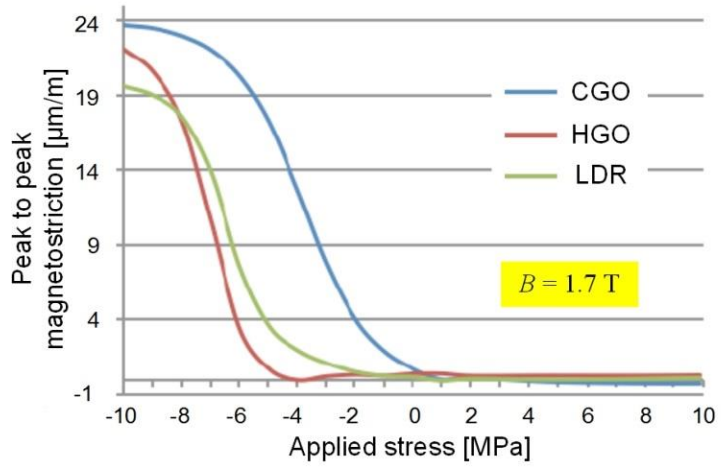

Fig.4-5: Magnetostriction-stress characteristics along the rolling direction of CGO, HGO and LDR materials at 1.7 T 50 Hz. [60].

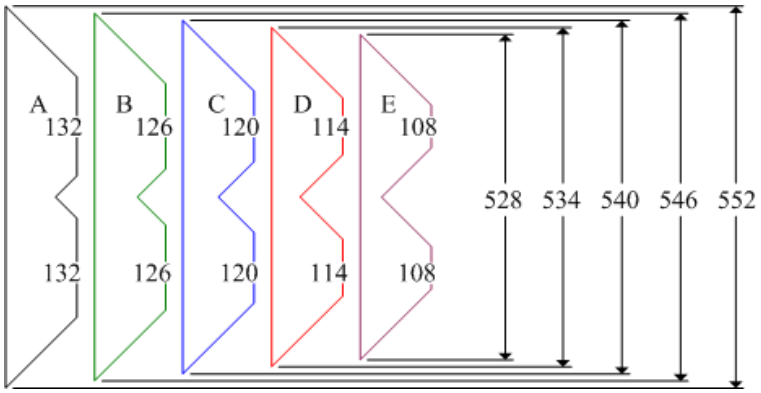

Dimensions in mm; not to scale

Fig. 4-6: Dimensions of the yoke of three phase three limb transformer core with multistep lap configuration

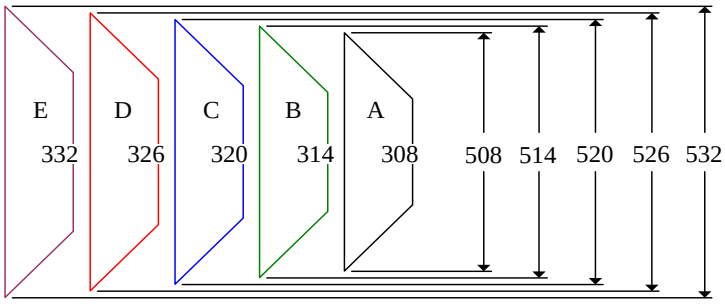

Dimensions in mm; not to scale

Fig. 4-7: Dimensions of the outer limb of three phase three limb transformer core with multistep lap configuration

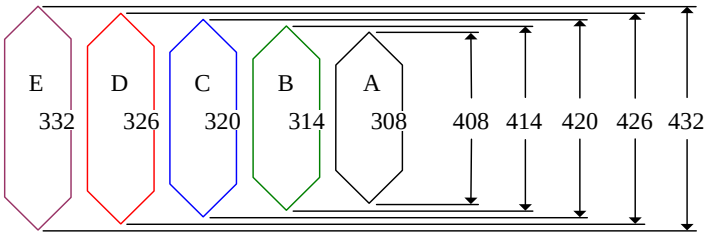

Dimensions in mm; not to scale

Fig. 4-8: Dimensions of the middle limb of three phase three limb transformer core with multistep lap configuration

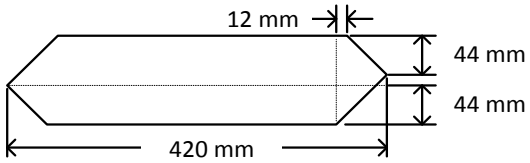

Fig. 4-9: Dimension of the middle limb of three phase three limb transformer core with single step lap configuration

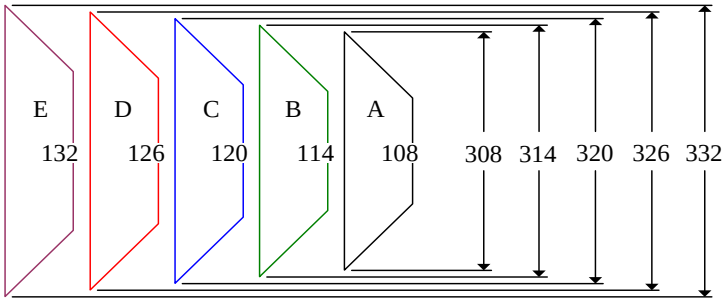

Dimensions in mm; not to scale

Fig. 4-10: Dimensions of yoke of the single phase transformer core

Three phase and single phase cores were built with the 3 materials in multistep and single step configurations. Therefore 12 core models were used in this study. To investigate the effect of core building, two cores of each configuration were built, 24 cores in all.

Tables 4-2 and 4-3 define the transformer core identification and describe material with step lap configuration. Photographs of the three phase and the single phase cores are shown in Fig.4-11. Fig. 4-12 shows photographs of the multi-step lap and the single step lap configuration. The transformer cores were clamped by 50 mm×30 mm wooden clamps on the yokes and 30 mm×20 mm clamps on each limb all tightened with fibre reinforced plastic bolts. The torque wrench, capacity 20 Nm was used for setting the clamping torque applied to the bolts.

Table 4-2: Number and specification of single phase transformer cores

Core No.	Material	Step lap	Core No.	Material	Step lap
1	LDR	MSL	7	LDR	SSL
2	LDR	MSL	8	LDR	SSL
3	HGO	MSL	9	HGO	SSL
4	HGO	MSL	10	HGO	SSL
5	CGO	MSL	11	CGO	SSL
6	CGO	MSL	12	CGO	SSL

Table 4-3: Number and specification of three phase transformer cores

Core No.	Material	Step lap	Core No.	Material	Step lap
13	LDR	MSL	19	LDR	SSL
14	LDR	MSL	20	LDR	SSL
15	HGO	MSL	21	HGO	SSL
16	HGO	MSL	22	HGO	SSL
17	CGO	MSL	23	CGO	SSL
18	CGO	MSL	24	CGO	SSL

It has been suggested that transformer core noise can be reduced by bonding laminations by adhesives [62]. To quantify the effect of bonding on core noise, a CGO single phase, multi-step lap core (Core No.5) which was assembled by the transformer manufacturer was tested and assessed using the procedure described in Section 4.3 after that it was coated with insulation vanish [66]. The noise experimental results are shown in Chapter 5.

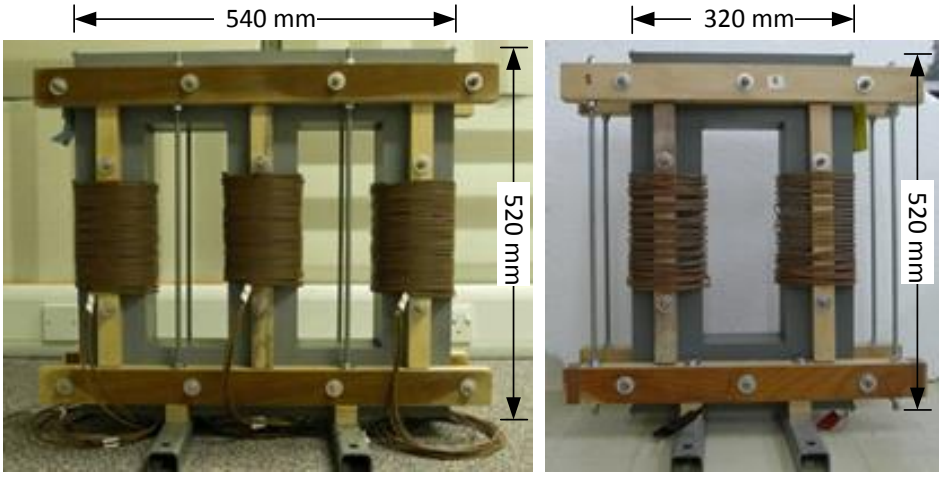

a) b)

Fig.4-11: Photographs of three phase and single phase transformer core

a) Three phase transformer core model, 115 kg.
b) Single phase transformer core model, 72 kg.

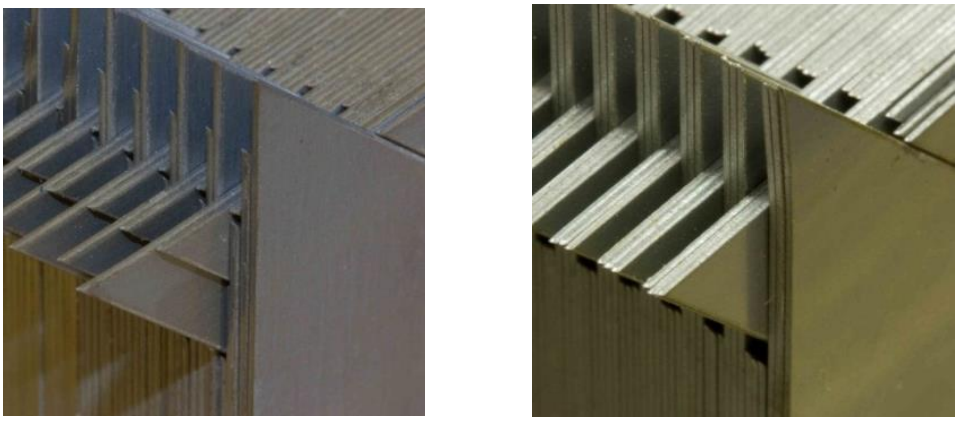

a) b)

Fig.4-12: Photographs of step lap configurations

a) Multi-step lap configuration 6/3/0/-3/-6 mm.
b) Single step lap configuration 6/-6 mm.

4.2 Magnetising System

A 15 kVA three phase variable transformer fed from a constant voltage transformer was used for magnetising the cores. The primary windings of the transformer core were connected to the variable transformer via a power analyser for measuring input voltage, magnetising current and power input. The induced voltage of the secondary was measured for calculating a magnetic flux density. A Norma D4000 power analyser was used for the measurement of single phase transformer cores and a Norma D6000 was used for the three phase cores. Schematic diagrams for single and three phase excitation are shown in Fig.4-13.

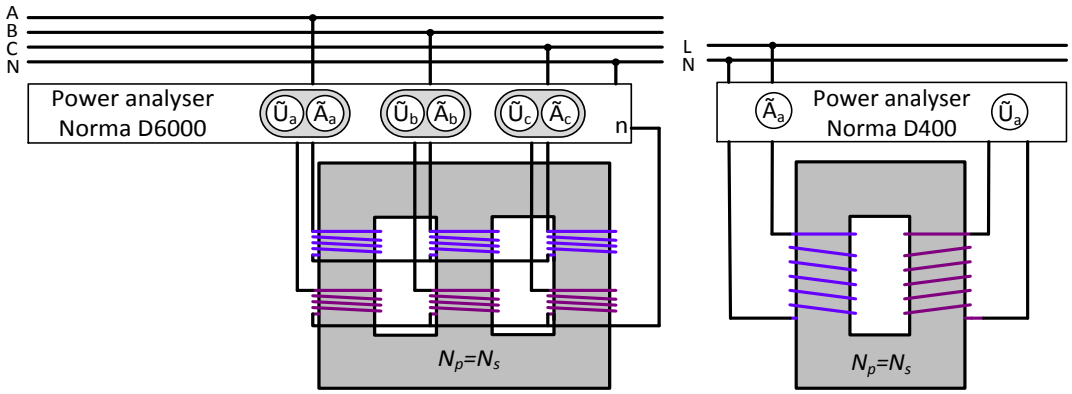

a) b)

Fig.4-13: Schematic diagram of the magnetising systems
a) Three phase magnetising system
b) Single phase magnetising system

4.3 Noise Measuring Procedure

The sound measuring system, described in section 3.4.1, was used for determining the sound emitted from the transformer cores. In order to compare all sounds from both three phase and single phase cores and to eliminate the effect of different dimensions between three phase core and single phase core, the A-weighted sound power level is

required. Fig. 4-14 shows the steps required to calculate A-weighted sound power level from sound pressure measurement [47].

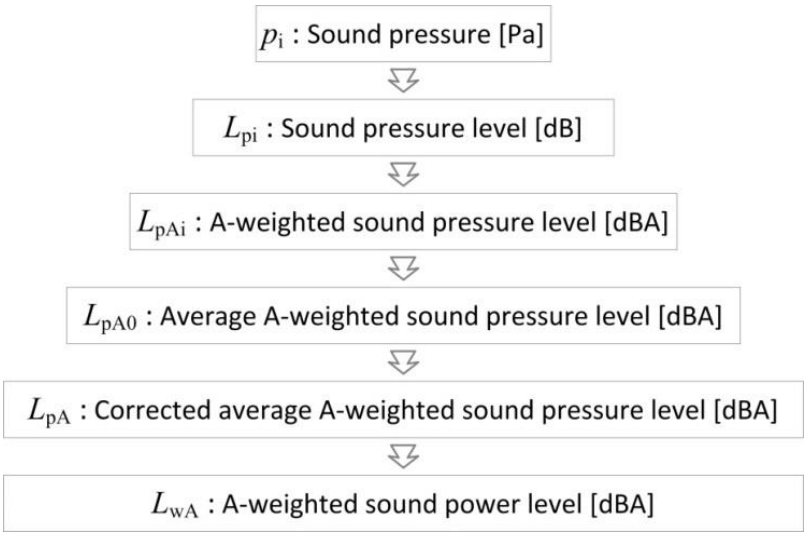

Fig.4-14: Flow chart of calculation of A-weighted sound power level from sound pressure

The following describes details in each step to calculate the A-weighted sound power levels. Sound pressure from each microphone, p_i, was calculated from the output voltage of the microphones and the open circuit sensitivities of the microphones as shown in Eq. 4-2.

$$p_i = \frac{\text{output voltage}}{\text{open circuit sensitivity}} \quad \text{Pa} \qquad (4\text{-}2)$$

where i represents the microphone position.

Sound pressure level, L_{pi}, was calculated from the sound pressure as shown in Eq. 4-3.

$$L_{pi} = 20 \times \log_{10}\left(\frac{p_i}{p_{ref}}\right) \quad \text{dB} \qquad (4\text{-}3)$$

Next, A-weighted sound pressure level, L_{pAi}, was calculated by applying the A-weighting scale.

The average A-weighted sound pressure level, L_{pA0}, was calculated from the A-weighted sound pressure level as shown in Eq. 4-4.

$$L_{\mathrm{pA0}} = 10\log_{10}\left(\frac{1}{N_{\mathrm{mic}}}\sum_{i=1}^{N_{\mathrm{mic}}} 10^{\frac{L_{\mathrm{pAi}}}{10}}\right) \qquad \text{dBA} \qquad (4\text{-}4)$$

where N_{mic} is the total number of measuring positions

The corrected average A-weighted sound pressure level, L_{pA}, was calculated from the average A-weighted sound pressure level as shown in Eq. 4-5.

$$L_{\mathrm{pA}} = 10\log_{10}\left(10^{\frac{L_{\mathrm{pA0}}}{10}} - 10^{\frac{L_{\mathrm{bgA}}}{10}}\right) - K \qquad \text{dBA} \qquad (4\text{-}5)$$

where L_{bgA} is the average A-weighted background noise pressure level and *K* is an environmental correction factor. Background noise was measured before and after measuring core noise. The environmental correction, *K*, was calculated from Eq. 4-6.

$$K = 10\log_{10}\left(1 + \frac{4}{A_{\mathrm{tr}}/S}\right) \qquad \text{dBA} \qquad (4\text{-}6)$$

The value of A_{tr} in square metres is given by Eq. 4-7.

$$A_{\mathrm{tr}} = \alpha S_v \qquad \mathrm{m}^2 \qquad (4\text{-}7)$$

where α is the average acoustic absorption coefficient. For full absorption such as cellulose fibre, α = 1 whilst for full reflective material such as plaster α is approximately 0. S_v is the total area of the surface of the test room (walls, ceilings

and floors) in square metres. Fig. 4-15 shows the relationship between the environment correction and the ratio of A_{tr} to the measurement area.

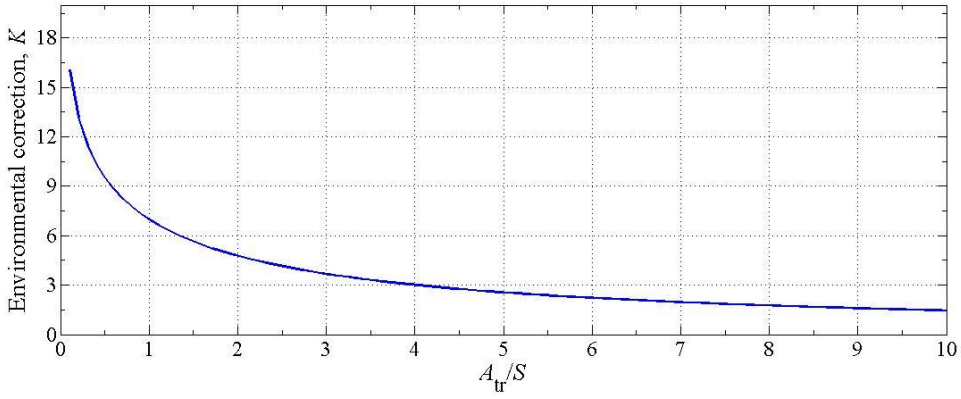

Fig.4-15: Relationship between environment correction and ratio of A_{tr} / S

The A-weighted sound power level of the transformer core, L_{WA}, was calculated from the corrected average A-weighted sound pressure level, L_{pA} as shown in Eq. 4-8.

$$L_{WA} = L_{pA} + 10\log_{10}\frac{S}{S_0} \qquad \text{dBA} \qquad (4\text{-}8)$$

where the measurement surface S is derived from Eq. 4-9.

$$S = 1.25hl_m \qquad \text{m}^2 \qquad (4\text{-}9)$$

where S_0 is a 1 m^2 reference area and *h* is a half the height of the core in metres, l_m is the length in metres of the prescribed contour. The 1.25 constant is based on experience for taking into account the sound energy radiated by the upper part of the transformer [47]. The last term of Eq. 4-8 is negative if $S < S_0$. Table 4-4 summarises the parameters used for calculating the sound power level of the transformer cores.

In the experiments, the sound pressure signals from the microphones were simultaneously recorded while the cores were magnetised at 1.0 T to 1.8 T with a clamping torque ranging from 2 Nm to 6 Nm. The results of the corrected average A-weighted sound pressure level, the A-weighted sound power level and frequency distribution of the sound pressure signals on each core are shown in Chapter 5.

Table 4-4: Summary of the parameter use for determine sound power level

	3 phase core	1 phase core
Room dimension [m^3]	2 × 2.2 × 3.5	2 × 2.2 × 3.5
average acoustic absorption coefficient, α	0.5	0.5
Total surface of the test room , S_v [m^2]	38.2	38.2
A_{tr} [m^2]	19.1	19.1
A half the height of the core, h [m]	275×10^{-3}	275×10^{-3}
Length of the prescribed contour , l_m [m]	3.115	2.675
Measurement surface, S [m^2]	1.071	0.920
Environmental correction, K	0.879	0.765
$10\log(S / S_0)$	0.298	-0.362

4.4 Vibration Measuring Procedure

The vibration measurement system, described in section 3.4.2, was used for investigating the vibration of the transformer core surfaces. A PSV-400 scanning vibrometer was hired for the experiments. To eliminate the building vibration, a single point vibrometer with Laser Head OFV-303 was used for cooperating with PSV-400. To reduce the size of the measurement area, an advantage of symmetry was used. The shaded area of Fig. 4-16 shows the symmetrical measurement area of the transformer surface for both the three phase and single phase cores. In the experiments, the mirror technique was utilised to scan three surfaces of the core without moving the laser head or the core. A photograph of the system is shown in Fig. 4-17. Single turn coils were

wound around the middle limbs of three phase cores and one limb of the single phase core for use as the reference flux density signal.

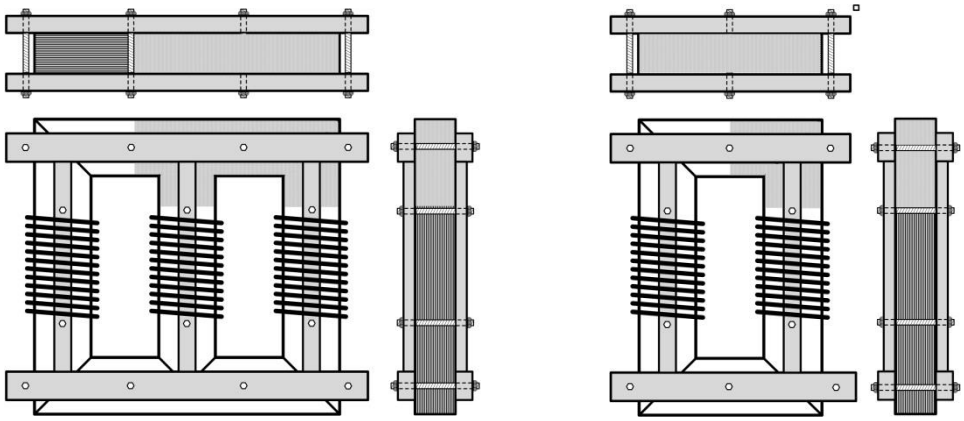

a) b)

Fig. 4-16: Area (grey) of the vibration measurements
a) Three phase transformer
b) Single phase transformer

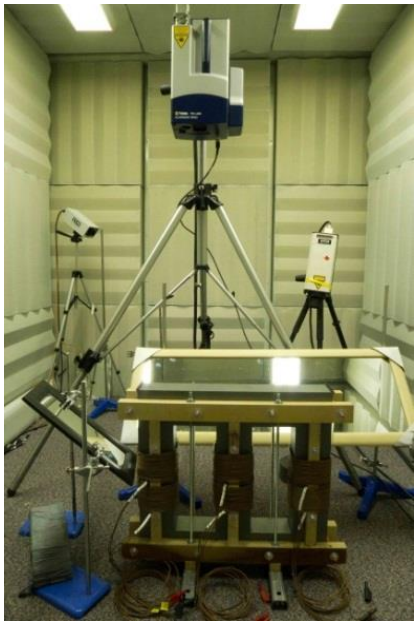

Fig.4-17: Photograph of the vibration measurement system

To prepare the experiments, the scanning vibrometer was setup by first defining the measurement area, i.e. the edges of the desired measurement areas were focused on. A spatial resolution of the measurement less than 1 cm × 1 cm was set. Next, the frequency bandwidth was specified. By preliminary testing using a wide frequency range (1 Hz to 20 kHz) and high frequency resolution (1 Hz), it was confirmed that the fundamental of the vibration was approximately 100 Hz to 200 Hz and that the natural frequency of the core lamination was less than 3 kHz [67]. Therefore, the frequency bandwidth was set at 5 kHz for covering the frequencies of interest.

In the experiments, the average of 3 vibration velocity signals from the scanning vibrometer in the frequency domain at each measuring point were recorded while the cores were magnetised from 1.0 T to 1.7 T, 50 Hz with a clamping torque ranging from 2 Nm to 6 Nm. The results of surface vibrations, vibration velocity, and frequency distribution on each core are presented in Chapter 5.

4.5 Localised magnetic flux density measuring procedure

To investigate the localised magnetic flux density at the corners and the T-joint, the search coil sensing technique was used. The middle lamination of a three phase CGO core was prepared with arrays of 10 mm long single turn search coils wound orthogonal to both rolling and transverse directions. Fig. 4-18 shows the positions of the search coils which were wound by threading 0.19 mm diameter (SWG-36) enamelled copper wire through 0.5 mm diameter hole. The leads of the coils were tightly twisted together to avoid stray voltage pick-up.

To measure the orthogonal components of localised magnetic flux density, the instantaneous induced voltage (v) of each search coil was acquired by a data acquisition card, NI-9215, with a sampling rate of 1 kS/s while the core was magnetised. The magnetic flux density components were obtained by integrating of

the instantaneous induced voltage signal and dividing by the lamination cross section area from Eq. 4-10.

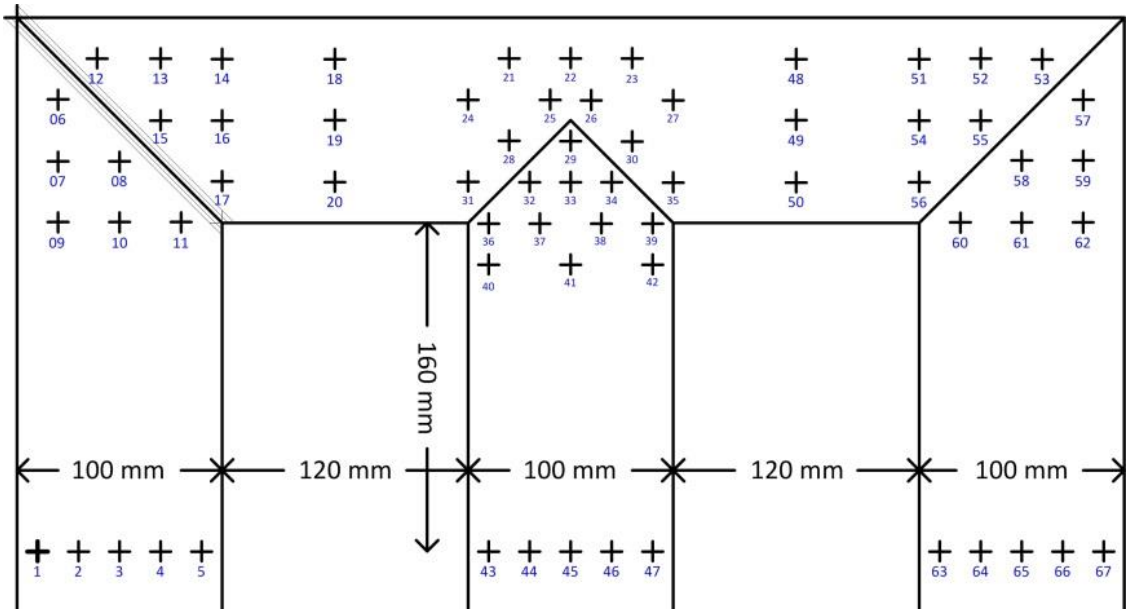

Fig.4-18: Positions of localised search coils in the middle layer of the core

$$b(t) = \frac{1}{A_c}\int v dt \tag{4-10}$$

where b is instantaneous magnetic flux density. The total localised magnetic flux (b_{total}) was calculated from the component in the rolling direction ($b_{r.d.}$) and transverse direction ($b_{t.d.}$) as shown in Eq. 4-11.

$$b_{total} = \sqrt{b_{r.d.}^2 + b_{t.d.}^2} \tag{4-11}$$

In the experiments, the VI for calculating magnetic flux density was developed as described in section 3.4.3. The orthogonal components of localised magnetic flux density were recorded while the cores were magnetised at 1.0 T to 1.7 T with a clamping torque of 4 Nm. They are presented and discussed in Chapter 5.

Chapter 5

Analysis and Discussion of Noise and Vibration Experimental Results on Transformer Cores

This chapter presents the experimental noise and vibration results of the transformer cores which were described in Chapter 4. In the noise experiments, transformer cores were tested under magnetic flux densities from 1.0 T to 1.8 T 50 Hz with clamping torques from 2 Nm to 6 Nm. The vibration experimental results were achieved from six MSL and one SSL three phase cores and three single phase cores at magnetic flux densities from 1.0 T to 1.7 T 50 Hz with clamping torques from 2 Nm to 6 Nm.

A-weighted sound power level (dBA), A-weighted sound pressure level (dBA) and sound pressure (Pa) were used for describing the quantity of the core noise in the appropriate situation. A-weighted sound power level is the quantity used to express sound energy generated from a sound source which is independent of the frequency of the sound, the distance of the measurement and the dimensions of the sound source. Hence, it is the appropriate parameter for comparing the noise generated by transformer cores. This is the reason for using sound power level as the reference quantity in the standard to classify the class of transformers [2]. However, it is not suitable for investigating the relationship between noise and vibration because an A-weighting scale is applied. Therefore, sound pressure is more suitable than A-weighted sound power level for this situation. When comparing the amount of noise emitted by transformer cores with identical dimensions, sound pressure level can be accepted. Because sound waves propagate through the air as a longitudinal wave with a velocity, experimental vibration results were expressed in terms of velocity. The experimental results yield both vibration velocity and phase of vibration both in time domain and frequency domain where the magnetic flux density signal at the middle limb was used as a phase reference.

The experimental noise and vibration results are presented starting with the effect of magnetostriction. Noise from three transformer cores assembled with the same size and step lap configuration but different magnetostriction characteristic materials are compared. Next, the effect of magnetic flux density is considered, and then an investigation of noise and vibration on each surface of transformer core is presented. Then, an investigation of the effect of the T-joint on transformer core noise is shown by comparing the A-weighted sound power level from the three phase core with the single phase core which has the same window size. Then, the effect of clamping torque is presented. Next, the effect of bonding a core is illustrated. Finally, localised magnetic flux density on the T-joint and corner are presented. Before considering the experimental results, a model of core deformation due to magnetostriction is proposed for explaining deformation of the core laminations.

5.1 Model of Transformer Core Deformation due to Magnetostriction

The causes of transformer core vibration are magnetic forces between laminations and lamination deformation due to magnetostriction. If a transformer core has a homogeneous structure, there is only in-plane vibration due to magnetostriction, however, in practice the core is usually built up from a stack of laminations and, there is a vibration in an out-plane direction of the lamination due to magnetic forces [62]. Magnetostriction and magnetic forces varies with the square of magnetic flux density [68], [69] which is proportional to induced voltage. In a three phase transformer, the primary windings are connected to a three phase electrical system. Therefore, instantaneous magnetic flux densities on phase A (b_a), phase B (b_b) and phase C (b_c) can be expressed by Eq. 5-1 to Eq. 5-3.

$$b_a(t) = B_m \sin\left(\omega t + 120^\circ\right) \quad \text{T} \quad (5\text{-}1)$$

$$b_b(t) = B_m \sin\left(\omega t\right) \quad \text{T} \quad (5\text{-}2)$$

$$b_c(t) = B_m \sin\left(\omega t - 120^\circ\right) \quad \text{T} \quad (5\text{-}3)$$

where B_m is maximum magnetic flux density, ω is angular frequency, t is time. The signal b_b was used as a phase reference.

Fig.5.1 shows variation of magnetic flux density in one cycle of magnetisation. A phase shift of one-third of the period occurs between each phase. Red, green and blue lines represent magnetic flux density phase A, B and C respectively.

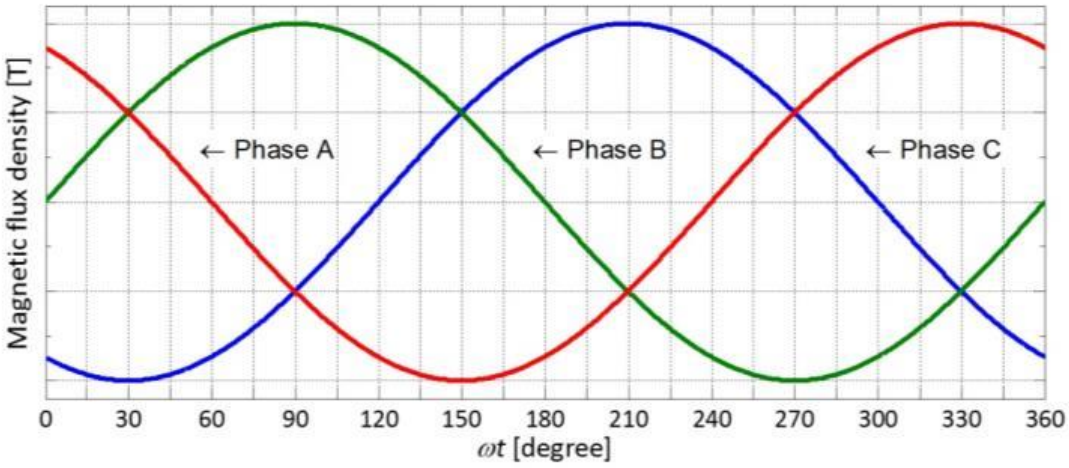

Fig. 5-1: Three phase magnetic flux density waveforms

Deformation of a lamination due to magnetostriction is shown in Fig.5-2. If a transformer core lamination is magnetised and magnetic flux flows uniformly along the rolling direction, the deformation due to transverse magnetostriction is neglected because the core lamination width is significantly shorter than the length by approximately 5 times and magnetostriction in the rolling direction is higher than in the transverse direction when flux flows uniformly along the rolling direction [61].

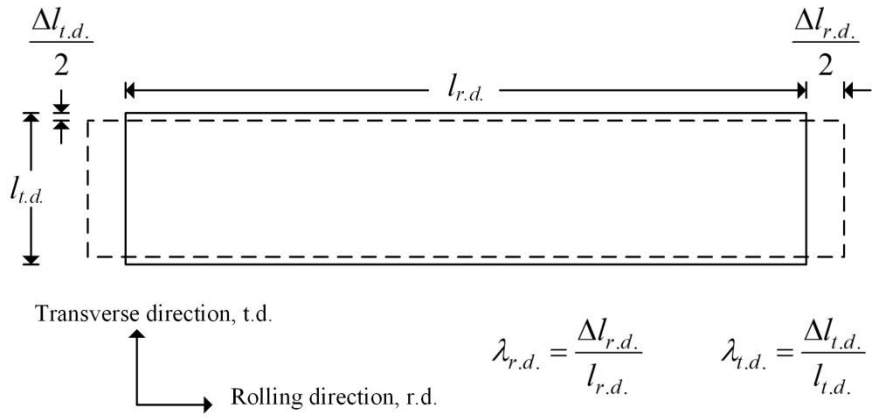

Fig. 5-2: Deformation of a lamination due to magnetostriction

Considering the dimensions of transformer core laminations, there are three different shapes for three phase core and two different shapes for single phase core as shown in Fig. 5-3. Each limb of a three phase core is magnetised with a 120° phase shift. Top and bottom yokes which are interlaced to the limbs have associated magnetic flux with the limbs.

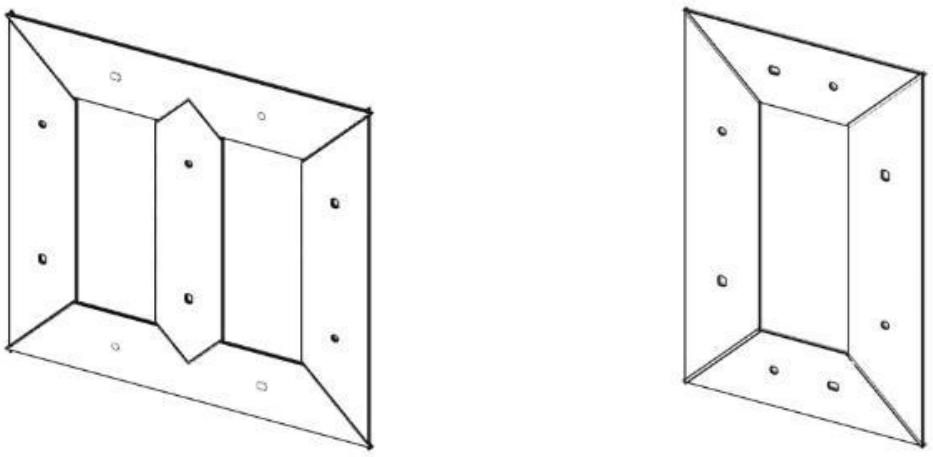

a) b)

Fig. 5-3: Shape of transformer core laminations

a) Three phase three limb core
b) Single phase core type

A model to obtain the deformation of a core lamination due to magnetostriction was developed in Matlab assuming that magnetic flux is distributed uniformly in the rolling direction and not taking in to account the effect of rotational or transverse magnetisation. Rotational magnetisation affects the magnetostriction characteristic of the materials depending on the loci [70]. Fig. 5-4 shows simulated core deformation of a three phase core under magnetic flux at ωt=0° to 180°. The core dimensions are to scale but in order to clearly present the difference in deformation, the magnetostriction is increased in amplitude. Because of symmetry, only the upper half is shown. The grey arrow represents the maximum amplitude of the magnetic flux density in the positive direction. The black dotted lines at the joints represent the un-deformed length of the laminations.

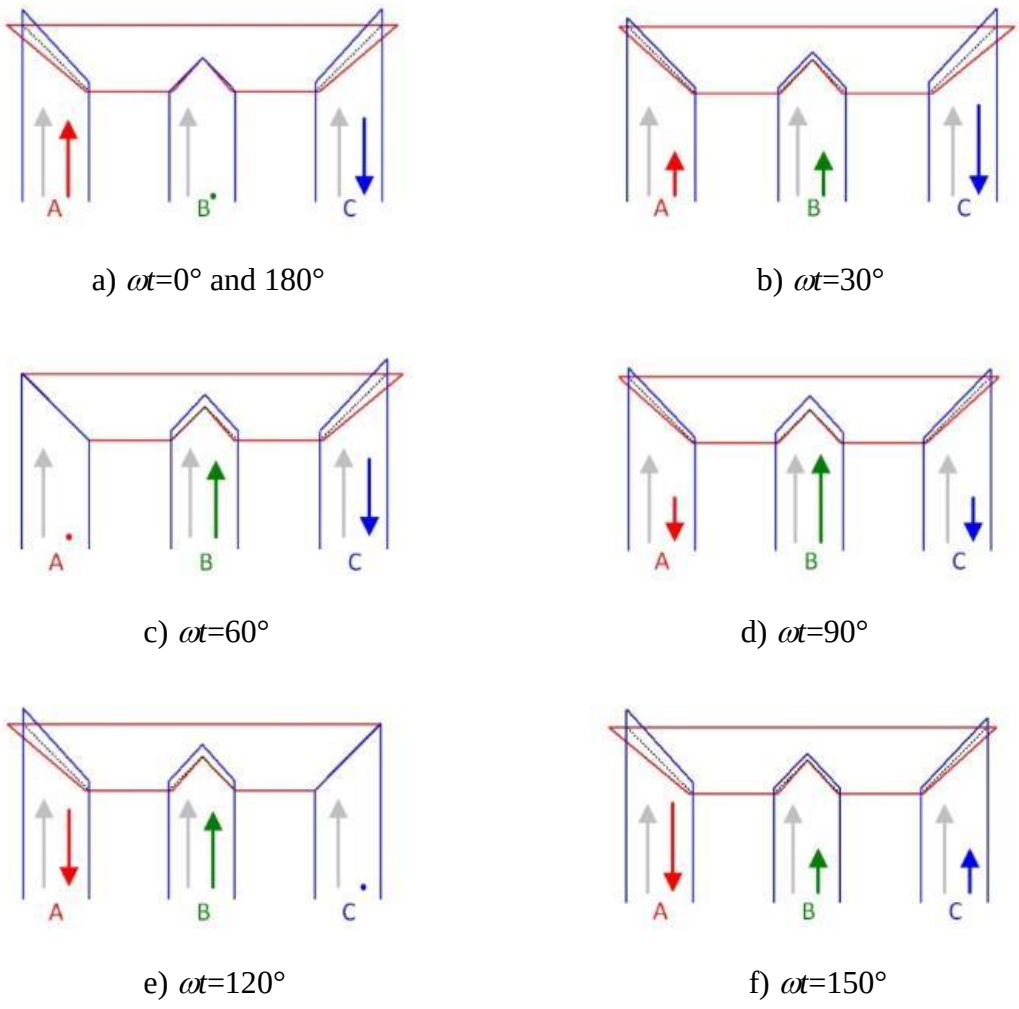

a) ωt=0° and 180°

b) ωt=30°

c) ωt=60°

d) ωt=90°

e) ωt=120°

f) ωt=150°

Fig. 5-4: Simulated core deformation due to magnetostriction in the rolling direction

At ωt=0°, the magnetic flux density at phase B is zero while phase A and phase C have the same amplitude but opposite direction. Opposite direction of magnetic flux does not affect the amplitude of magnetostriction. From Fig.5-4 at ωt=0°, it can be seen that the middle limb does not change the dimension because $b_b = 0$. However, there is a deformation on the yoke because of an influence of the magnetic flux in phase A and phase C. The outer limbs are strained due to the influence of b_a and b_c, hence the outer limbs strained approximately 75 %, $\sin\left((0)\pm 120^{\circ}\right)^2$ = 0.75, of the maximum magnetostriction. In addition, magnetic flux b_a and b_c also influence the yokes.

At ωt=30°, the magnetic flux density on phase C decreases to the maximum in the negative direction. While the magnetic flux densities on phase A and B have the same amplitude, half that of phase C but with opposite polarity to that in phase C. The laminations in limb C strain to the maximum magnetostriction whilst the laminations in limb A and the middle limb strain to 25 % of the maximum magnetostriction. At this time, the yokes which are connected to limb A and limb C were magnetised to an amplitude of 50 % magnetic flux from phase A and 100% magnetic flux from phase C. The yoke which is connected to limb C is strained more than the side which is connected to limb A.

At ωt=60°, b_a is zero whilst b_b and b_c have the same amplitude but different directions. The length of limb C is reduced to the same length as at ωt=0°. The middle limb has a larger strain than at ωt=30° and limb A is un-deformed.

The middle limb shows the largest strain when ωt=90°. This time b_b rises to the maximum. The laminations continually deform from shortest to longest length in half a cycle of magnetic flux. It can be seen that the largest strain in each limb occurs twice in one period of magnetic flux density.

In reality, there are repelling stresses between the laminations in the in-plane direction and an attractive interlaminar stress between the lamination in the normal direction on

the overlap area. These stresses result in vibration in both the in-plane and out of plane direction of the core. In the case of single phase cores, there are no phase differences of magnetic flux flow in the core therefore all laminations deform to their longest and shortest length at the same time. This model is used for explaining the vibration experimental results.

5.2 Influence of Magnetostriction on Transformer Core Noise

To investigate the effect of magnetostriction, the experimental results from three phase transformer cores built with different materials but the same dimensions, step lap configuration, and clamping torque were compared.

The results of A-weighted sound power level from CGO material (core No.18), HGO material (core No.15) and LDR material (core No.13) with clamping torque 4 Nm at magnetic flux density 1.0 T to 1.8 T are shown in Fig.5-5.

The results show the highest A-weighted sound power level emitted from the CGO core and the lowest emitted from the HGO core at all levels of magnetisation. A-weighted sound power level from CGO and HGO cores displays a similar trend. The difference in A-weighted sound power level between CGO core and HGO core is approximately 5 dB.

The A-weighted sound power level of the LDR core slightly increases (36.5 dBA to 39.5 dBA) when the flux density is increased from 1.0 T to 1.5 T and significantly increases (39.5 dBA to 53 dBA) when it is increased from 1.5 T to 1.8 T.

To investigate the contribution of magnetostriction to transformer core noise, the results in Fig. 5-5 were considered with the magnetostriction characteristic of the materials shown in Chapter 4. Because all of the cores were built with the same size, step lap configuration, and clamping torque, magnetic forces on each core were assumed to be similar. Hence, the parameter which affects any changes in transformer

core noise can be assumed to be magnetostriction. As expected, the CGO core emitted the highest noise and the CGO material had the highest magnetostriction. The HGO core emitted the lowest noise and the HGO material had the lowest magnetostriction.

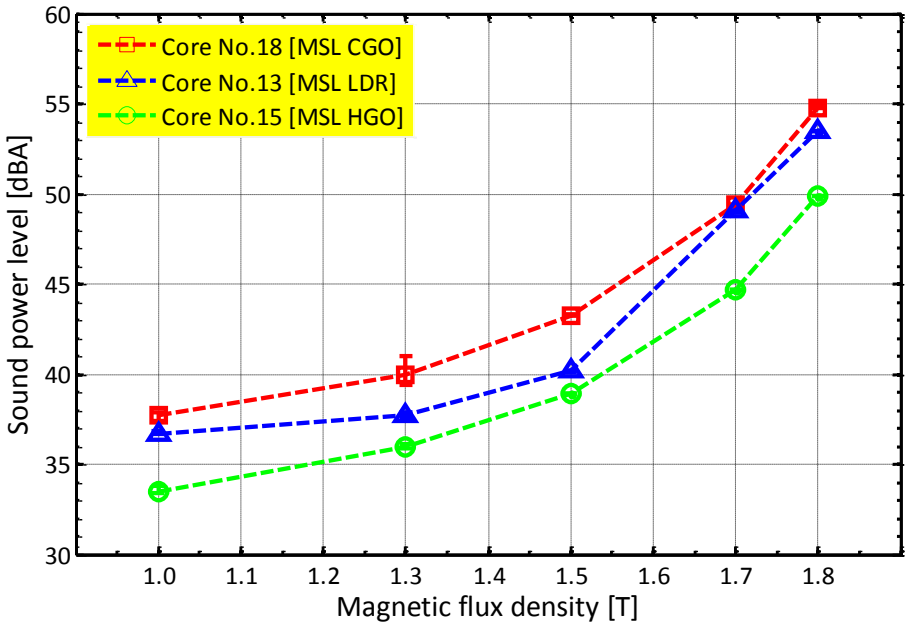

Fig. 5-5: Comparison of A-weighted sound power level of 3 phase multi step lap configuration transformer core assembled with different materials: CGO, HGO and LDR, with clamping torque 4 Nm at 1.0 T to 1.8 T, 50 Hz.

Hence the magnetostriction is a significant factor affecting transformer core noise. However, the difference of noise emitted from these three cores did not show the same trend with magnetostriction characteristic. From Figs. 4-1 to 4-3 there is a small difference between magnetostriction characteristic of HGO and LDR materials and there is a significant difference between these two materials with CGO for all levels of magnetic flux density. At 1.0 T, the LDR core emitted noise similar to that of the CGO core whilst at 1.5 T it emitted noise close to the HGO core and close to the CGO core again at 1.7 T. Therefore, there are other parameters affecting the transformer core noise. The CGO core was chosen for further investigation of these other factors.

5.3 Influence of Magnetic Flux Density on Transformer Core Noise and Vibration

Magnetic flux density was chosen as the first parameter to investigate because it directly affects both the magnetostriction and magnetic forces. From Fig. 5.5, L_{wA} of the CGO core increases from 37.3 dBA to 42.9 dBA at magnetic flux densities ranging from 1.0 T to 1.5 T and considerably increases to 49.1 dBA and 54.6 dBA when the magnetic flux density is increased to 1.7 T and 1.8 T respectively. The significant increase of L_{wA} is due to the effect of the change in the closure domains and the supplementary domain structure, which affects the magnetic forces and vibration, when the core is magnetised above a critical induction level. Due to the fact that the LDR has smaller domains and more supplementary domain structure, the magnetostriction is high for LDR material at higher magnetic flux density.

The vibration experimental results from the core are shown in Figs.5-6 to 5-8. The results yield both vibration velocity and phase of vibration where the average magnetic flux density signal from the middle limb was used as a phase reference. The results show that the vibrations on the surfaces are not uniform. The variation of the vibration on each surface is increased when the magnetic flux density is increased due to the effect of saturation induction near the joints.

When operating the core at low induction, the noise and vibration are less than operating at high flux density. This seems to be a simple way to reduce the core noise and vibration; however this leads to an increase in cost and a larger core size. Noise and vibration on each surface are investigated in the next section.

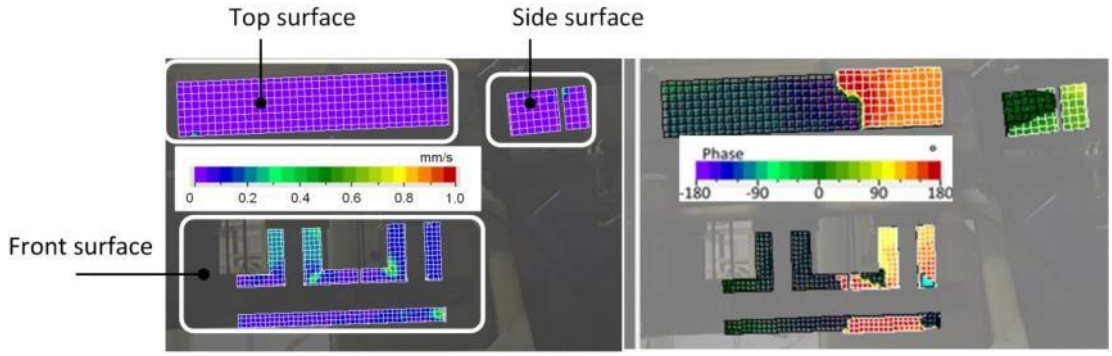

Fig.5-6: Vibration distribution on core No.18 surfaces, 3 phase MSL CGO, with clamping torque 4 Nm at magnetic flux density 1.0 T, 50 Hz.

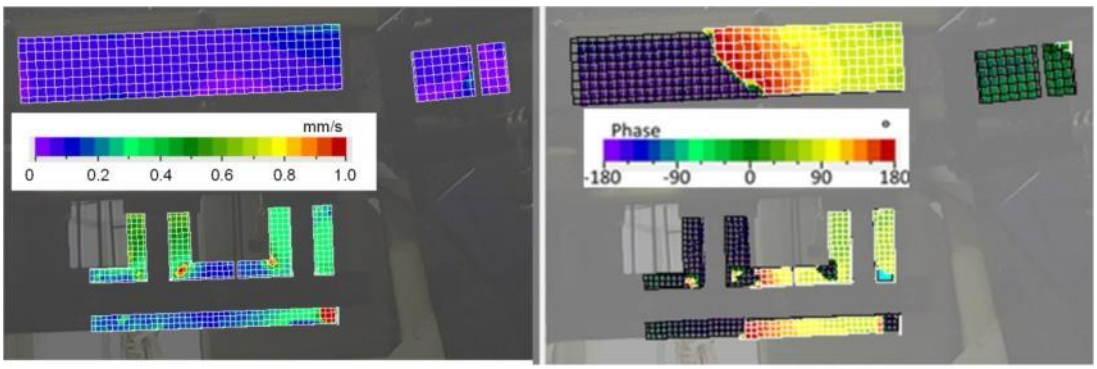

Fig.5-7: Vibration distribution on core No.18 surfaces, 3 phase MSL CGO, with clamping torque 4 Nm at magnetic flux density 1.5 T, 50 Hz.

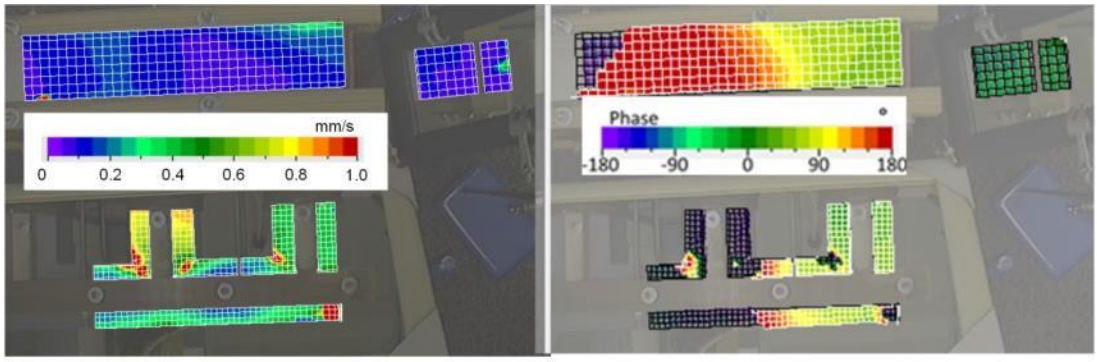

Fig.5-8: Vibration distribution on core No.18 surfaces, 3 phase MSL CGO, with clamping torque 4 Nm at magnetic flux density 1.7 T, 50 Hz.

5.4 Investigation of Transformer Core Noise and Vibration on Transformer Core Surfaces

To investigate the characteristic of sound emitted by each surface of the transformer core, the experimental A-weighted sound pressure level results from the array of nine microphones were considered separately. The positions of the microphones were described in Chapter 3. In positions 1 and 5, microphones were located perpendicular to the outer limbs of the core on the side surface. This surface is located parallel to the in-plane direction of the laminations. Whereas, at positions 3 and 7 microphones were located perpendicular to the front surface of the middle limb and the position 9 microphone was fixed perpendicularly above the top yoke. Positions 2, 4, 6 and 8 were fixed equally spaced between positions 1, 3, 5 and 7 on the prescribed contour.

Fig. 5-9 shows a comparison of the A-weighted sound pressure level emitted from each surface of core no.18 with a clamping torque 4 Nm at flux densities ranging from 1.0 T to 1.8 T. The highest A-weighted sound pressure level was found on the front surface when the core was magnetised between 1.3 T and 1.8 T. Whilst, at 1.0 T the highest noise was found at the side surface (position 1) because it is assumed that there is no effect of saturation induction in the laminations at low magnetic flux density. Therefore lamination deformation due to magnetostriction is the only cause of vibration and noise. The influence of magnetic forces is higher when the magnetic flux density is increased. The experimental results depend significantly on the microphone positions. This demonstrates the need for averaging the A-weighted sound pressure level from all microphones on the prescribed contour for quantifying the sound power level of the core. Due to each transformer core surface has different characteristics each surface was separately investigated as shown in the next subsection.

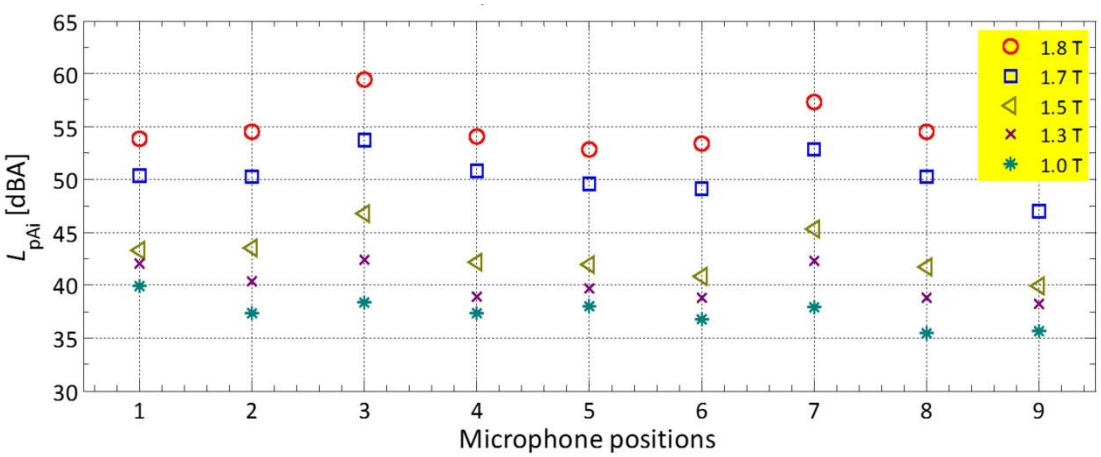

Fig. 5-9: Comparison of A-weighted sound pressure level between 9 microphones positions of core No.18, 3 phase MSL CGO, with clamping torque 4 Nm at flux density 1.0 T to 1.8 T, 50 Hz.

5.4.1 Noise and Vibration on Front Surface

Figs. 5-10 to 5-12 show the frequency distribution of sound pressure on the front surface position of core No.18, 3 phase MSL CGO, with a clamping torque of 4 Nm at magnetic flux densities from 1.0 T to 1.7 T. Fig.5-13 shows frequency distribution of the background noise in the hemi anechoic chamber which was measured from the 9 microphones located as normal but with no core present. From the results in Fig.5-13, the highest component is at approximately 50 Hz, 1 mPa which is equivalent to 31 dB or 1 dBA. The background noise is assumed to be mostly generated by electrical system, vibration of the building and vibration of the machines installed in the building. The background noise was measured before and after measuring transformer core noise and used for calculating the average A-weighted sound pressure level as shown in Eq.4-5. The average A-weighted background noise was approximately 22 dBA.

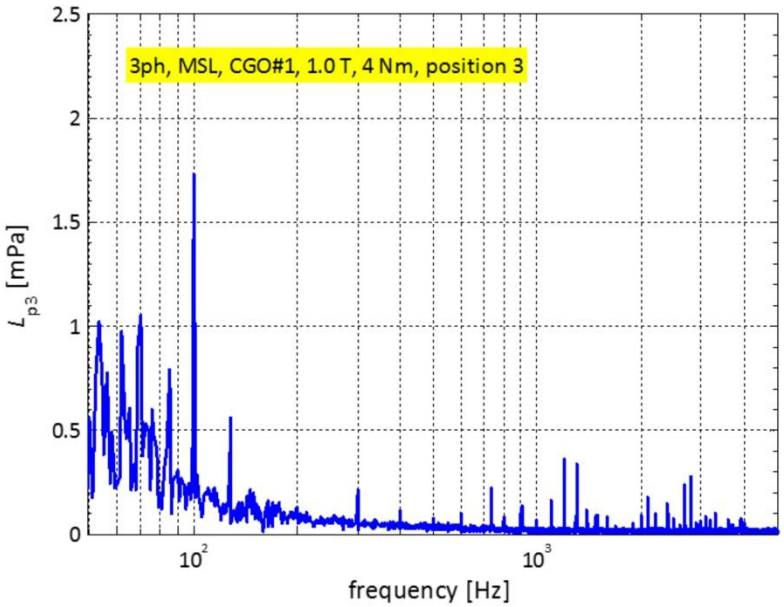

Fig. 5-10: Frequency distribution of sound pressure emitted from front surface of core No.18, 3 phase MSL CGO, with clamping torque 4 Nm at flux density 1.0 T, 50 Hz.

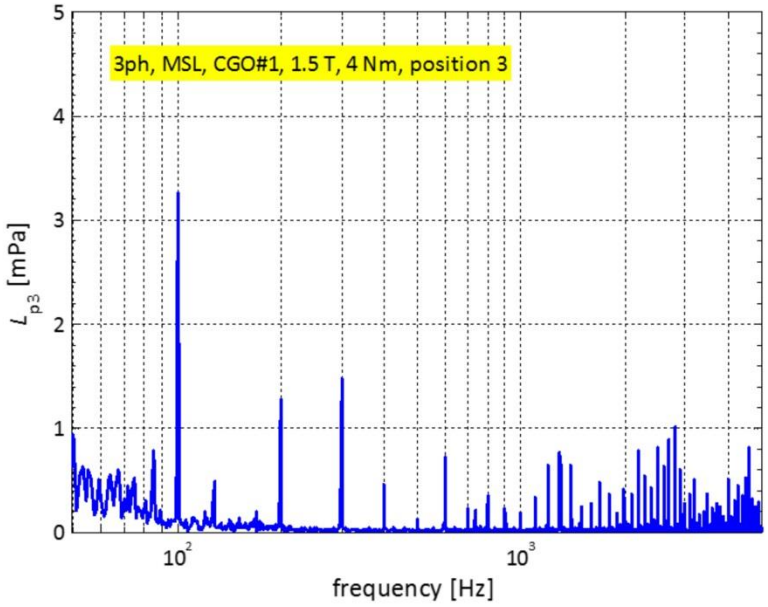

Fig. 5-11: Frequency distribution of sound pressure emitted from front surface of core No.18, 3 phase MSL CGO, with clamping torque 4 Nm at flux density 1.5 T, 50 Hz.

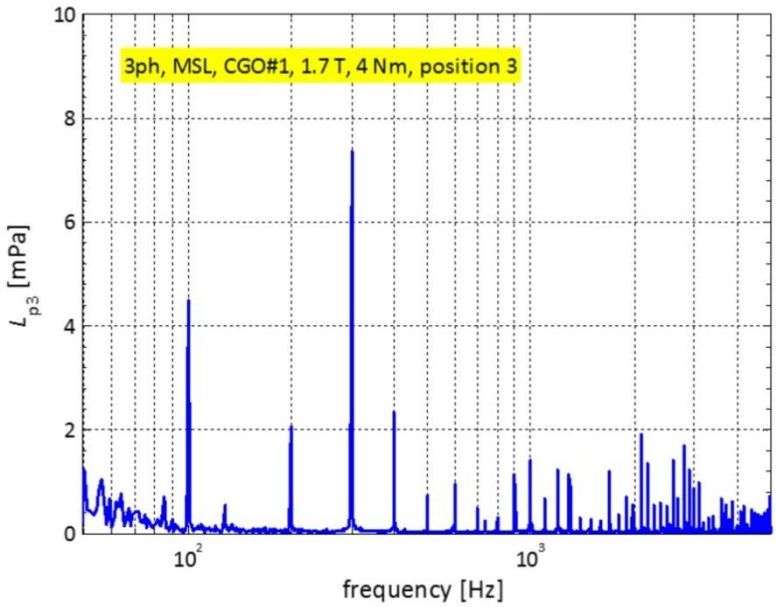

Fig. 5-12: Frequency distribution of sound pressure emitted from front surface of core No.18, 3 phase MSL CGO, with clamping torque 4 Nm at flux density 1.7 T, 50 Hz.

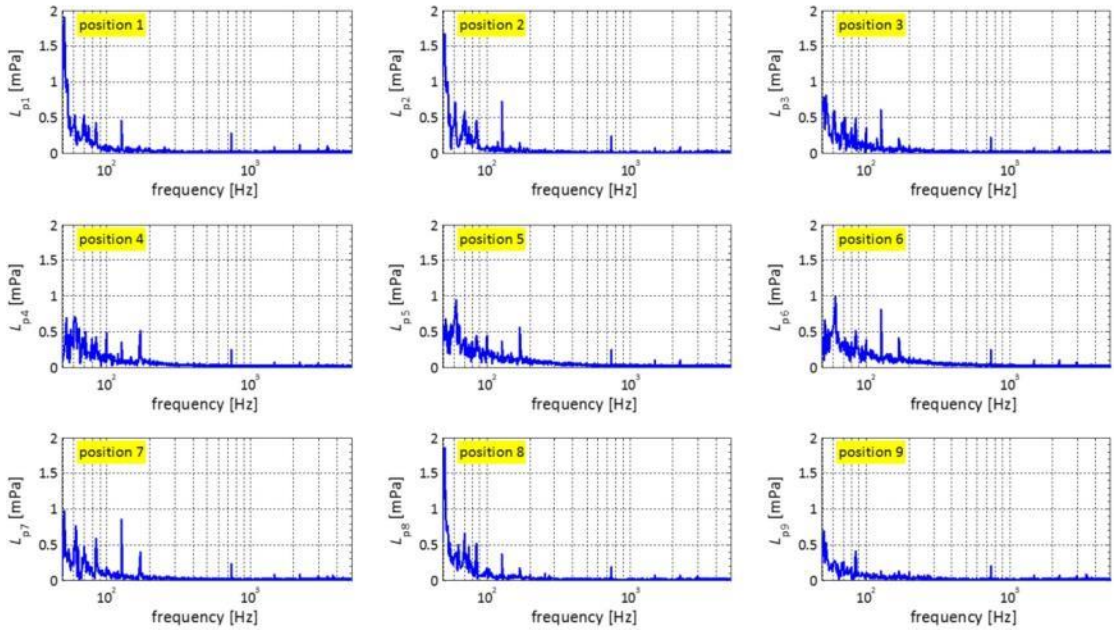

Fig. 5-13: Frequency distributions of background noise in the hemi anechoic chamber from 9 microphones.

The results from Figs. 5-10 to 5-12 include significant 100 Hz components as expected because it is the fundamental frequency component of magnetostriction and

magnetic forces. Although the highest component of sound pressure at 1.7 T is at 300 Hz, the component at 100 Hz is clearly seen. The component at 300 Hz is increased when the magnetic flux density is increased due to the distortion of the magnetic flux density signal. The vibration distributions on the front surface of the core at flux densities from 1.0 T to 1.7 T are shown in Fig.5-14 to 5-16. The content is identical to that shown in Figs. 5-6 to 5-8 but in order to clearly present the difference of vibration they are shown with new scales.

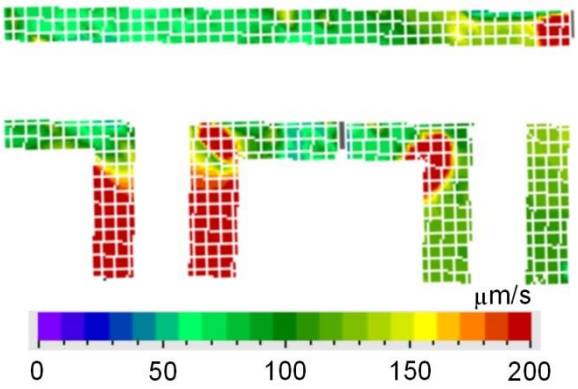

Fig.5-14: Vibration distribution on front surface of core No.18, 3 phase MSL CGO, with clamping torque 4 Nm and magnetic flux density 1.0 T, 50 Hz.

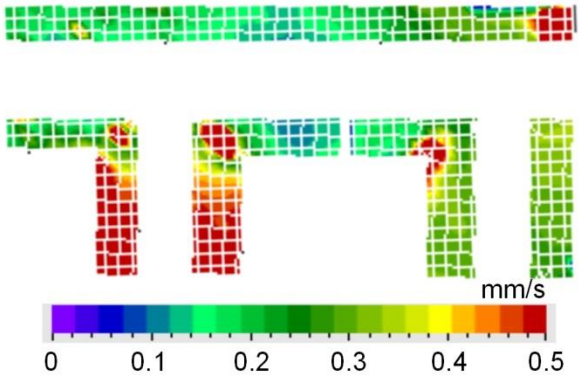

Fig.5-15: Vibration distribution on front surface of core No.18, 3 phase MSL CGO, with clamping torque 4 Nm and magnetic flux density 1.5 T, 50 Hz.

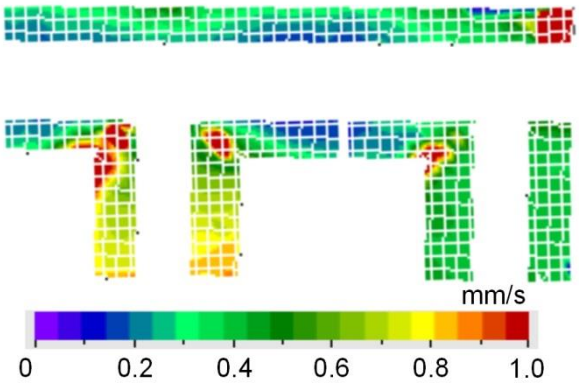

Fig.5-16: Vibration distribution on front surface of core No.18, 3 phase MSL CGO, with clamping torque 4 Nm and magnetic flux density 1.7 T, 50 Hz.

From the results in Figs. 5-14 to 5-16, it can be seen that vibrations on the front surface are not uniform. The limb vibration is slightly higher than that of the yoke. Whilst between limbs, the middle limb is higher than the outer limb. If we consider the magnetostriction of the lamination under rotational magnetic flux which is significantly higher than with alternating flux [70], higher vibration of the middle limb could be due to the additional rotational magnetostriction at the T-joint. The laminations on the middle limb interlace with the notches of the top and bottom yoke laminations. If the gap at the joint is assumed to be zero, therefore there is no space for magnetostrictive strain to occur in the in-plane direction. If there is the gap at the joint, a magnetic force is set up and closure domains are also set up then laminations are deformed into a curve in the normal direction.

Loci of the magnetic flux density at the T-joint in positions 32, 33 and 34, at an average peak magnetic flux density of 1.7 T are shown in Fig. 5-17 to 5-19. The loci are distorted because there are harmonic components due to localised magnetic properties of the material. The localised flux at corresponding positions in different parts of the laminations differ a little because they are highly dependent on local grain and domain structures [71]. Discussion of the effect of harmonic components on magnetostriction is given in section 5.12.

From the results in Fig. 5-14 to 5-16, it can be observed that the vibration at the T-joint was unsymmetrical although the core was symmetrically designed. The reason for this result is because the core joints are not perfectly symmetrical when assembled with variable gaps between the joints.

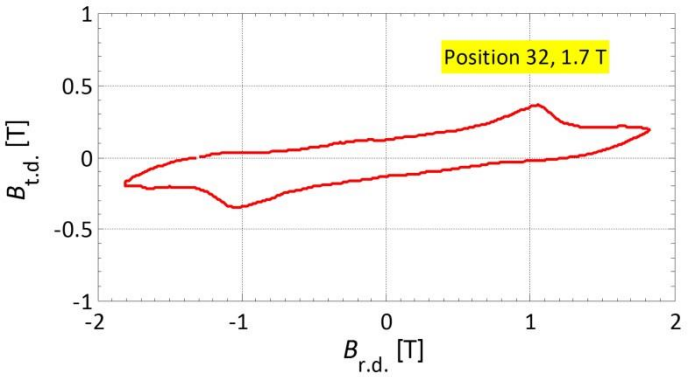

Fig. 5-17: Loci flux densities at the position 32 at the average maximum flux density 1.7 T, 50 Hz.

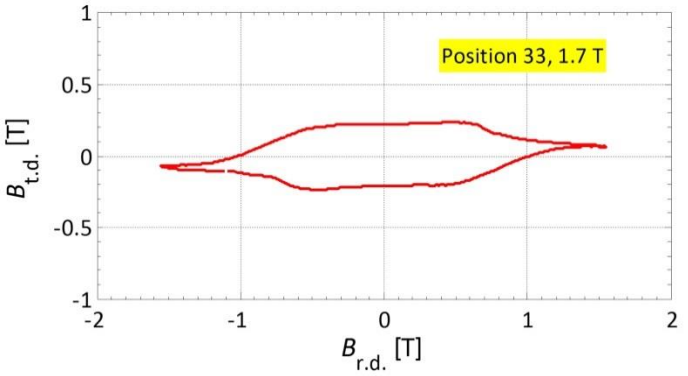

Fig. 5-18: Loci flux densities at the position 33 at the average maximum flux density 1.7 T, 50 Hz.

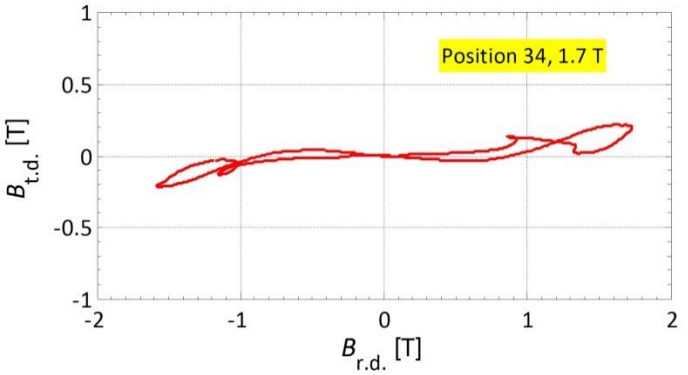

Fig. 5-19: Loci flux densities at the position 34 at the average maximum flux density 1.7 T, 50 Hz.

In the case of gaps close to zero, there is almost no effect of saturation induction in the laminations. Therefore there is also little effect from attractive interlaminar stress in the normal direction. The cause of core vibration is then assumed to be only in-plane due to magnetostriction and in-plane attractive stress at any operating flux density. In the case of the joint with gaps the magnetic flux density at the end of the laminations, approximately 1 mm either side, are saturated when the laminations are magnetised over B_c [72]. Magnetic flux flows across the air gap in the normal direction to neighbouring laminations on the different layers and some flux flows through the air gap to the lamination in the same plane. Therefore in this case the causes of vibration are magnetostriction, attractive stress in both the in-plane direction and the out of plane direction. Hence, when operating the core at flux densities higher than B_c, vibration of the joint with gaps is higher than the joint without gaps. The gaps cause more vibration because of increased demagnetisation field causing more closure domains [58]. Investigation of contribution of the fundamental component of magnetostriction and magnetic force is described in section 5.6.

Next, frequency distribution of vibration on the front core surface was investigated. Fig. 5-20 shows the positions of investigation on the front surface. The area on the front surface is separated by the characteristic of the magnetisation pattern into three regions: limb (position B, alternating magnetisation), T-joint (position D, rotational magnetisation) and corner (position E, alternating magnetisation out of the rolling direction). In addition, the effect of the non-uniform clamping area on the limb surface is investigated by comparing the vibration velocity at three points with different distances away from the clamp as shown in positions A, B and C in Fig. 5-20. The results in Figs.5-21 to 5-29 show the frequency distribution on the limb surface at positions A, B and C with a clamping torque of 4 Nm at magnetic flux densities from 1.0 T to 1.7 T.

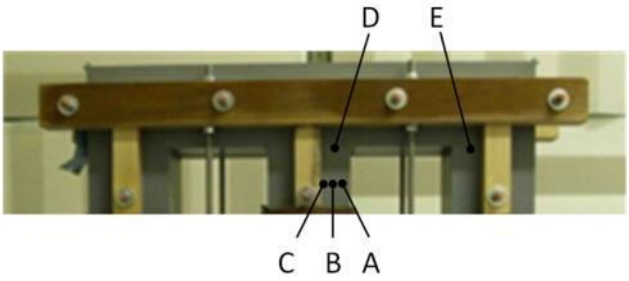

Fig. 5-20: Investigating positions of velocity frequency distribution on front surface of core No.18, 3 phase MSL CGO, with clamping torque 4 Nm.

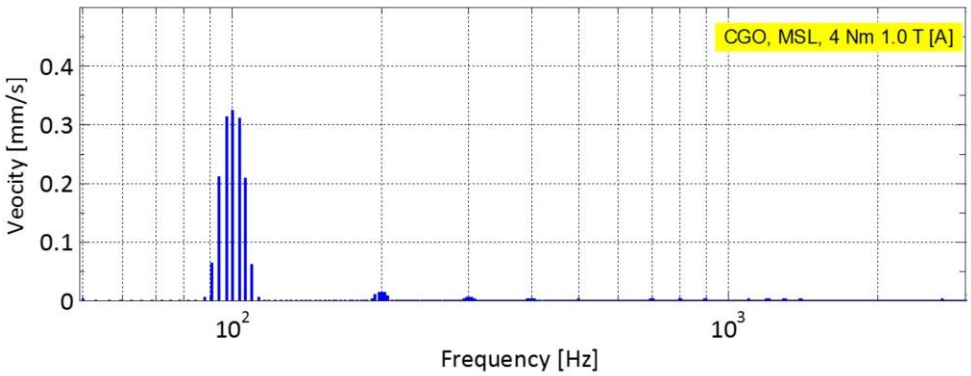

Fig. 5-21: Frequency distribution of vibration velocity on core No.18, 3 phase MSL CGO, at positions A with clamping torque 4 Nm at 1.0 T, 50 Hz.

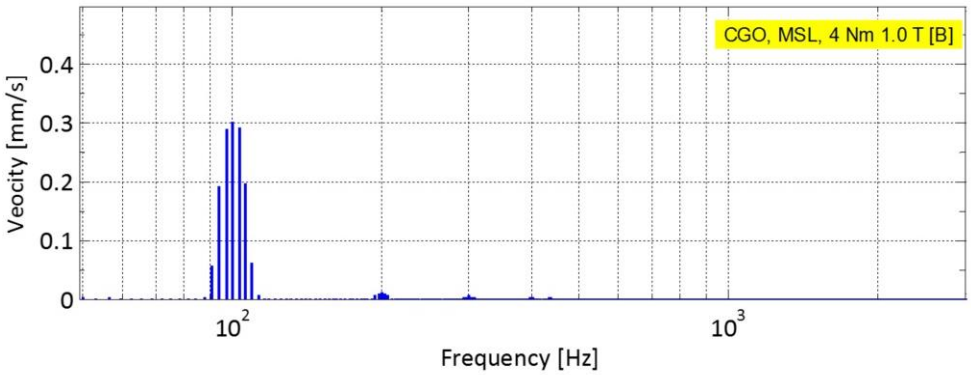

Fig. 5-22: Frequency distribution of vibration velocity on core No.18, 3 phase MSL CGO, at positions B with clamping torque 4 Nm at 1.0 T, 50 Hz.

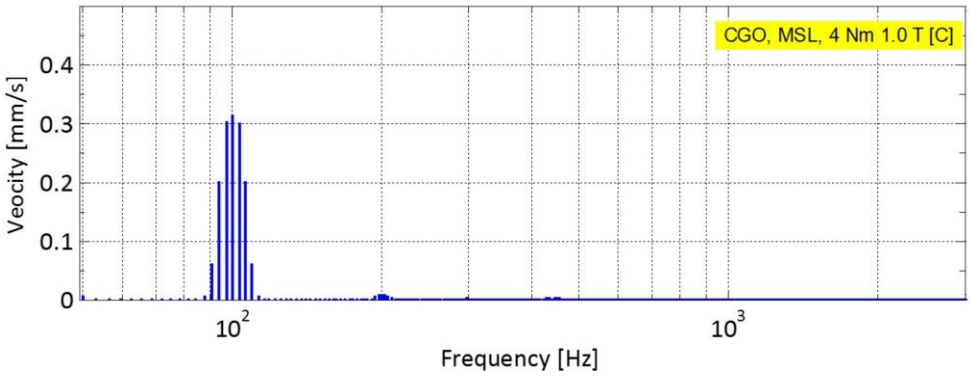

Fig. 5-23: Frequency distribution of vibration velocity on core No.18, 3 phase MSL CGO, at positions C with clamping torque 4 Nm at 1.0 T, 50 Hz.

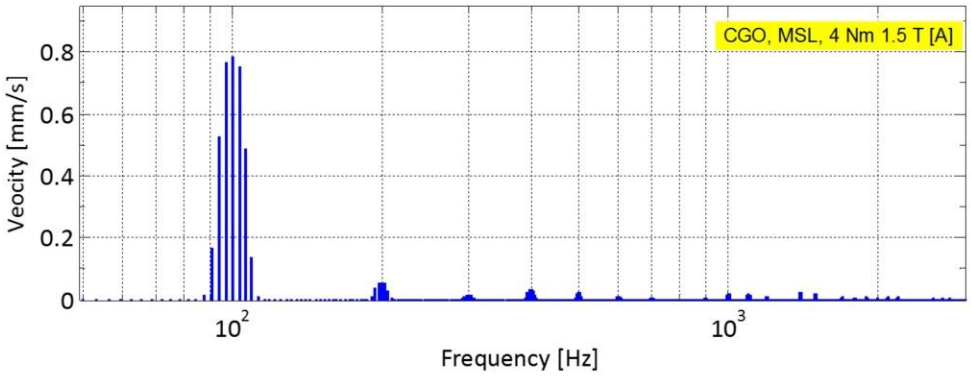

Fig. 5-24: Frequency distribution of vibration velocity on core No.18, 3 phase MSL CGO, at positions A with clamping torque 4 Nm at 1.5 T, 50 Hz.

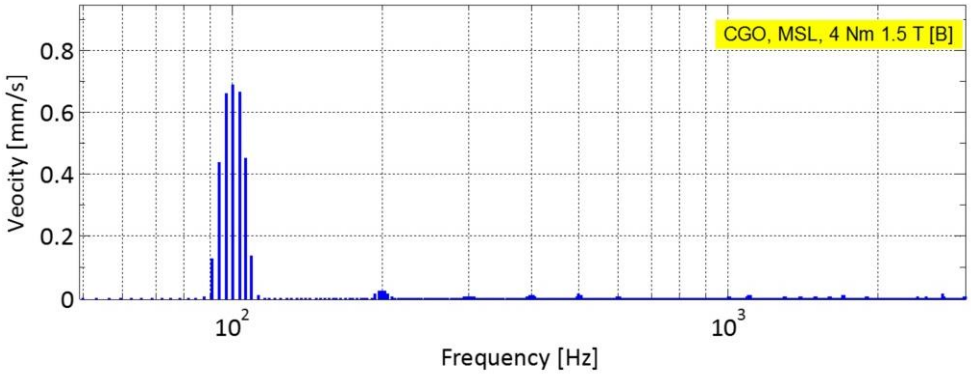

Fig. 5-25: Frequency distribution of vibration velocity on core No.18, 3 phase MSL CGO, at positions B with clamping torque 4 Nm at 1.5 T, 50 Hz.

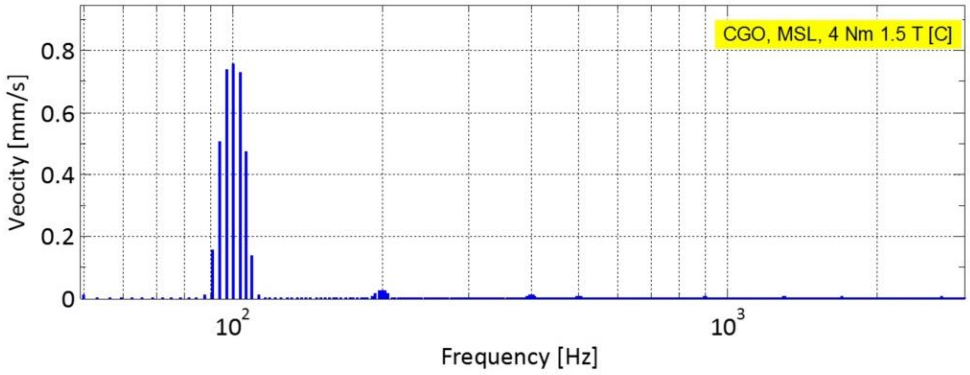

Fig. 5-26: Frequency distribution of vibration velocity on core No.18, 3 phase MSL CGO, at positions C with clamping torque 4 Nm at 1.5 T, 50 Hz.

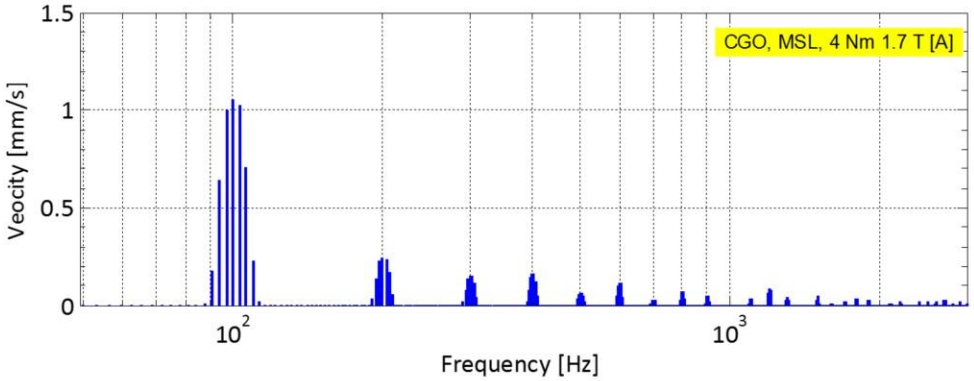

Fig. 5-27: Frequency distribution of vibration velocity on core No.18, 3 phase MSL CGO, at positions A with clamping torque 4 Nm at 1.7 T, 50 Hz.

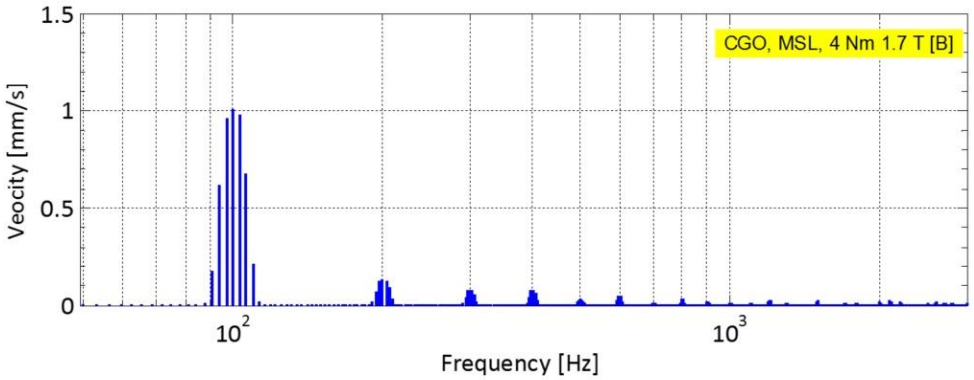

Fig. 5-28: Frequency distribution of vibration velocity on core No.18, 3 phase MSL CGO, at positions B with clamping torque 4 Nm at 1.7 T, 50 Hz.

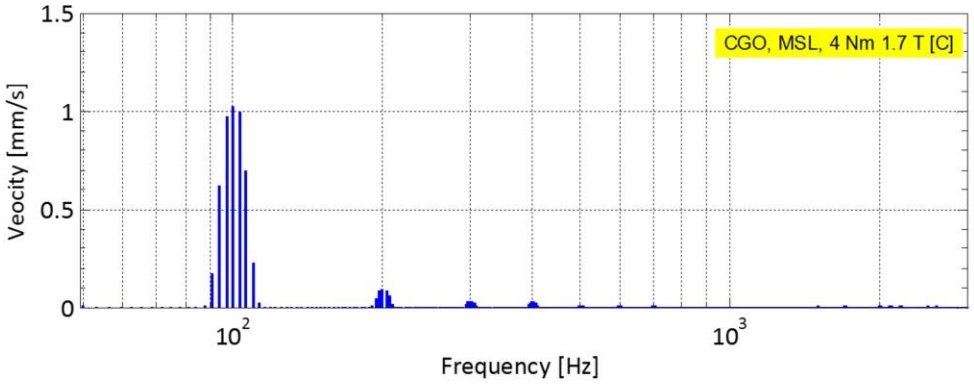

Fig. 5-29: Frequency distribution of vibration velocity on core No.18, 3 phase MSL CGO, at positions C with clamping torque 4 Nm at 1.7 T, 50 Hz.

From the results in Figs.5-21 to 5-29, it can be seen that the highest component was found at 100 Hz as expected for all levels of magnetic flux density. Comparing the vibration between position A, B and C, there is no significant difference in the amplitude of the fundamental component at the same level of magnetic flux density. At 1.0 T, there is also no significant difference in harmonic components between positions A, B and C. However, when the magnetic flux density is increased to 1.5 T, it can be seen that the vibration velocity at position A has some harmonics appearing at 200 Hz to 500 Hz. The harmonics of vibration velocity increase when the magnetic flux density is increased, while there is no significant difference of harmonic components of vibration velocity at positions B and C. The harmonics at position A caused by the effect of harmonics in *B* due to localised magnetic properties of the laminations and the effect of stress at the edge of the lamination due to the slitting process [73]. The higher harmonics of vibration are another cause of transformer core noise.

Figs. 5-30 to 5-32 show the frequency distribution of vibration velocity at the T-joint (position D) and corner (position E) surfaces at magnetic flux densities from 1.0 T to 1.7 T. Comparing the vibration velocity between three positions, B, D and E at 1.0 T, there is no significant difference between those three positions. Whilst, at 1.5 T, it can be clearly seen that at position D (T-joint) the amplitude of velocity component at

100 Hz is the highest. It is almost twice the value of the vibration on the limb (position B). Moreover, there is also a high amplitude harmonic at 200 Hz. At position E (corner), although the amplitude at 100 Hz is lower than on the limb, there are higher amplitudes of other harmonic components.

At 1.7 T, there is no significant difference of vibration velocity component at 100 Hz between positions B, D and E. Vibration at 100 Hz is approximately 1 mm/s. The harmonic component at 200 Hz on the T-joint and corner have higher amplitude than the fundamental component.

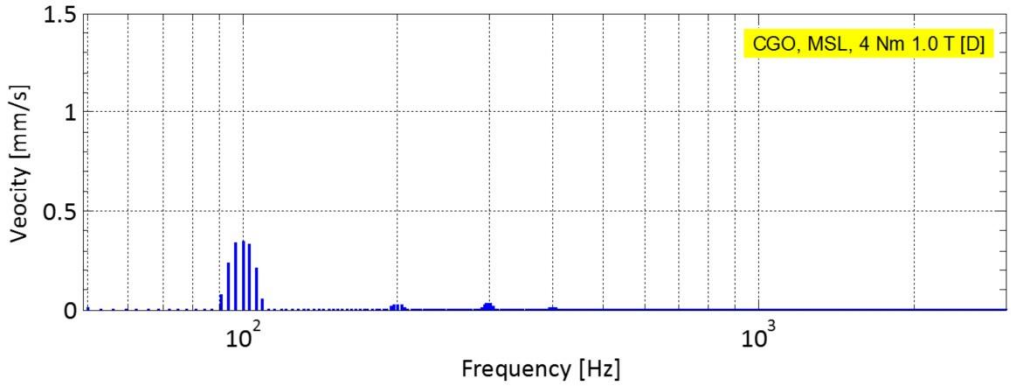

Fig. 5-30: Frequency distribution of vibration velocity on core No.18, 3 phase MSL CGO, at position D (T-joint) with clamping torque 4 Nm at 1.0 T, 50 Hz.

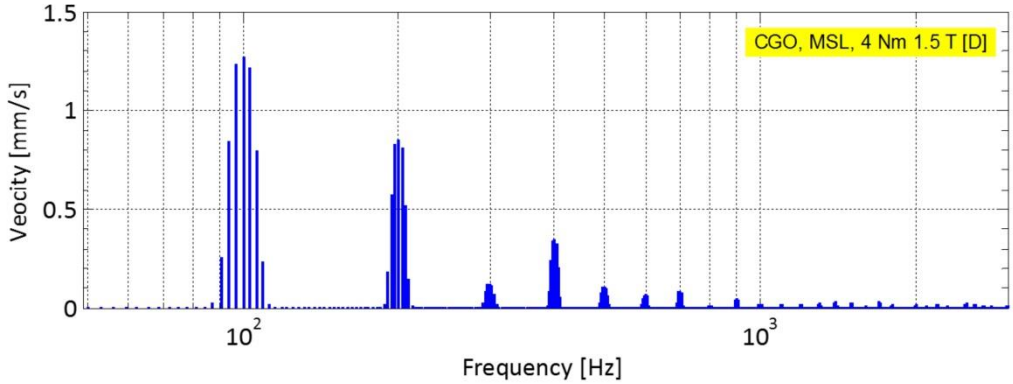

Fig. 5-31: Frequency distribution of vibration velocity on core No.18, 3 phase MSL CGO, at position D (T-joint) with clamping torque 4 Nm at 1.5 T, 50 Hz.

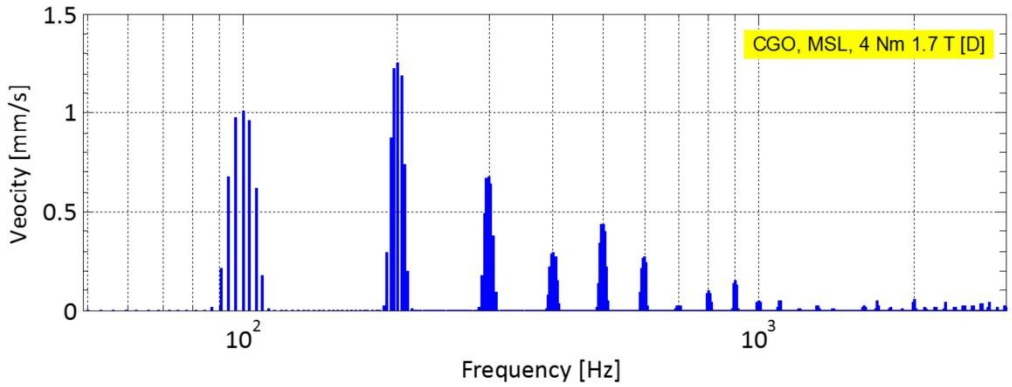

Fig. 5-32: Frequency distribution of vibration velocity on core No.18, 3 phase MSL CGO, at position D (T-joint) with clamping torque 4 Nm at 1.7 T, 50 Hz.

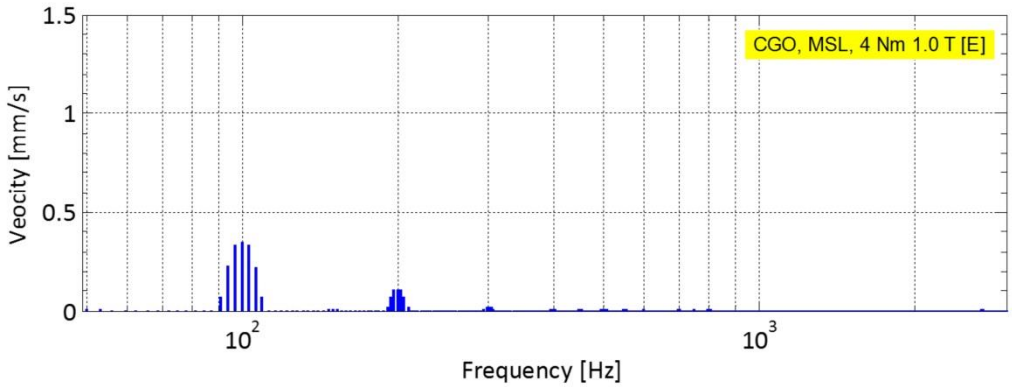

Fig. 5-33: Frequency distribution of vibration velocity on core No.18, 3 phase MSL CGO, at position E (corner)with clamping torque 4 Nm at 1.0 T, 50 Hz.

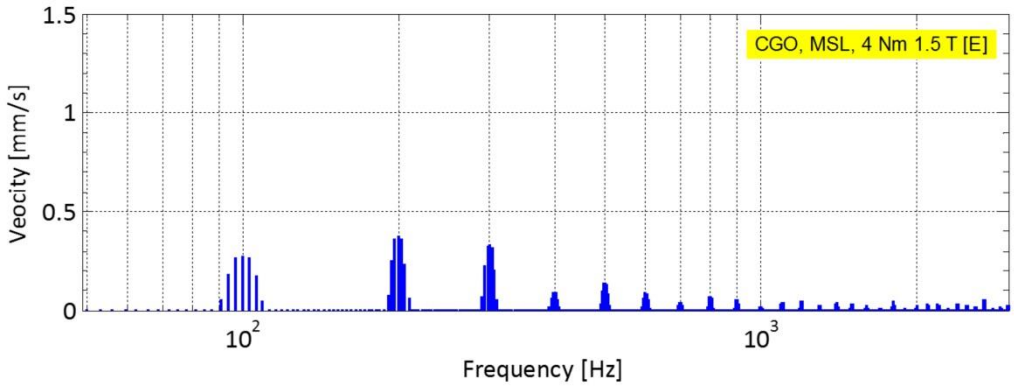

Fig. 5-34: Frequency distribution of vibration velocity on core No.18, 3 phase MSL CGO, at position E (corner)with clamping torque 4 Nm at 1.5 T, 50 Hz.

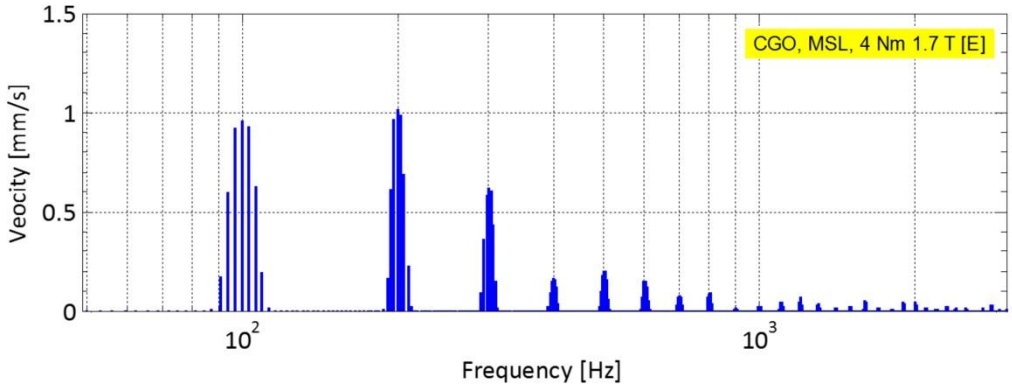

Fig. 5-35: Frequency distribution of vibration velocity on core No.18, 3 phase MSL CGO, at position E (corner)with clamping torque 4 Nm at 1.7 T, 50 Hz.

Finally, it can be concluded that there is no significant difference in the fundamental components of vibration velocity on the front surface. However, there are significant harmonic components at the T-joint, corner and the un-clamped areas.

5.4.2 Noise and Vibration on Top and Side Surfaces

Figs. 5-36 to 5-41 show the frequency distribution of vibration velocity on the top and side surfaces of core No.18, 3 phase MSL CGO, with clamping torque of 4 Nm at magnetic flux densities from 1.0 T to 1.7 T, 50 Hz.

At 1.0 T, the highest component was found at 100 Hz. However, at 1.5 T and 1.7, the fundamental component does not show the highest amplitude at 100 Hz as expected. The highest component is found at 200 Hz.

Comparing the amplitude of the sound pressure between the top and side surfaces, it can be seen from Figs. 5-36 to 5-41 that at 1.0 T the sound pressure emitted from the side surface is slightly higher than the top surface and the harmonic components become higher due to the magnetostriction harmonics increasing when the magnetic flux density is increased [74].

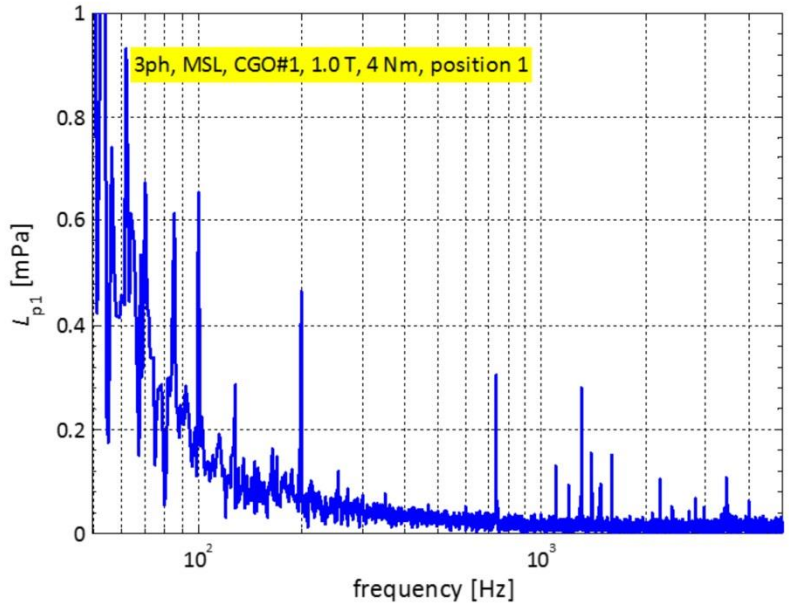

Fig. 5-36: Frequency distribution of sound pressure emitted from side surface of core No.18, 3 phase MSL CGO, with clamping torque 4 Nm at flux density 1.0 T, 50 Hz.

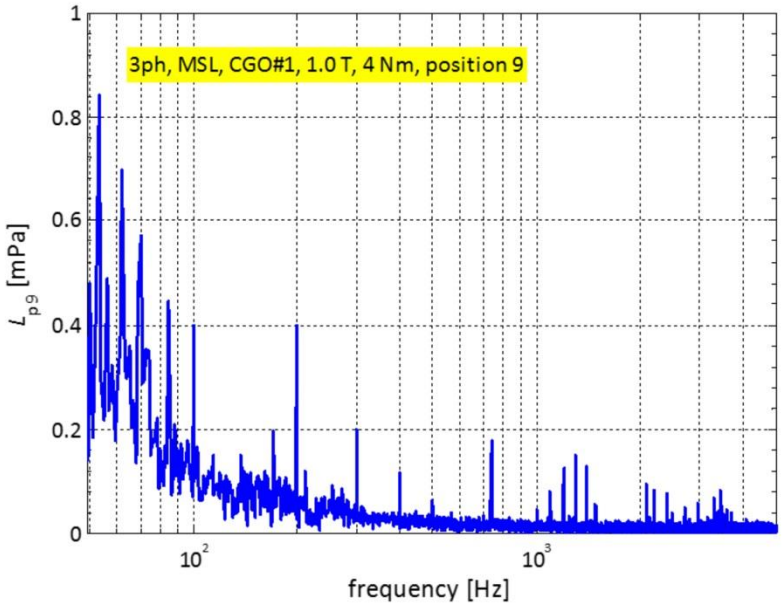

Fig. 5-37: Frequency distribution of sound pressure emitted from top surface of core No.18, 3 phase MSL CGO, with clamping torque 4 Nm at flux density 1.0 T, 50 Hz.

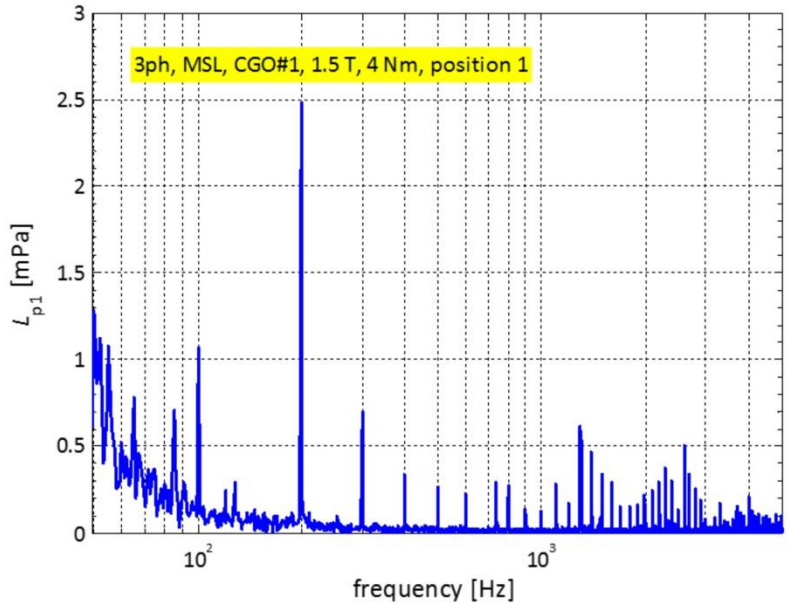

Fig. 5-38: Frequency distribution of sound pressure emitted from side surface of core No.18, 3 phase MSL CGO, with clamping torque 4 Nm at flux density 1.5 T, 50 Hz.

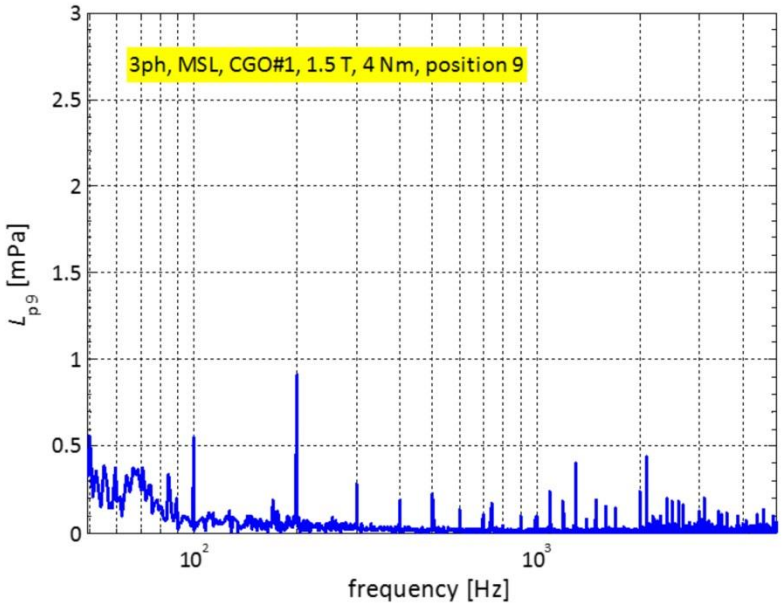

Fig. 5-39: Frequency distribution of sound pressure emitted from top surface of core No.18, 3 phase MSL CGO, with clamping torque 4 Nm at flux density 1.5 T, 50 Hz.

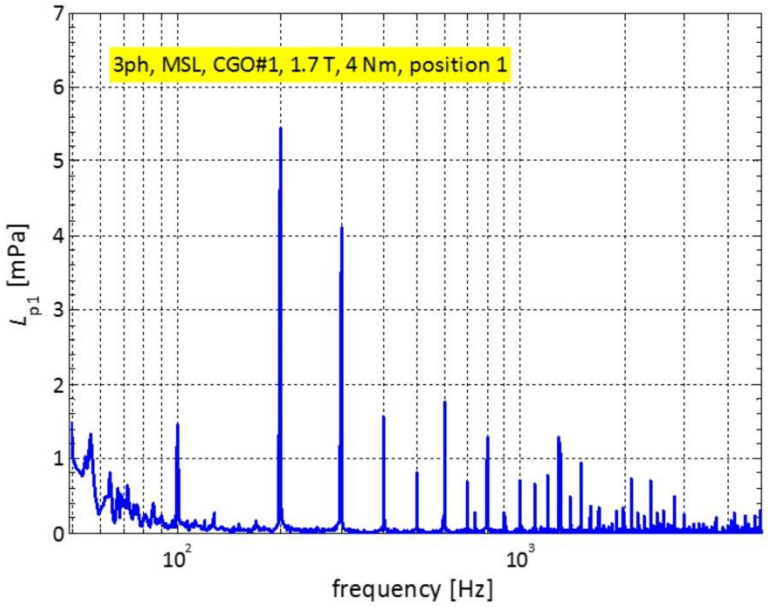

Fig. 5-40: Frequency distribution of sound pressure emitted from side surface of core No.18, 3 phase MSL CGO, with clamping torque 4 Nm at flux density 1.7 T, 50 Hz.

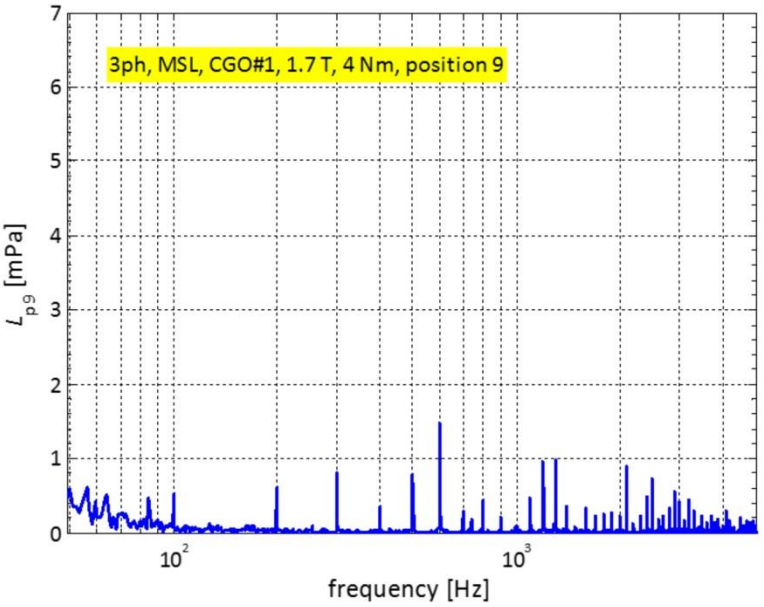

Fig. 5-41: Frequency distribution of sound pressure emitted from top surface of core No.18, 3 phase MSL CGO, with clamping torque 4 Nm at flux density 1.7 T, 50 Hz.

Table 5-1 shows numerical results of noise emitted from core No.18 extracted from the experimental data, with clamping torque 4 Nm. The results show a comparison of noise between each surface in different units: sound pressure (Pa), sound pressure

level (dB) and A-weighted sound pressure level (dBA). The relationship between the three units are sound pressure can be converted to sound pressure level by Eq.3-3. The sound pressure level in the time domain is transformed to the frequency domain and weighted with the A-weighting scale then converts to units of dBA.

Table 5-1: Numerical results of noise on core No.18 with clamping torque 4 Nm at 1.0 T to 1.7 T, 50 Hz between each surface

	Side surface			Front surface			Top surface		
	mPa	dB	dBA	mPa	dB	dBA	mPa	dB	dBA
1.0 T	34.4	64.7	40.4	28.7	63.1	38.9	25.5	62.1	35.8
1.3 T	32.9	64.3	43.2	27.1	62.7	43.2	23.7	61.5	38.9
1.5 T	31.7	64.0	43.4	26.9	62.6	46.9	23.2	61.3	39.2
1.7 T	36.2	65.2	48.9	32.7	64.3	52.2	28.4	63.0	46.1
1.8 T	196.8	79.9	53.6	193.8	79.7	59.3	174.4	78.8	49.7

It can be seen that noise in the unit of Pascals is proportional with that in decibels by Eq.3-3 but not proportional to the unit of dBA due to the varying harmonic components of the sound signal and the A-weighting scale. For example, at 1.5 T the side surface has a higher sound pressure than the front surface but lower in A-weighted sound pressure level. It means the side surface emitted the human ear responds to louder noise but it is not in a good frequency range.

At 1.0 T, the highest sound pressure (dB) and A-weighted sound pressure level (dBA) were found at the side surface. When the magnetic flux density is increased to 1.3 T and 1.5 T, sound pressures emitted from front and side surfaces slightly decrease but the A-weighted sound pressure level, dBA, is increased. The reason for this result is the noise signal at 1.5 T contains frequency components in the good response region of the human ear, although the amplitude is slightly lower. The A-weighted sound pressure level increases when magnetic flux density is increased. These results agree with the investigator's perception of the sound level during the experiments.

Sound pressure and sound pressure level do not take into account the frequency of the noise emitted from the cores. Whilst A-weighted sound pressure level reduces the

amplitude of frequencies which not affect the human ear, approximately lower than 1 kHz and higher than 6 kHz. Decreasing the 100 Hz component of sound pressure level resulted in decreasing of the sound pressure which occurs due to the fundamental component of magnetostriction and magnetic forces. Hence, when investigating the relationship between noise and vibration, the data should be analysed in the frequency domain.

The vibration distribution on the top and side surfaces of the core at magnetic flux density from 1.0 T to 1.7 T, 50 Hz are shown in Figs.5-42 to 5-47. They are the identical data in Figs. 5-6 to 5-8 but in order to clearly present the difference in vibration they are shown with new scales.

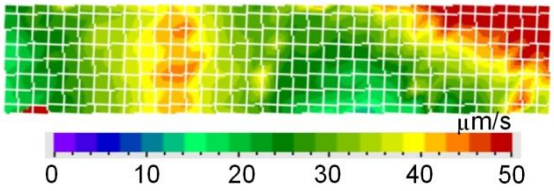

Fig.5-42: Vibration distribution on top surface of core No.18, 3 phase MSL CGO, with clamping torque 4 Nm and magnetic flux density 1.0 T, 50 Hz.

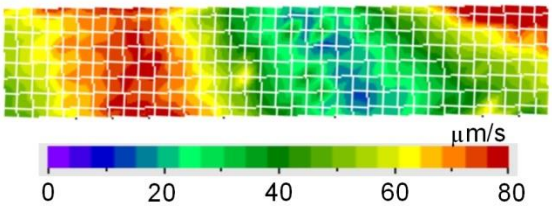

Fig.5-43: Vibration distribution on top surface of core No.18, 3 phase MSL CGO, with clamping torque 4 Nm and magnetic flux density 1.5 T, 50 Hz.

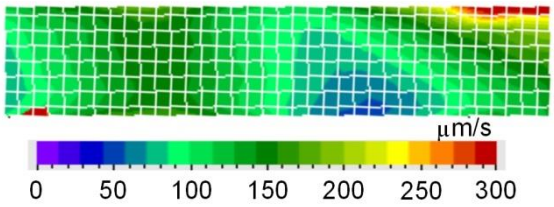

Fig.5-44: Vibration distribution on top surface of core No.18, 3 phase MSL CGO, with clamping torque 4 Nm and magnetic flux density 1.7 T, 50 Hz.

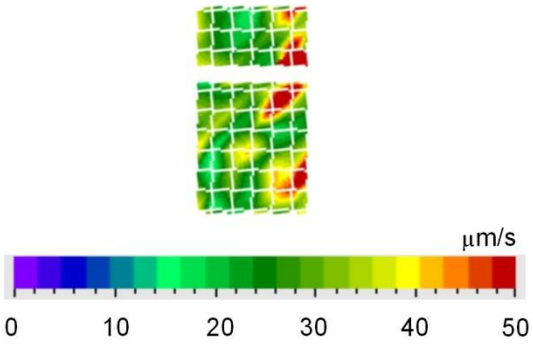

Fig.5-45: Vibration distribution on side surface of core No.18, 3 phase MSL CGO, with clamping torque 4 Nm and magnetic flux density 1.0 T, 50 Hz.

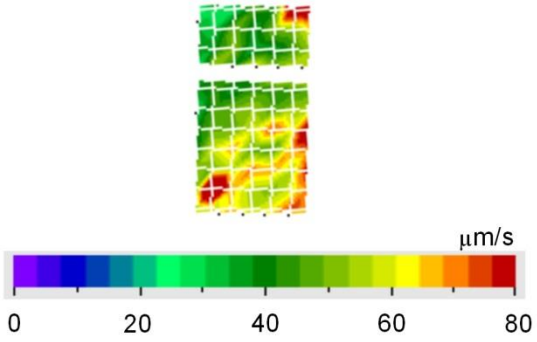

Fig.5-46: Vibration distribution on side surface of core No.18, 3 phase MSL CGO, with clamping torque 4 Nm and magnetic flux density 1.5 T, 50 Hz.

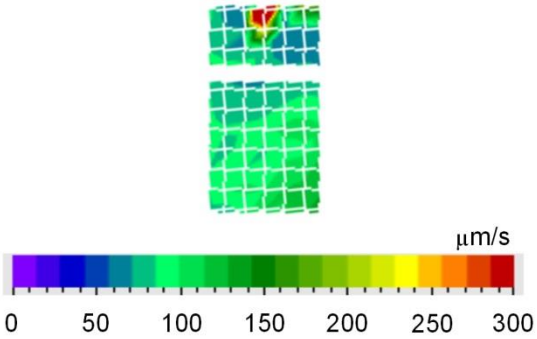

Fig.5-47: Vibration distribution on side surface of core No.18, 3 phase MSL CGO, with clamping torque 4 Nm and magnetic flux density 1.7 T, 50 Hz.

The results in Figs. 5-42 to 5-44 show vibration velocity on the top surface in the shaded area as shown in Fig. 4-15; it is not the full area of the top surface. Vibration velocity on the top surface above the limbs is higher than above the core window.

This result agrees with the model of the transformer core deformation due to magnetostriction as described in section 5.1. There is deformation of the laminations on the limbs which affects the yokes joined to the limbs. Moreover, there is a phase difference between the vibration above the middle limb and above the outer limb of approximately 120° due to the phase difference of magnetic flux density on each limb which affect the yoke as shown in Figs.5-6 to 5-8.

Comparing the amplitude of vibration between top and side surfaces, it can be seen that the top surface has a higher amplitude of vibration but lower sound pressure as shown in Table 5-1. This is the effect of phase difference on the top surface whilst there is no phase difference on the side surface. The discussion on phase difference is shown in the next section.

Fig. 5-48 shows the investigation points on the top and side surfaces. The investigation points on top surface are at the middle of lamination stack above the middle limb (point F), above the core window (point G) and above the outer limb (point H) while on the side surface are at the points I and J.

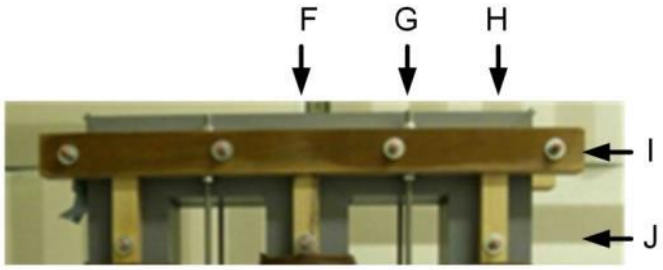

Fig. 5-48: Investigation positions of velocity on top and side surfaces of core No.18, 3 phase MSL CGO, with clamping torque 4 Nm.

Figs. 5-49 to 5-57 show the frequency distribution of vibration velocity on the top surface at magnetic flux densities from 1.0 T to 1.7 T. The results agree with the model of transformer core vibration due to magnetostriction. Straining of laminations in the limbs affects the vibration on the yoke especially on the top surface above the limbs. From the results in Figs. 5-49 to 5-57, it can be seen that vibration velocity

components above the outer limb are slightly higher than above the middle limb due to laminations at the outer corner which is likely to be due to the greater freedom of the laminations to out of plane vibration at this point.

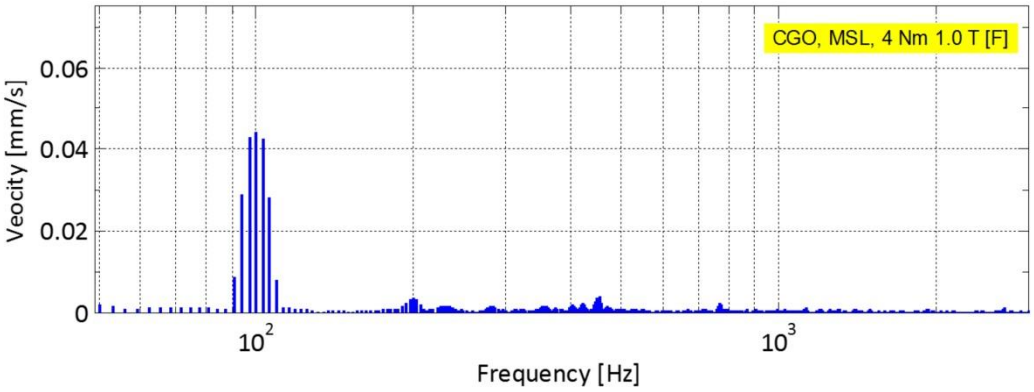

Fig. 5-49: Frequency distribution of vibration velocity on top surface of core No.18, 3 phase MSL CGO, at position F with clamping torque 4 Nm at 1.0 T, 50 Hz.

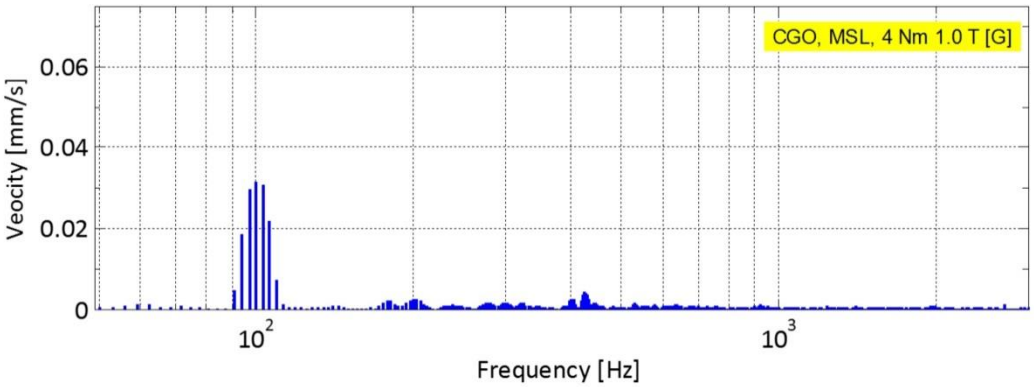

Fig. 5-50: Frequency distribution of vibration velocity on top surface of core No.18, 3 phase MSL CGO, at position G with clamping torque 4 Nm at 1.0 T , 50 Hz.

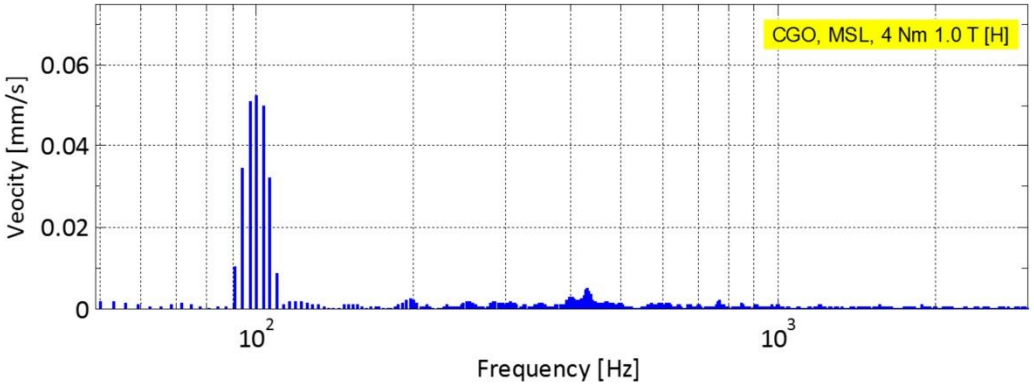

Fig. 5-51: Frequency distribution of vibration velocity on top surface of core No.18, 3 phase MSL CGO, at position H with clamping torque 4 Nm at 1.0 T , 50 Hz.

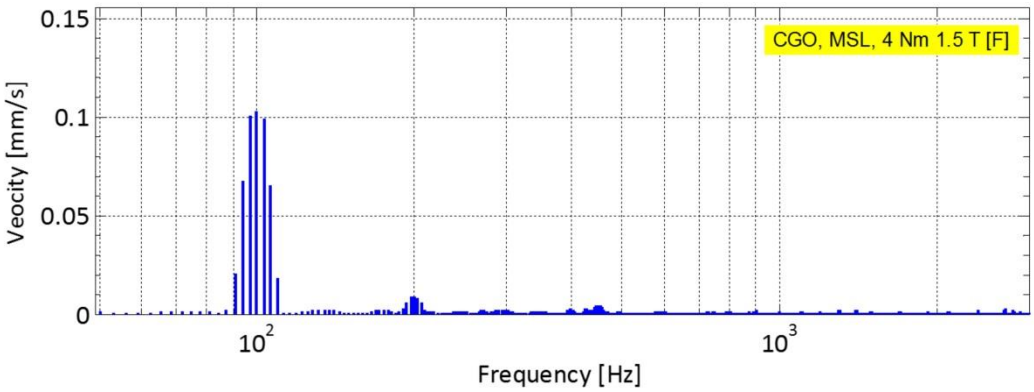

Fig. 5-52: Frequency distribution of vibration velocity on top surface of core No.18, 3 phase MSL CGO, at position F with clamping torque 4 Nm at 1.5 T, 50 Hz.

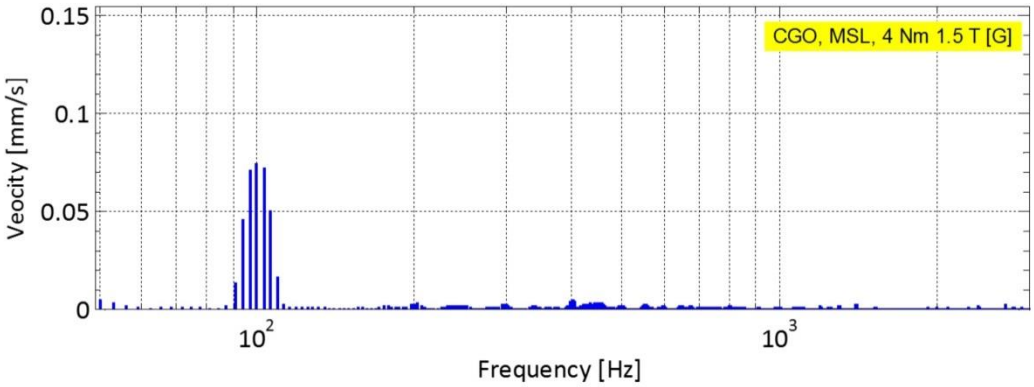

Fig. 5-53: Frequency distribution of vibration velocity on top surface of core No.18, 3 phase MSL CGO, at position G with clamping torque 4 Nm at 1.5 T, 50 Hz.

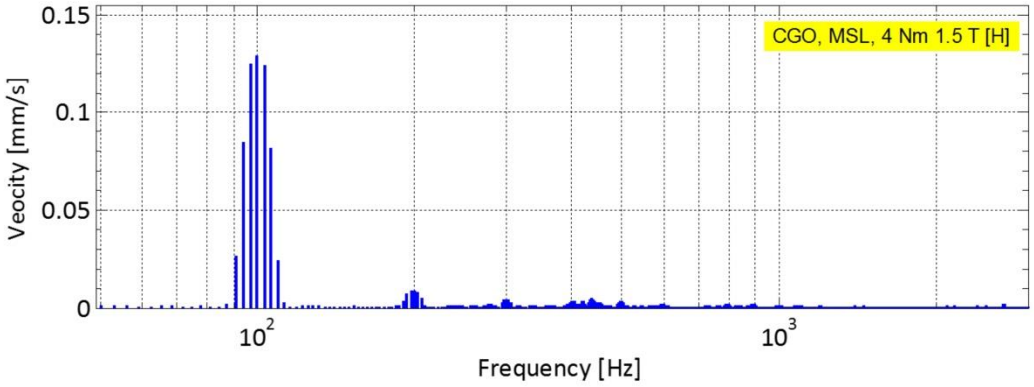

Fig. 5-54: Frequency distribution of vibration velocity on top surface of core No.18, 3 phase MSL CGO, at position H with clamping torque 4 Nm at 1.5 T, 50 Hz.

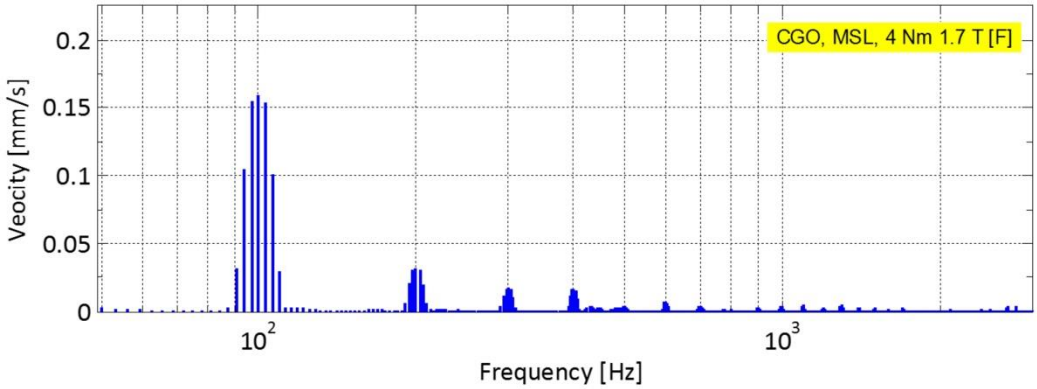

Fig. 5-55: Frequency distribution of vibration velocity on top surface of core No.18, 3 phase MSL CGO, at position F with clamping torque 4 Nm at 1.7 T, 50 Hz.

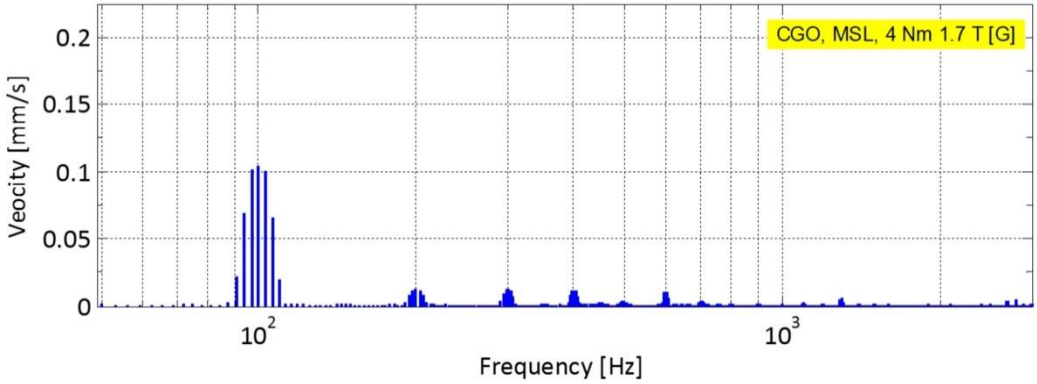

Fig. 5-56: Frequency distribution of vibration velocity on top surface of core No.18, 3 phase MSL CGO, at position G with clamping torque 4 Nm at 1.7 T, 50 Hz.

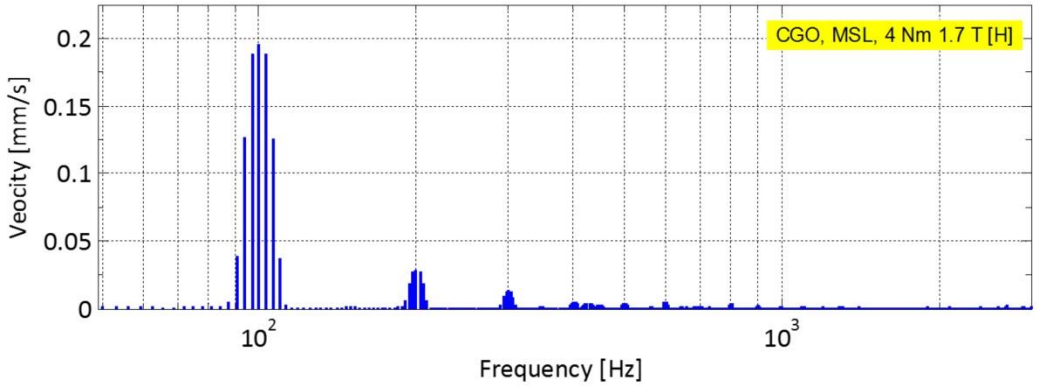

Fig. 5-57: Frequency distribution of vibration velocity on top surface of core No.18, 3 phase MSL CGO, at position H with clamping torque 4 Nm at 1.7 T, 50 Hz.

Figs. 5-58 to 5-63 show the frequency distribution of vibration velocity on the side surface at magnetic flux densities from 1.0 T to 1.7 T. The highest amplitude was found at 100 Hz as expected. Position J, which is further from the lamination end than position I, has a higher amplitude of vibration than position I. Comparing the noise and vibration velocity between top and side surfaces, the top surface has higher vibration but less noise due to the phase difference between them. The phase of the vibration on the top surface is associated with the magnetic flux on the limbs which have a phase difference of 120° but the phase of the vibration on the side surface only depends on the magnetic flux in its limb.

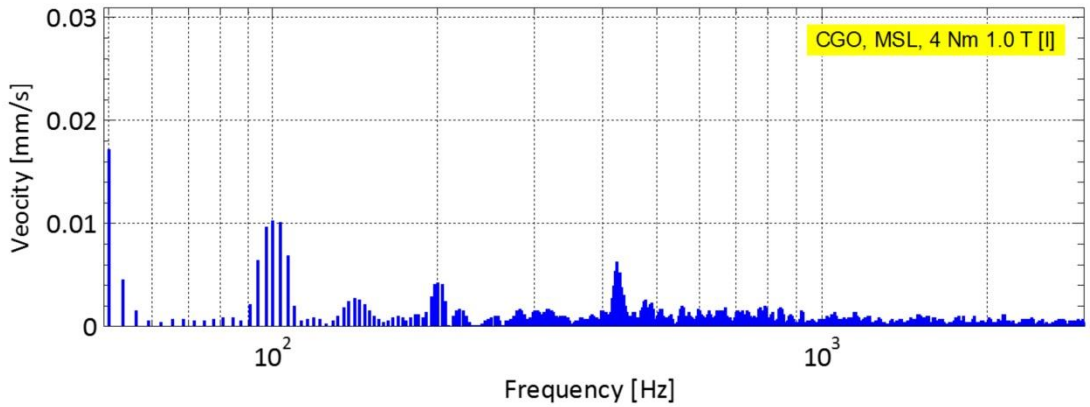

Fig. 5-58: Frequency distribution of vibration velocity on side surface of core No.18, 3 phase MSL CGO, at position I with clamping torque 4 Nm at 1.0 T, 50 Hz.

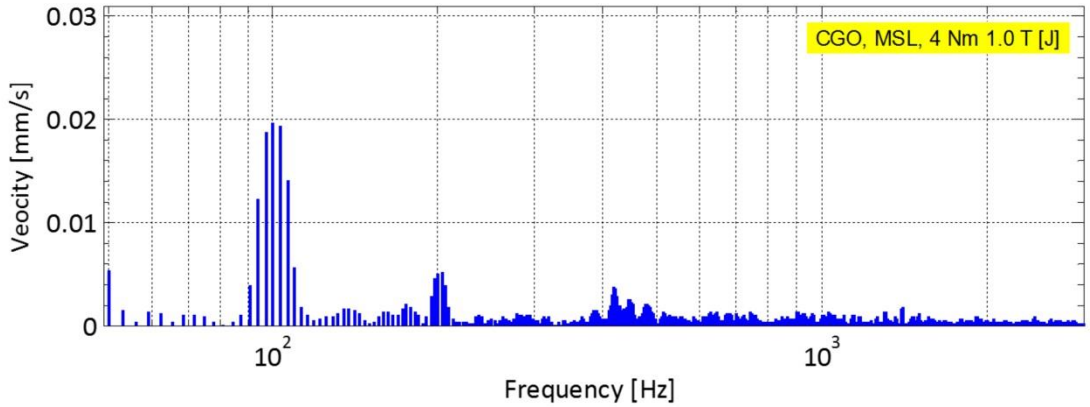

Fig. 5-59: Frequency distribution of vibration velocity on side surface of core No.18, 3 phase MSL CGO, at position J with clamping torque 4 Nm at 1.0 T, 50 Hz.

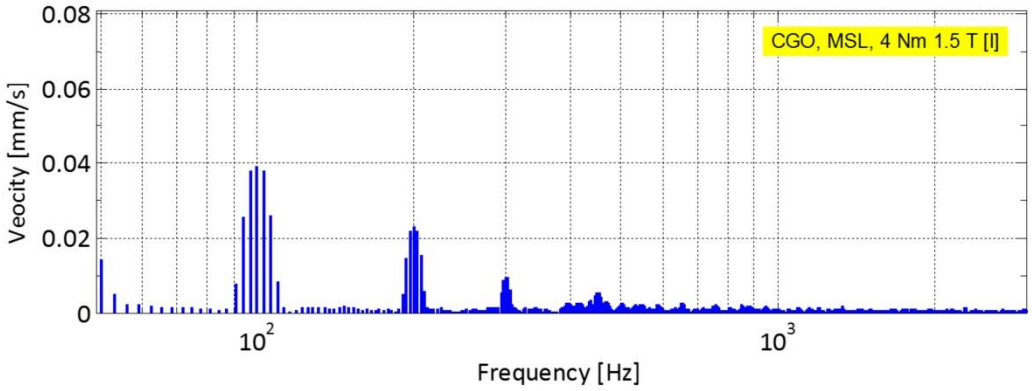

Fig. 5-60: Frequency distribution of vibration velocity on side surface of core No.18, 3 phase MSL CGO, at position I with clamping torque 4 Nm at 1.5 T, 50 Hz.

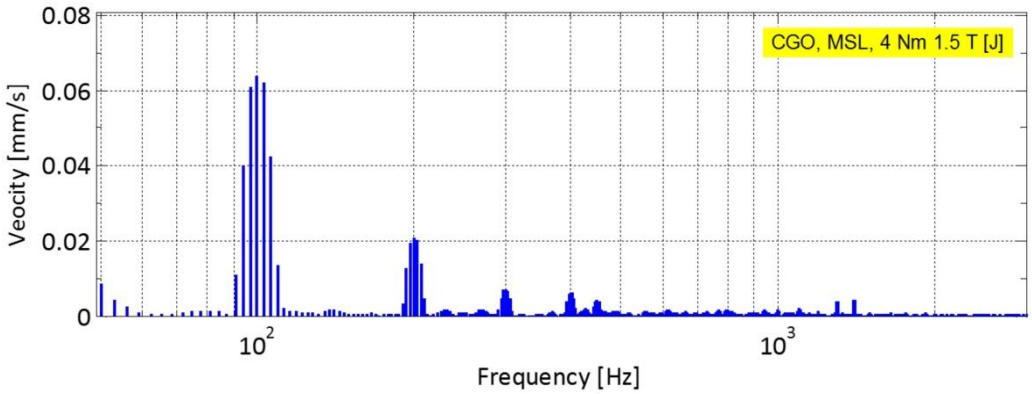

Fig. 5-61: Frequency distribution of vibration velocity on side surface of core No.18, 3 phase MSL CGO, at position J with clamping torque 4 Nm at 1.5 T, 50 Hz.

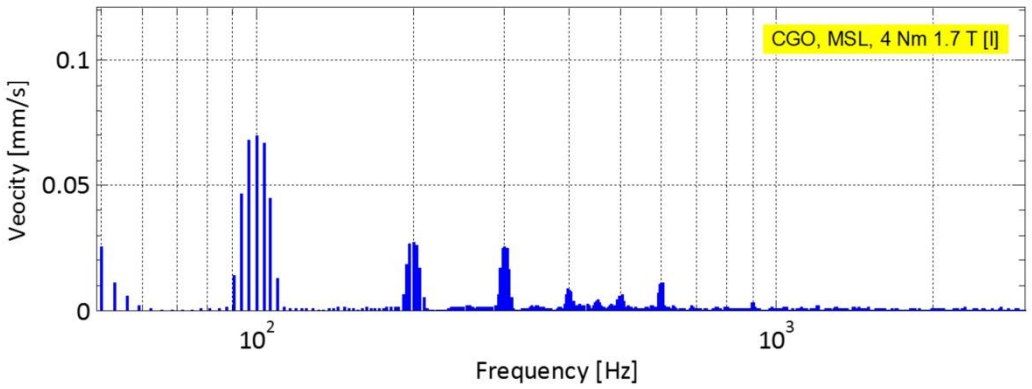

Fig. 5-62: Frequency distribution of vibration velocity on side surface of core No.18, 3 phase MSL CGO, at position I with clamping torque 4 Nm at 1.7 T, 50 Hz.

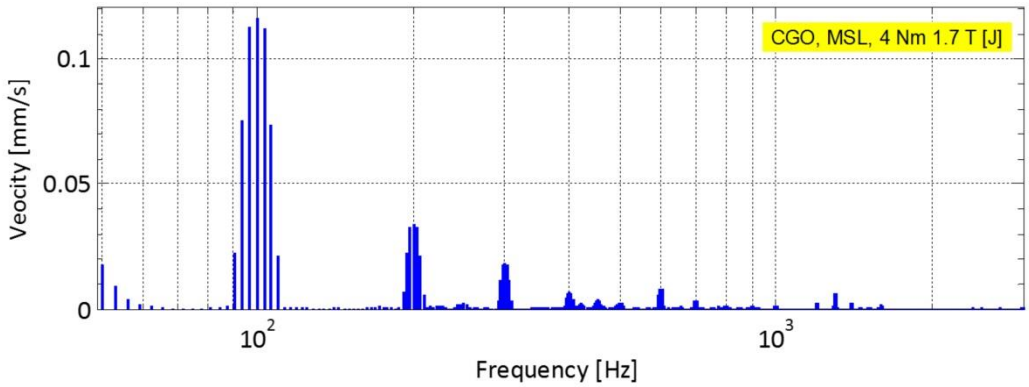

Fig. 5-63: Frequency distribution of vibration velocity on side surface of core No.18, 3 phase MSL CGO, at position J with clamping torque 4 Nm at 1.7 T, 50 Hz.

5.5 Effect of Vibration Phase Difference on Transformer Core Noise

The results from the previous section showed that the front surface had the highest vibration and the highest component was 100 Hz. To investigate in detail the vibration on this surface at 100 Hz, the whole front surface was measured. The results of the front surface vibration velocity and phase of the component at 100 Hz with clamping torque at 4 Nm and magnetic flux density of 1.5 T, 50 Hz are shown in Figs. 5-64 to 5-75. It is different to the results in Fig. 5-15 which show average rms of vibration for all frequency components while the results in Figs. 5-64 to 5-75 show only the component of the vibration at 100 Hz. In the experiment, the signal of magnetic flux density in the middle limb was used as a phase reference.

Vibration on the middle limb referred to the 0° and 180° instances of magnetic flux density in the middle limb show lowest vibration. This result agrees with the model of transformer core deformation due to magnetostriction as shown in Section 5.1. At 0° and 180° magnetic flux density at the middle limb is zero therefore magnetostriction of the laminations on the middle limb is also zero. However, in reality, there are magnetic forces applied to the end of the laminations on the middle limb due to magnetic flux from phases A and C which flow in the yoke so there is a small vibration on the middle limb. The highest vibration on the middle limb was found at

90° and 270° when the magnetic flux density, and therefore the magnetostriction, in the middle limb rises to its maximum amplitude. Although there are no experimental results at the centre of the middle limb, it can be extrapolated from the trend of the data near the centre that the highest vibration of the middle limb is at the centre of the lamination length with an amplitude approximately twice that of the outer limbs as shown in Fig. 5-76. The highest vibration of the outer limbs is not at the centre of the limb length but is at the end of laminations. Moreover, there is a phase difference between the outer limbs. If the limbs vibrate with identical phase, the sound pressure waves generated from them are also in phase. However, the experimental results show there is the phase difference between each limb.

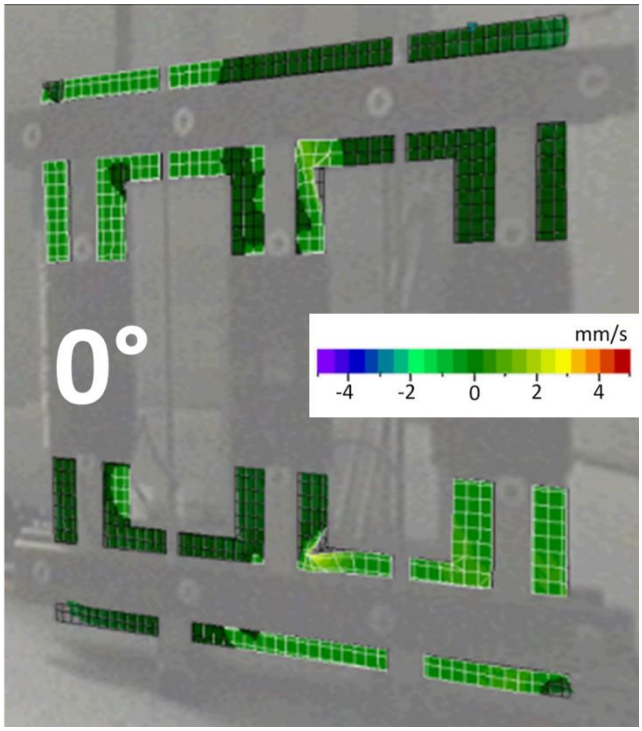

Fig.5-64: Measured phase vibration contour on front surface of core No.18, 3 phase MSL CGO, with clamping torque 4 Nm and magnetic flux density 1.5 T, 50 Hz at 0° of the magnetic flux density at the middle limb.

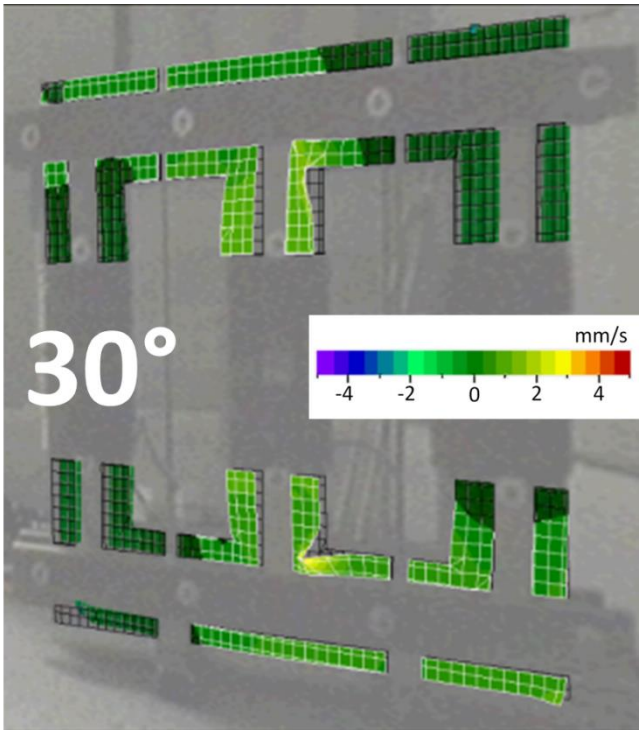

Fig.5-65: Measured phase vibration contour on front surface of core No.18, 3 phase MSL CGO, with clamping torque 4 Nm and magnetic flux density 1.5 T, 50 Hz at 30° of the magnetic flux density at the middle limb.

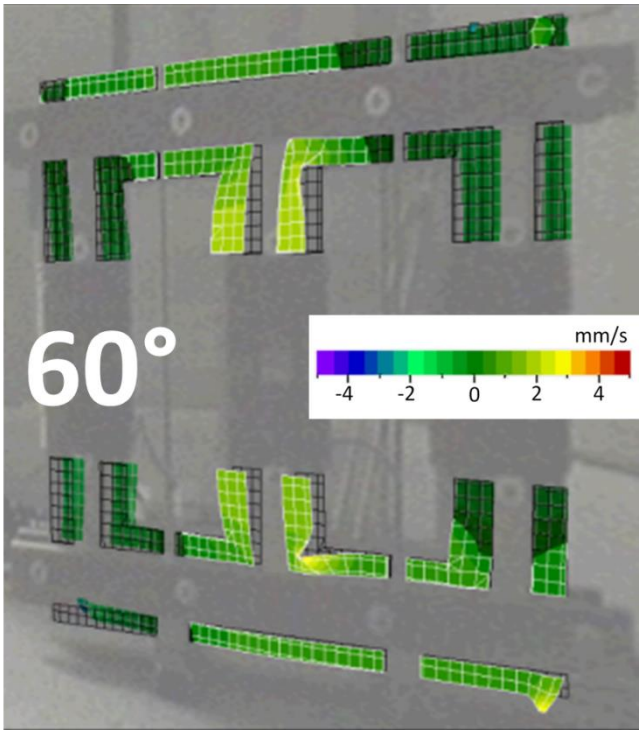

Fig.5-66: Measured phase vibration contour on front surface of core No.18, 3 phase MSL CGO, with clamping torque 4 Nm and magnetic flux density 1.5 T, 50 Hz at 60° of the magnetic flux density at the middle limb.

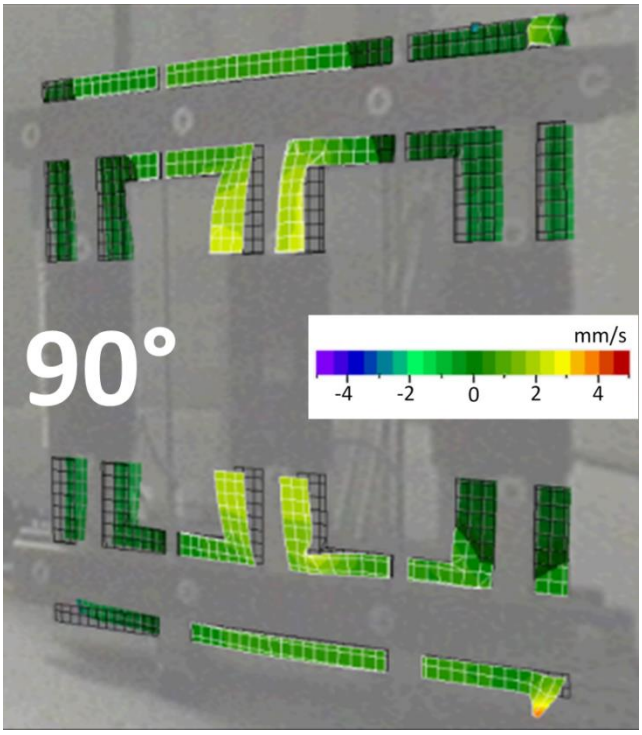

Fig.5-67: Measured phase vibration contour on front surface of core No.18, 3 phase MSL CGO, with clamping torque 4 Nm and magnetic flux density 1.5 T, 50 Hz at 90° of the magnetic flux density at the middle limb.

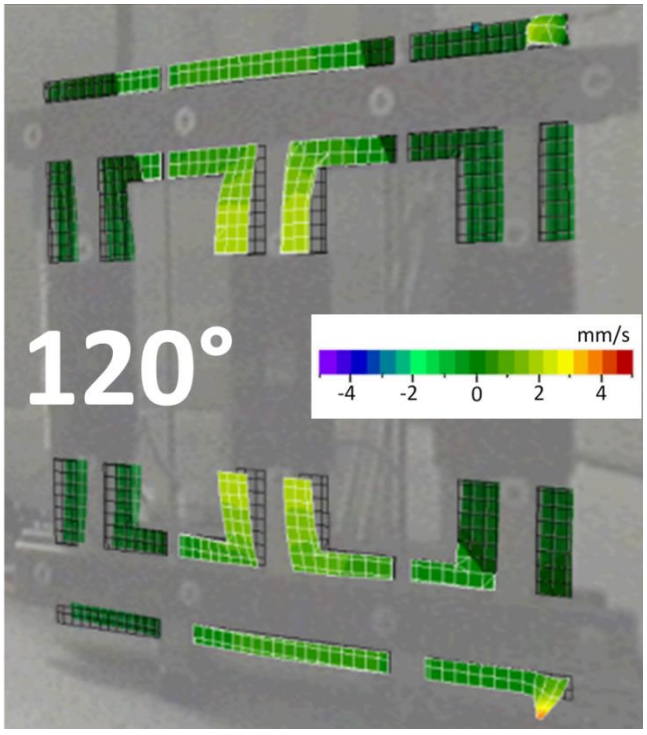

Fig.5-68: Measured phase vibration contour on front surface of core No.18, 3 phase MSL CGO, with clamping torque 4 Nm and magnetic flux density 1.5 T, 50 Hz at 120° of the magnetic flux density at the middle limb.

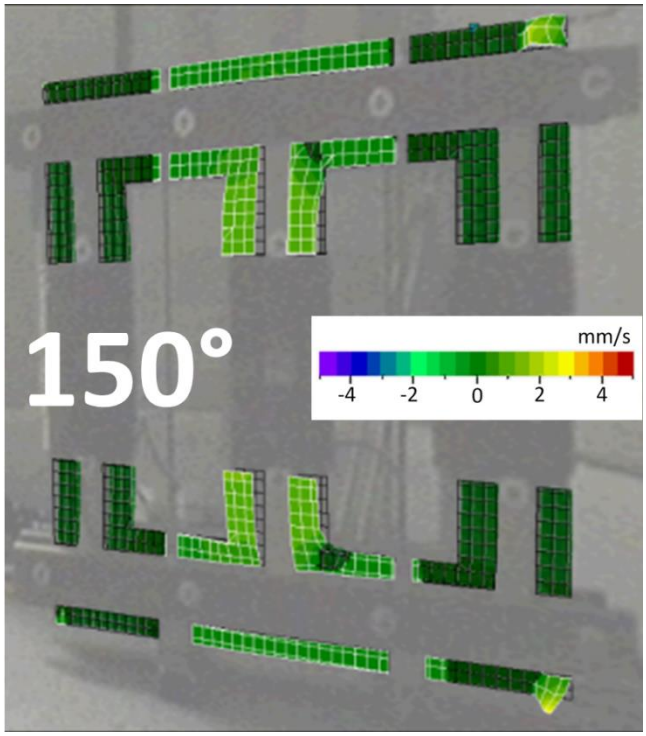

Fig.5-69: Measured phase vibration contour on front surface of core No.18, 3 phase MSL CGO, with clamping torque 4 Nm and magnetic flux density 1.5 T, 50 Hz at 150° of the magnetic flux density at the middle limb.

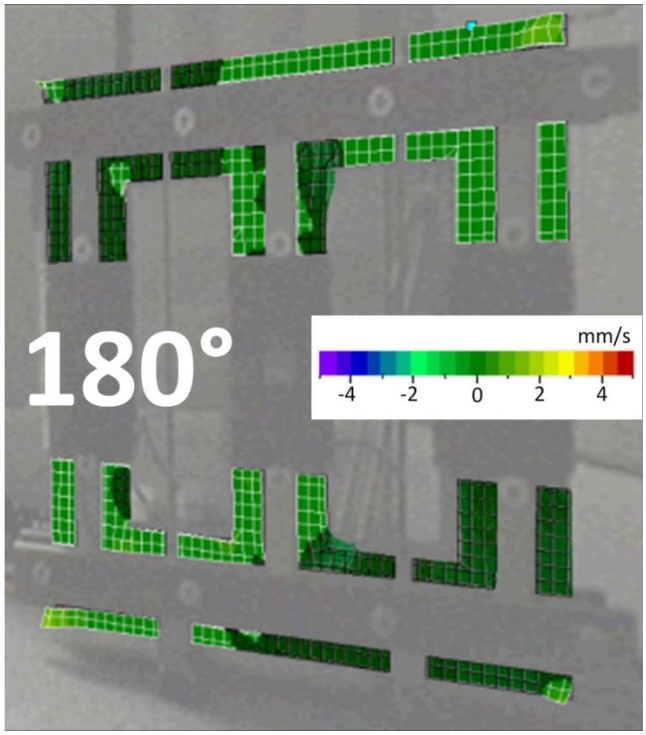

Fig.5-70: Measured phase vibration contour on front surface of core No.18, 3 phase MSL CGO, with clamping torque 4 Nm and magnetic flux density 1.5 T, 50 Hz at 180° of the magnetic flux density at the middle limb.

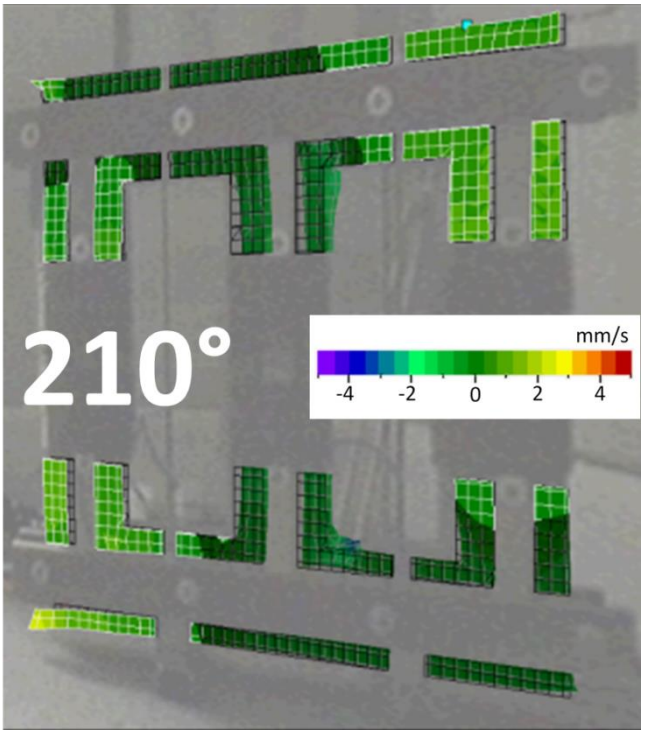

Fig.5-71: Measured phase vibration contour on front surface of core No.18, 3 phase MSL CGO, with clamping torque 4 Nm and magnetic flux density 1.5 T, 50 Hz at 210° of the magnetic flux density at the middle limb.

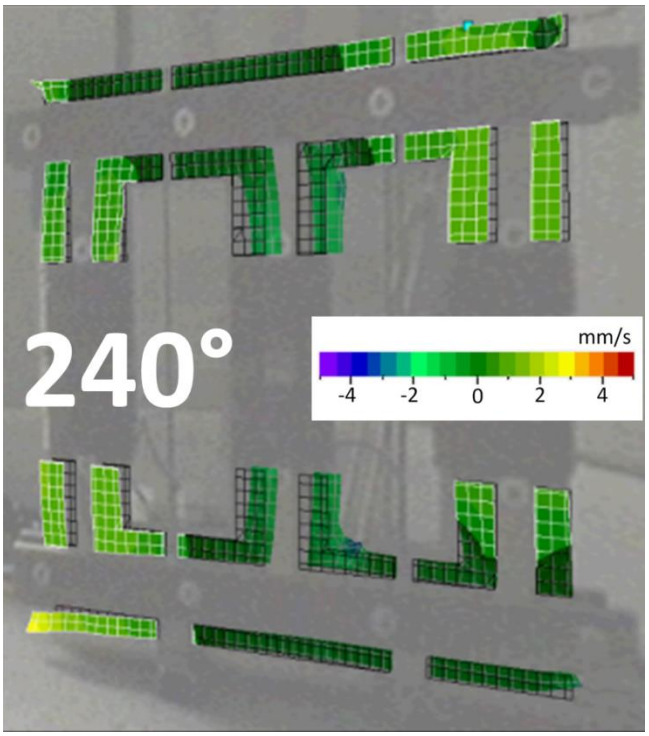

Fig.5-72: Measured phase vibration contour on front surface of core No.18, 3 phase MSL CGO, with clamping torque 4 Nm and magnetic flux density 1.5 T, 50 Hz at 240° of the magnetic flux density at the middle limb.

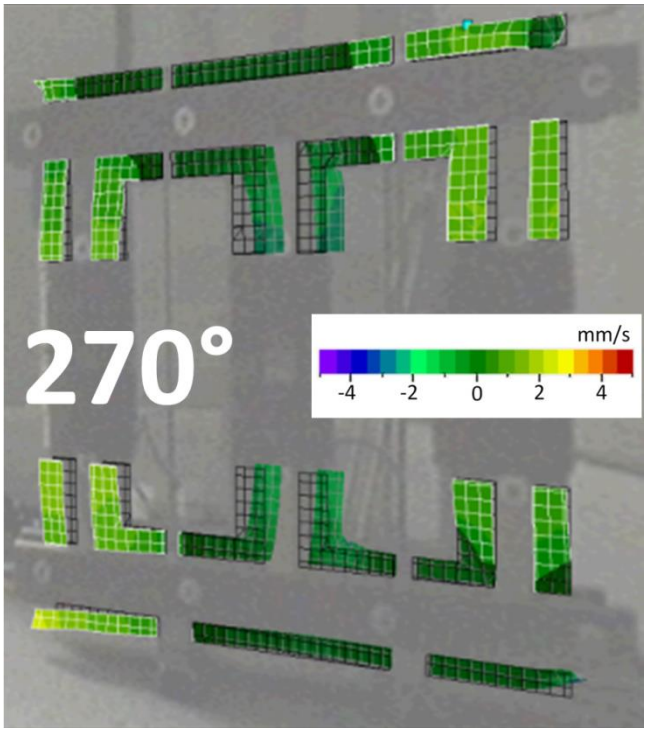

Fig.5-73: Measured phase vibration contour on front surface of core No.18, 3 phase MSL CGO, with clamping torque 4 Nm and magnetic flux density 1.5 T, 50 Hz at 270° of the magnetic flux density at the middle limb.

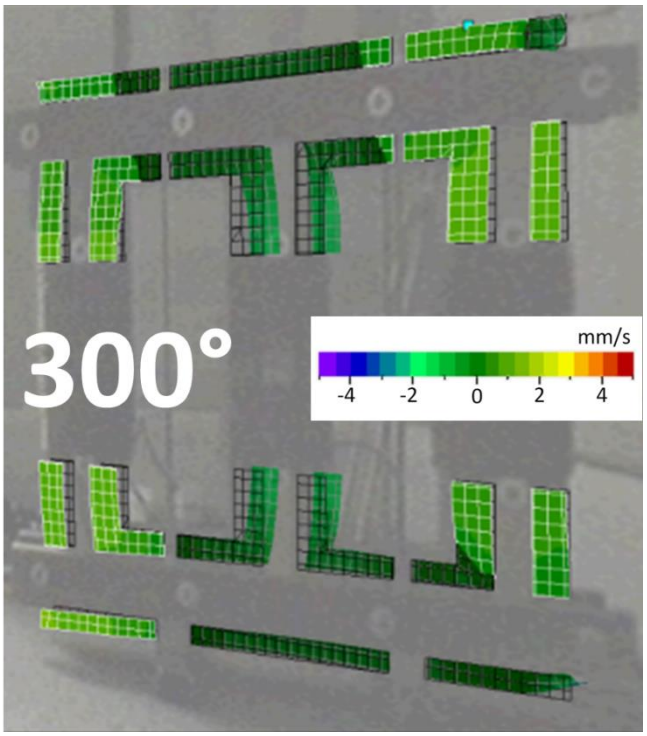

Fig.5-74: Measured phase vibration contour on front surface of core No.18, 3 phase MSL CGO, with clamping torque 4 Nm and magnetic flux density 1.5 T, 50 Hz at 300° of the magnetic flux density at the middle limb.

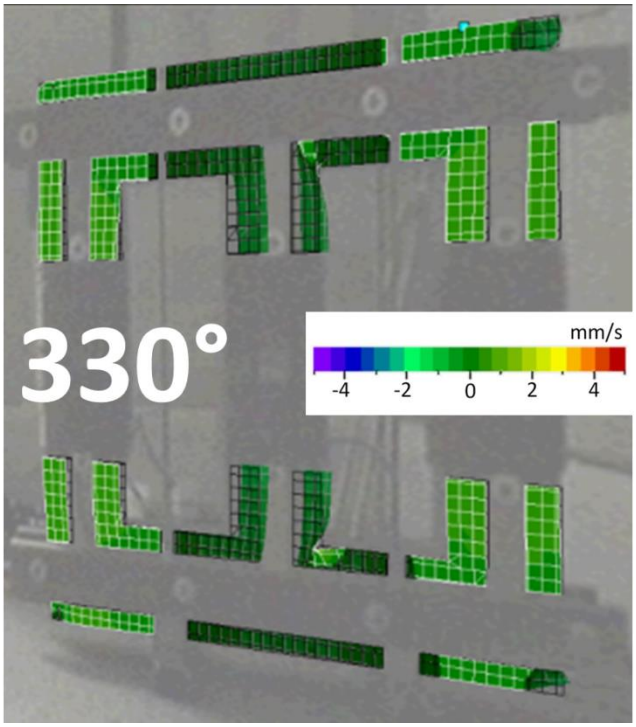

Fig.5-75: Measured phase vibration contour on front surface of core No.18, 3 phase MSL CGO, with clamping torque 4 Nm and magnetic flux density 1.5 T, 50 Hz at 330° of the magnetic flux density at the middle limb.

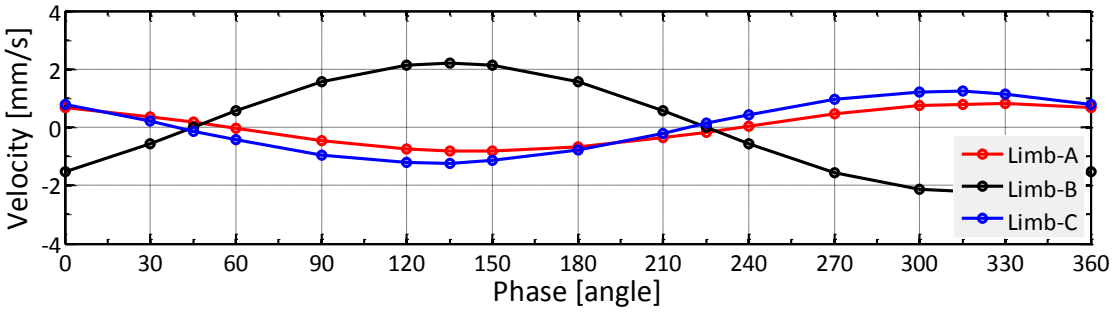

Fig.5-76: Comparison measured vibration phase difference between the core limb A (left hand side), B (middle limb) and C (right hand side)

Equations 5-4 and 5-5 show two sound wave equations ζ_1 and ζ_2 .[75]

$$\zeta_1(x,t) = A_1 \sin(mx - \omega t + \phi_1) \tag{5-4}$$

$$\zeta_2(x,t) = A_2 \sin(mx - \omega t + \phi_2) \tag{5-5}$$

when A_1 and A_2 are the maximum amplitude of sound waves ζ_1 and ζ_2, ϕ_1 and ϕ_2 are the phase constants of sound waves ζ_1 and ζ_2, and the minus (-) in front of ωt shows that the two sound waves move in the same direction. To investigate the effect of the difference of the phase constant, mx and ωt are defined as a constant. The superposition of these two waves, ζ_{total} can be expressed by Eq. 5-6.

$$\zeta_{total} = R \times \cos\left(mx - \omega t + \theta\right) \tag{5-6}$$

R is the amplitude of the superposition, $\cos\left(mx - \omega t + \theta\right)$ is the wave function and phase. R and θ can be calculated from Eq. 5-7 and Eq. 5-8.

$$R^2 = \left(A_1 + A_2\cos\left(\phi_2 - \phi_1\right)\right)^2 + \left(A_2\sin\left(\phi_2 - \phi_1\right)\right)^2 \tag{5-7}$$

$$= A_1^2 + A_2^2 + 2A_1A_2\cos\left(\phi_2 - \phi_1\right)$$

$$\text{and } \tan\theta = \frac{A_1\sin\phi_1 + A_2\sin\phi_2}{A_1\cos\phi_1 + A_2\cos\phi_2} \tag{5-8}$$

Comparing the amplitude R with $A_1 + A_2$

from $\left(A_1 + A_2\right)^2 = A_1^2 + A_2^2 + 2A_1A_2$, and $R^2 = A_1^2 + A_2^2 + 2A_1A_2\cos\left(\phi_2 - \phi_1\right)$

so $R^2 \le \left(A_1 + A_2\right)^2$

Therefore, if there is a phase difference between the waves the amplitude of the superposition is decreased due to factor of the cosine of the phase difference.

5.6 Vibration Separation Model

This section presents a simple model for separating the effect of magnetostriction and magnetic forces affecting transformer core vibration. The model considers the fundamental component of vibration at 100 Hz. From the experimental results in

Figs. 5-64 to 5-75, the deformation of the laminations on the middle limb due to magnetostriction and magnetic force can be expressed by the assumed circular segment as shown in Fig. 5-77. The chord represents the un-deformed length of the middle limb laminations (≈420 mm). The arc represents the deformed length of the lamination. The height of the segment (peak of displacement at 100 Hz) can be estimated by the peak of vibration velocity at 100 Hz as shown in Eq. 5-9.

$$\text{Displacement} = \int \text{velocity}\, dt \quad \text{m} \qquad (5\text{-}9)$$

The heights of the segment at magnetic flux densities from 1.0 T to 1.7 T are shown in Table 5-2.

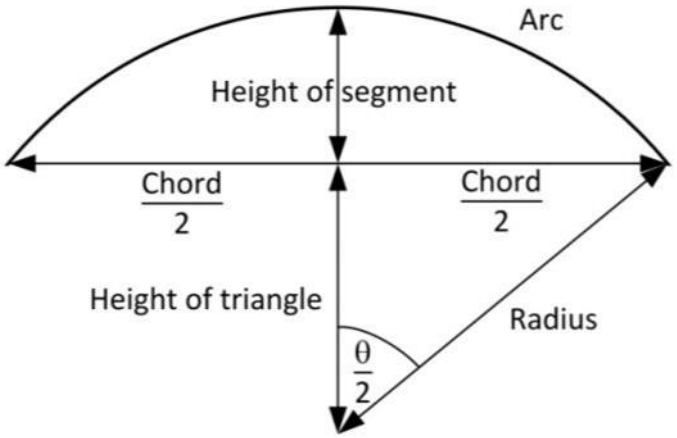

C : Chord

H : Height of segment

R : Radius

Fig. 5-77: Circular segment represent the deformation of the lamination on the middle limb of three phase three limb transformer core.

Table 5-2: Peak of vibration velocity and displacement at the centre of the middle limb of core No. 18, three phase transformer core with multistep lap and CGO material, at magnetic flux densities from 1.0 T to 1.7 T, 50 Hz.

B [T]	Peak of velocity [μm/s]	Peak of displacement [μm]	Δl_{total} [μm]
1.0	300	0.5	1.5
1.5	800	1.3	10.3
1.7	1000	1.6	16.1

The arc can be calculated from the relationship of the assumed circular segment as shown in Eq. 5-10 to Eq. 5-12.

$$R = \frac{C^2}{8H} + \frac{H}{2} \tag{5-10}$$

$$\theta = 2\tan^{-1}\left(\frac{4CH}{C^2 - 4H^2}\right) \tag{5-11}$$

$$\text{Arc} = Rd\theta \tag{5-12}$$

The difference between arc and chord is the lamination deformation due to magnetostriction and magnetic forces. Since magnetostriction $\propto B^2$ and magnetic forces $\propto B_g^2$, the deformation of the middle limb, Δl_{total} , can be expressed as shown in Eq. 5-13.

$$\Delta l_{total} \propto \Delta l_{\lambda,B} + \Delta l_{M,B_g} \tag{5-13}$$

where Δl_{λ} is the deformation due to magnetostriction and Δl_M is deformation due to magnetic forces.

At B = 1.0 T there is no effect of saturation induction in the laminations therefore $B_g << B$ hence, B_g is assumed to be zero.

Then (at B = 1.0 T) $\Delta l_{total} \propto \Delta l_{\lambda,1.0\text{T}} + \Delta l_{M,0\text{T}}$ or $\Delta l_{total} \propto \Delta l_{\lambda,1.0\text{T}}$

From the definition of magnetostriction, $\lambda = \frac{\Delta l}{l}$ we can write

$$\lambda_{1.0\text{T}} \propto \frac{1.45\times10^{-6}}{420\times10^{-3}} \propto 3.45\ \mu\varepsilon$$

Comparing the calculated magnetostriction at 1.0T with the magnetostriction stress characteristics of CGO material in Chapter 4, it was found that the magnetostriction is

equivalent to a stress of approximately 3.5 MPa. Since the vibration experiments at 1.0 T to 1.7 T were tested under the same clamping conditions, the effect of clamping torque on the stress applied on the lamination should be the same. Therefore, at 3.5 MPa the magnetostriction is 7.85 με and 10 με at 1.5 T and 1.7 T respectively. Then, the deformation due to magnetostriction can be calculated by the magnetostriction and the length of the lamination. The difference between the total deformation and the deformation due to magnetostriction is the deformation due to magnetic forces. Table 5-3 shows the numerical result of the total deformation, deformation due to magnetostriction, deformation due to magnetic forces and percentage of the contribution of magnetostriction and magnetic forces on the vibration of the middle limb at 1.0 T to 1.7 T.

Table 5-3: Summary of contribution of deformation due to magnetostriction and magnetic forces on the middle limb of three phase three limb transformer core at 1.0 T to 1.7 T, 50 Hz.

B [T]	Δl_{total} [μm]	Δl_{λ} [μm]	λ [με]	Δl_{M} [μm]	Δl_{λ} [%] : Δl_{M} [%]
1.0	1.45	1.45	3.45	0.0	100 : 0
1.5	10.29	3.30	7.85	7.0	32 : 68
1.7	16.08	4.20	10.00	11.9	26 : 74

It can be seen from the results in Table 5-3 that, if there is no saturation induction, then no magnetic flux flows through the gap, therefore the vibration is only due to magnetostriction. The influence of the magnetic forces on the vibration of the lamination on the middle limb significantly increases when the operating magnetic flux density is increased to 1.5 T (68 %) and 1.7 T (74 %). On the other hand, the influence of magnetostriction on the vibration decreases when the magnetic flux density is increased.

This numerical analysis is limited since it does not take into account the harmonic components of vibration which might have a higher effect on transformer core noise

than the fundamental component. Therefore the ratio between Δl_{λ} and Δl_{M} does not represent the contribution of magnetostriction and magnetic force to the total transformer core noise. However, it can be used for estimation of the relative effect of magnetostriction and magnetic forces on transformer core vibration.

5.7 Influence of Vibration of T-joint on Transformer Core Noise

The results from the previous section showed that the vibration amplitude of the middle limb had approximately twice that of the outer limb. This section presents a comparison of the noise experimental results between the three phase core, weighing 115 kg, and single phase core, weighing 72 kg, for investigating the effect of vibration on the middle limb on transformer core noise. The cores were assembled with the CGO material, step lap configuration, and cross sectional area. The three phase core has larger front and top surfaces. The extra area is in the T-joint region as shown in Fig. 5-78. Therefore a difference on noise should be the effect of the T-joint.

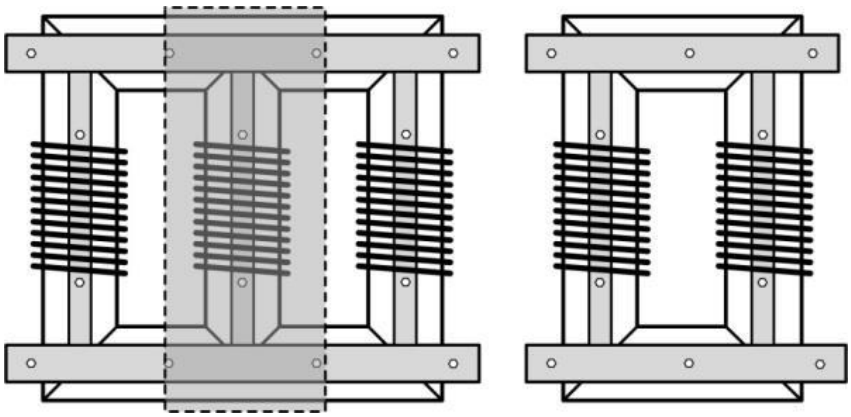

Fig.5-78: Comparison of front surface area between three phase and single phase cores.

Fig. 5-79 shows comparison of A-weighted sound power level between the three phase and single phase cores at magnetic flux density from 1.5 T to 1.8 T.

Unexpectedly, the A-weighted sound power level of the single phase core is higher than the three phase core. At 1.5 T, the A-weighted sound power level of the single phase core is 1.5 dB higher and at 1.7 T it is 2 dB higher. No significant difference of A-weighted sound power level between these two cores was found at 1.8 T. The reason for the difference in A-weighted sound power level is due to the vibration phase difference between each limb of the three phase core as can be seen in Figs.5-64 to 5-75. While no phase difference occurs between the limbs of single phase core since the magnetising currents are of course in phase.

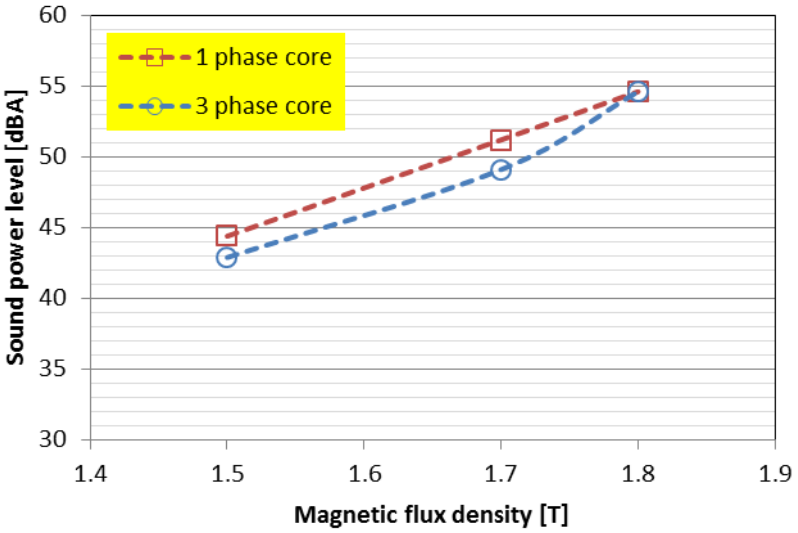

Fig.5-79: Comparison of sound power level between three phase and single phase cores with clamping torque 4 Nm at magnetic flux density 1.5 T to 1.8 T, 50 Hz.

5.8 Influence of Clamping Torque on Transformer Core Noise

Magnetostriction strongly depends on stress therefore clamping torque applied to the clamps affects the magnetostriction properties of the laminations as well as influencing air gaps, and therefore magnetic forces, and the mechanical behaviour of the cores. To investigate the effect of clamping torque, noise and vibration of transformer core No.18 were measured under magnetic flux density from 1.0 T to

1.7 T with clamping torque from 2 Nm to 6 Nm. Numerical results of A-weighted sound pressure level emitted from the core measured from microphone #1 (side surface), #3 (front surface) and #9 (top surface) are shown in Table 5-4.

Table 5-4: A-weighted sound pressure level (dBA) of transformer core No.18, 3 phase MSL, CGO, with clamping torque 2 Nm to 6 Nm at magnetic flux density 1.0 T to 1.7 T, 50 Hz.

	1.0 T			1.5 T			1.7 T		
Torque/Position	#1	#3	#9	#1	#3	#9	#1	#3	#9
2 Nm	39.9	38.5	36.0	43.3	46.8	40.1	50.3	53.6	46.9
4 Nm	40.4	38.9	35.8	43.4	46.9	39.2	48.9	52.2	46.1
6 Nm	40.3	38.3	36.9	44.8	48.1	42.7	50.5	53.7	47.8

At 1.0 T, the A-weighted sound pressure level is not significantly affected by clamping torque. At 1.5 T the highest sound pressure level is found at a clamping torque of 6 Nm on all surfaces whereas at 1.7 T, the lowest noise occurs at 4 Nm. The random variation of sound pressure on the effect of clamping torque is due to the core surface not being clamped especially at the inner and outer corners.

Positions and shape of clamps affect transformer core vibration [25], [26]. Also the wooden clamps on the yokes and the limbs are different sizes. The different sizes lead to different stress distribution to the laminations and different stresses could cause different magnetostriction characteristics. Practically, for a large transformer, the core cross-sectional area is not quadrilateral in order to optimise the core utilisation area and to reduce stress on the winding. Hence, the core is designed to have an approximate circular area and in bound with insulation as shown in Fig. 5-80.

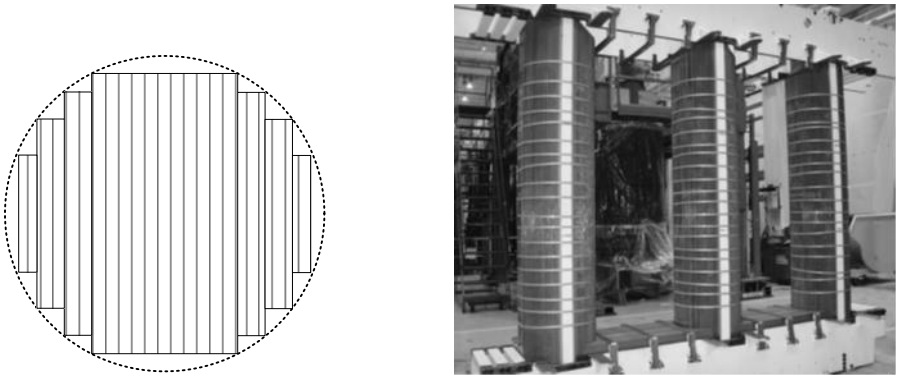

a) b)

Fig.5-80: (a) An approximate circular core area (b) stack core binds with tape [76]

To investigate the relationship between vibration and noise of the core, vibration distribution on the front, side and top surfaces of the core with 2 Nm to 6 Nm clamping torques at magnetic flux density 1.7 T were measured, the results are shown in Figs. 5-81 to 5-87.

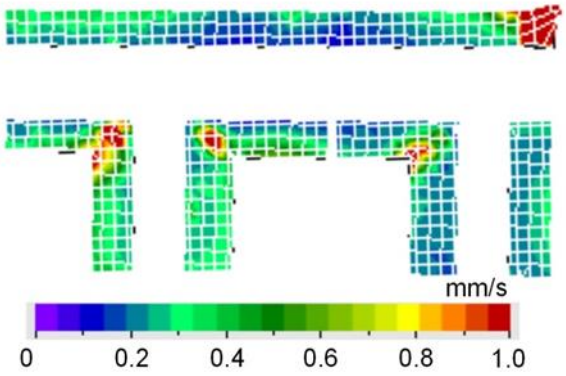

Fig.5-81: Vibration distribution on front surface of core No.18, 3 phase MSL CGO, with clamping torque 2 Nm at magnetic flux density 1.7 T, 50 Hz.

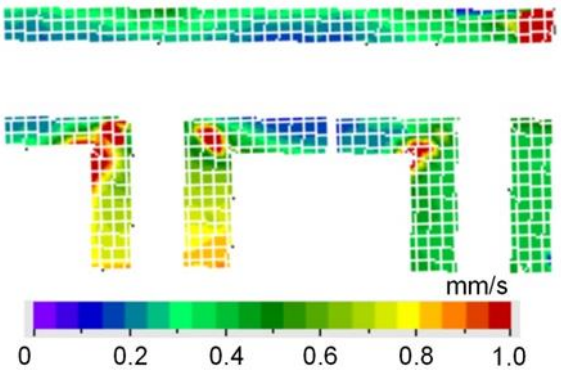

Fig.5-82: Vibration distribution on front surface of core No.18, 3 phase MSL CGO, with clamping torque 4 Nm at magnetic flux density 1.7 T, 50 Hz.

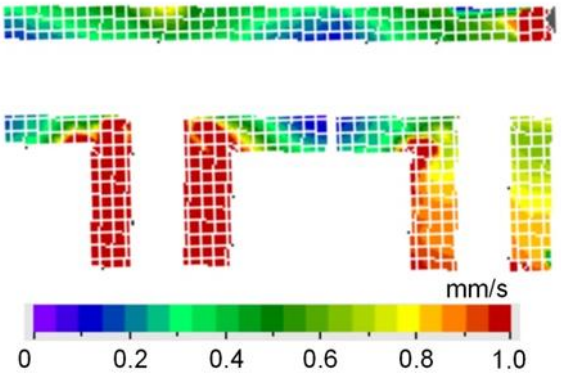

Fig.5-83: Vibration distribution on front surface of core No.18, 3 phase MSL CGO, with clamping torque 6 Nm at magnetic flux density 1.7 T, 50 Hz.

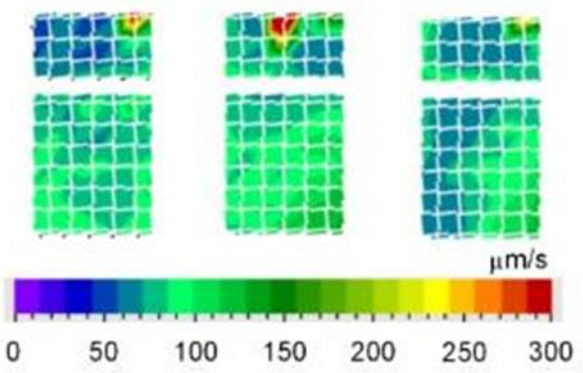

a) 2 Nm b) 4 Nm c) 6 Nm

Fig.5-84: Vibration distribution on side surface of core No.18, 3 phase MSL CGO, with clamping torque 2 Nm to 6 Nm at magnetic flux density 1.7 T, 50 Hz.

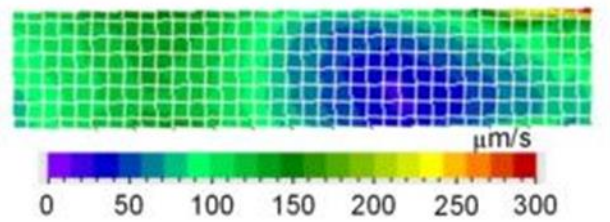

Fig.5-85: Vibration distribution on top surface of core No.18, 3 phase MSL CGO, with clamping torque 2 Nm at magnetic flux density 1.7 T, 50 Hz.

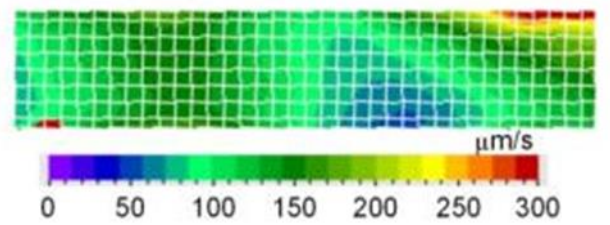

Fig.5-86: Vibration distribution on top surface of core No.18, 3 phase MSL CGO, with clamping torque 4 Nm at magnetic flux density 1.7 T, 50 Hz.

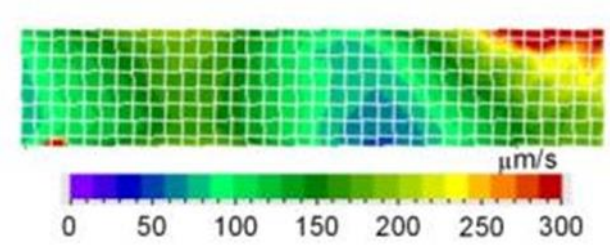

Fig.5-87: Vibration distribution on top surface of core No.18, 3 phase MSL CGO, with clamping torque 6 Nm at magnetic flux density 1.7 T, 50 Hz.

For the front surface, it can be seen that as the clamping torque increases from 2 Nm to 4 Nm the lamination is restricted from flapping at the outer corner. Increasing the clamping torque to 6 Nm leads to an increase in magnetostriction due to increase in the stress. For the side and top surfaces, at 4 Nm the vibration is the most uniform. It can be seen that an optimal pressure is needed to minimise the core vibration.

5.8.1 Relationship of Clamping Torque and Stress on Lamination

The relationship between bolt torque, T, and stress, σ applied to the layer, n, of lamination can be estimated from Eq. 5-14 and Eq. 5-15. [77]

$$\sigma_n = \frac{F_n}{A_{c,n}} \qquad \text{N/m}^2 \qquad (5\text{-}14)$$

$$F_n = \frac{T}{Jd_b} \qquad \text{N} \qquad (5\text{-}15)$$

where F is the force applied on the lamination in N, J is torque coefficient, 0.45, which can be estimated from the material properties of the bolts [78], [79] , d_b is bolt diameter in m, $A_{c,n}$ is the cross sectional area of the applied force on the lamination which can be estimated from the general cone geometry as shown in Fig. 5-88. The force distributes approximately 30° [77] from the clamp to the lamination. Therefore each layer of lamination has different stress. The stress on each layer on the lamination is shown in Fig. 5-89 and the average stress on the 240 laminations stack for clamping torque from 2 Nm to 6 Nm is shown in Table 5-5.

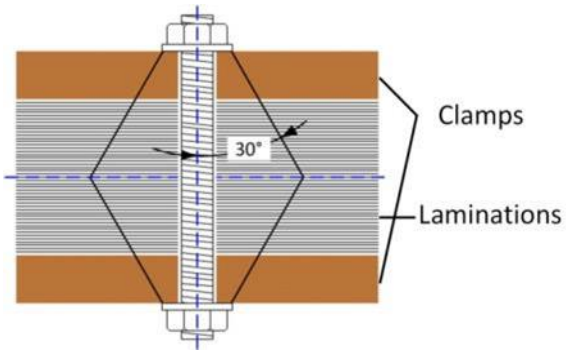

Fig.5-88: Force distribution from clamp to stack of lamination

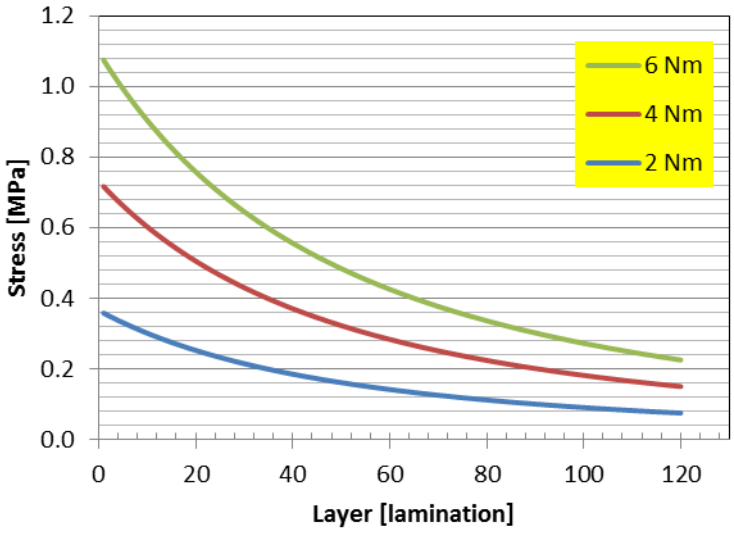

Fig. 5-89: Relationship between torque bolt and stress on the lamination stack.

Table 5-5: Relationship between torque bolt and average stress on the lamination stack.

Bolt torque [Nm]	Clamping force [N]	Average stress [MPa]
2 Nm	350	0.16
4 Nm	700	0.33
6 Nm	1050	0.49

5.9 Influence of Step Lap Design on Transformer Core Noise

The advantage of the MSL over the SSL core configuration is to reduce the effect of saturation induction at the end of the laminations. The saturation induction affects power losses and interlaminar forces at the joints. The critical induction level depends on the number of step laps. To investigate the influence of step lap configuration, transformer core No.24, 3 phase SSL CGO, was tested under the same condition as core No.18, 3 phase MSL CGO. Comparison of the variation of noise with flux density at a clamping torque of 4 Nm is shown in Fig. 5-90.

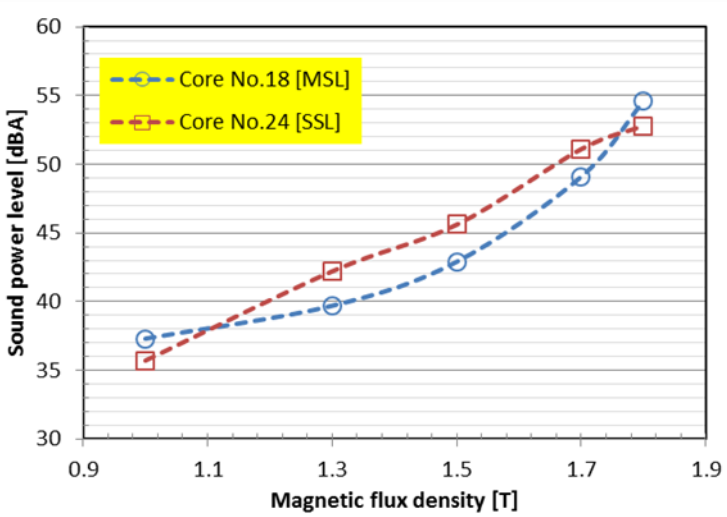

Fig.5-90: Comparison of sound power level between multistep lap and single step lap transformer core with clamping torque 4 Nm at 1.0 T to 1.8 T, 50 Hz.

The results show that at 1.0 T and 1.8 T the SSL core produces lower A-weighted sound power level than the MSL core. It can be seen that the SSL configuration has a lower average sound power level than the MSL configuration when they are operated at the same level of magnetic flux density and the SSL is operated at lower than its critical induction. On the other hand, the MSL configuration has higher sound power level than the SSL configuration when they are operated above their critical inductions. The critical induction of SSL and MSL (4 steps) configurations are approximately 1.0 T and 1.6 T respectively.

Figs. 5-91 to 5-96 show the vibration distribution on the front, top and side surfaces of core No.24, the 3 phase SLL CGO. The frequency distribution of the vibration on the front surface at the positions which were described in Fig.5-20 is shown in Figs.5-97 to 5-111. Comparing the vibration distribution on the front surface between the MSL (Figs.5-14 to 5-16) and SSL (Figs.5-91 to 5-93) configurations, it can be clearly seen that vibration on front surface of the SSL is less than the MSL configuration for all levels of magnetic flux density. However, the A-weighted sound power level of the SSL core is higher than the MSL core at 1.5 T and 1.7 T due to the effect of the harmonic components of vibration and magnetic forces due to saturation induction.

Considering the frequency distribution of the vibration component at 1.5 T and 1.7 T, on the limb surface the frequency component at 100 Hz of the SSL is approximately half the amplitude of the MSL configuration (approximately 0.70 mm/s on MSL core and 0.35 mm/s on SSL core), whilst there are higher amplitude of harmonic components near 1 kHz. This is the reason for higher A-weighted sound power level in the SSL core. The harmonics of vibration on SSL core might be due to unsymmetrical dimension of the lamination of the middle limb.

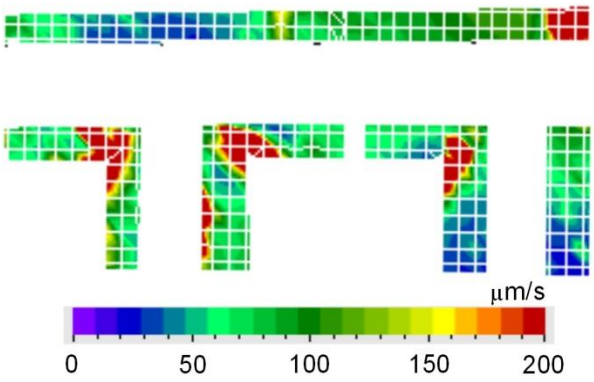

Fig. 5-91: Vibration distributions on front surface of core No.24, 3 phase SSL CGO, with clamping torque 4 Nm at magnetic flux density 1.0 T, 50 Hz.

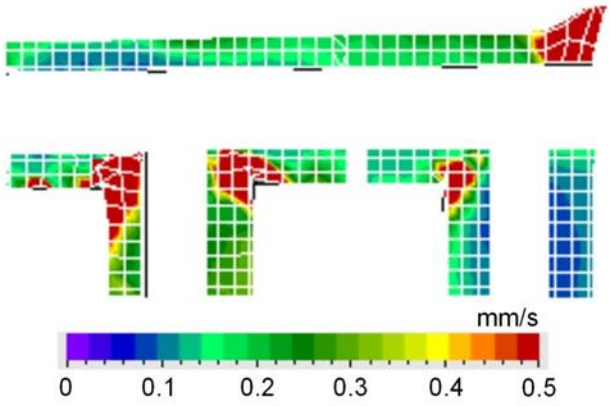

Fig. 5-92: Vibration distributions on front surface of core No.24, 3 phase SSL CGO, with clamping torque 4 Nm at magnetic flux density 1.5 T, 50 Hz.

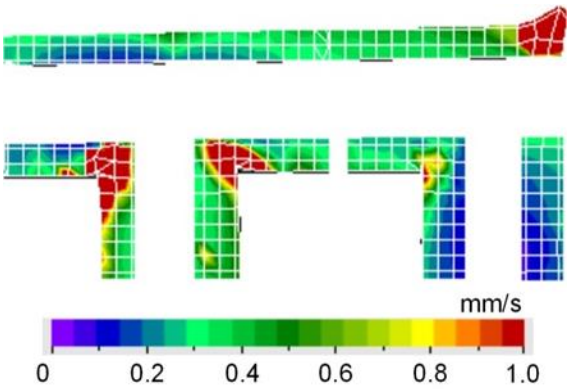

Fig. 5-93: Vibration distributions on front surface of core No.24, 3 phase SSL CGO, with clamping torque 4 Nm at magnetic flux density 1.7 T, 50 Hz.

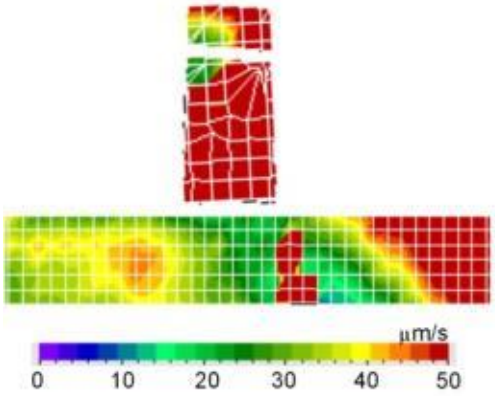

Fig. 5-94: Vibration distributions on top and side surfaces of core No.24, 3 phase SSL CGO, with clamping torque 4 Nm at magnetic flux density 1.0 T, 50 Hz.

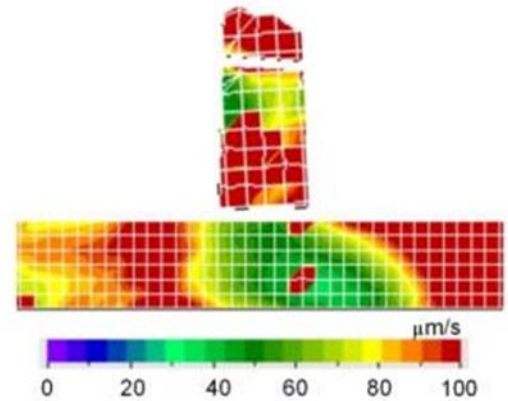

Fig. 5-95: Vibration distributions on top and side surfaces of core No.24, 3 phase SSL CGO, with clamping torque 4 Nm at magnetic flux density 1.5 T, 50 Hz.

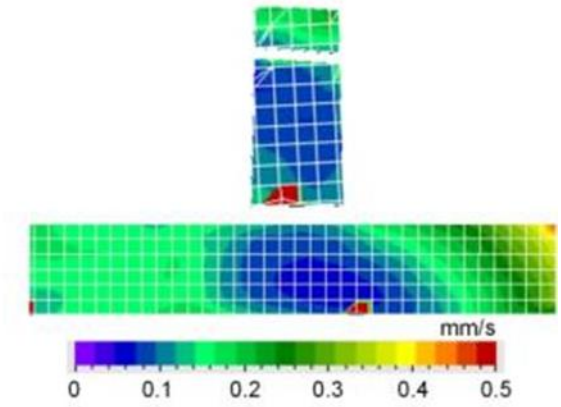

Fig. 5-96: Vibration distributions on top and side surfaces of core No.24, 3 phase SSL CGO, with clamping torque 4 Nm at magnetic flux density 1.7 T, 50 Hz.

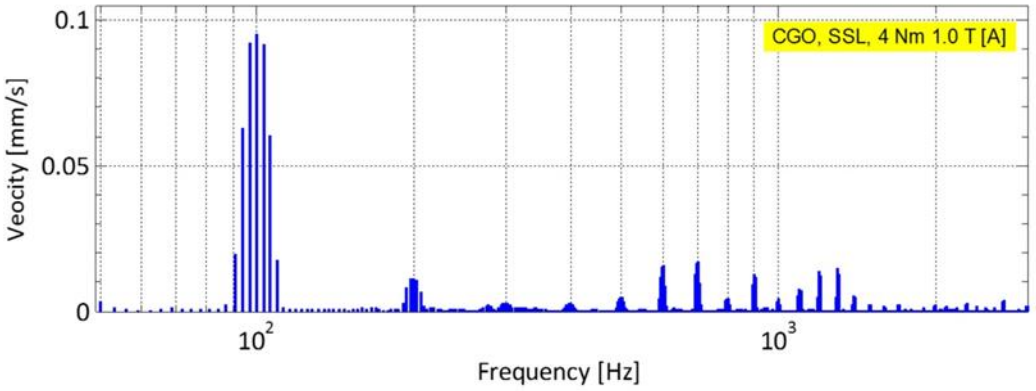

Fig. 5-97: Frequency distribution of vibration velocity on core No.24, 3 phase SSL CGO, at position A with clamping torque 4 Nm at 1.0 T, 50 Hz.

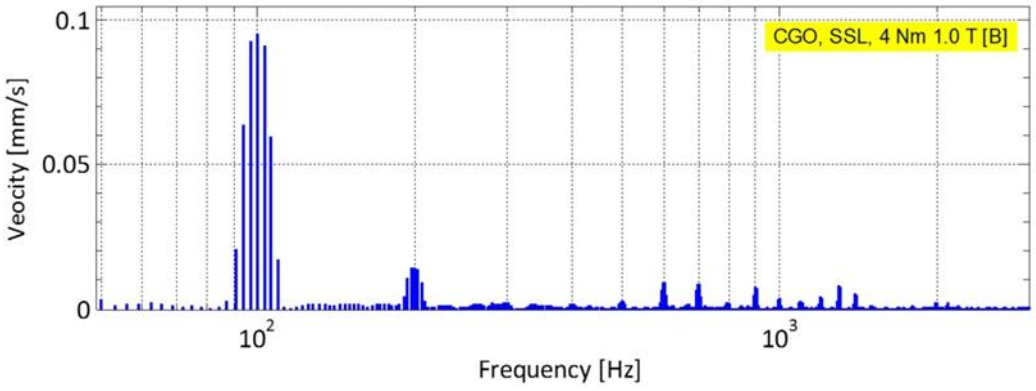

Fig. 5-98: Frequency distribution of vibration velocity on core No.24, 3 phase SSL CGO, at position B with clamping torque 4 Nm at 1.0 T, 50 Hz.

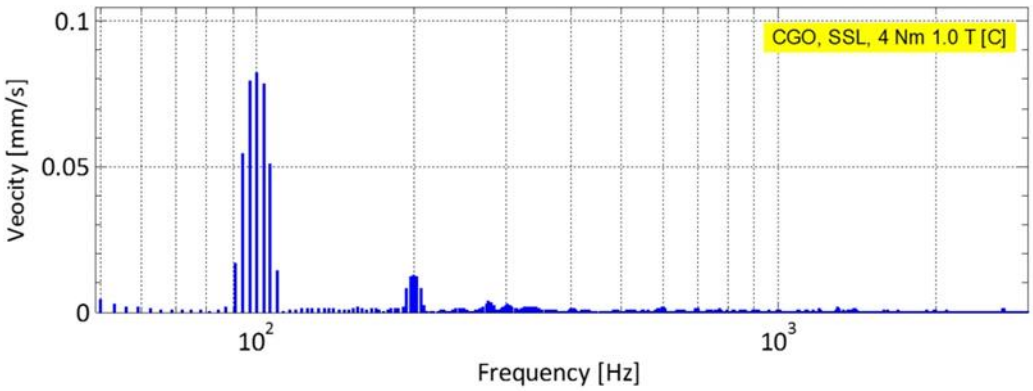

Fig. 5-99: Frequency distribution of vibration velocity on core No.24, 3 phase SSL CGO, at position C with clamping torque 4 Nm at 1.0 T, 50 Hz.

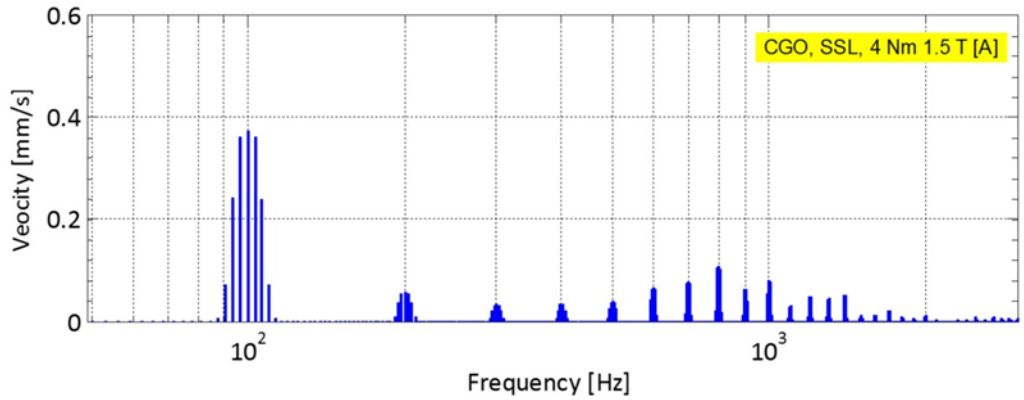

Fig. 5-100: Frequency distribution of vibration velocity on core No.24, 3 phase SSL CGO, at position A with clamping torque 4 Nm at 1.5 T, 50 Hz.

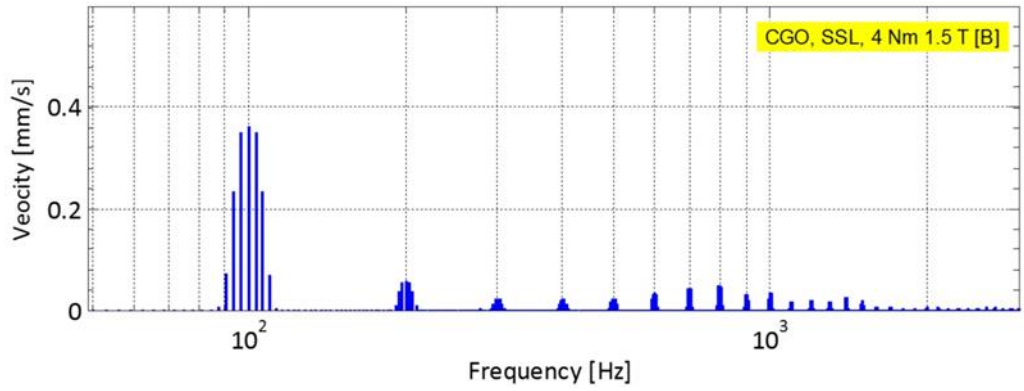

Fig. 5-101: Frequency distribution of vibration velocity on core No.24, 3 phase SSL CGO, at position B with clamping torque 4 Nm at 1.5 T, 50 Hz.

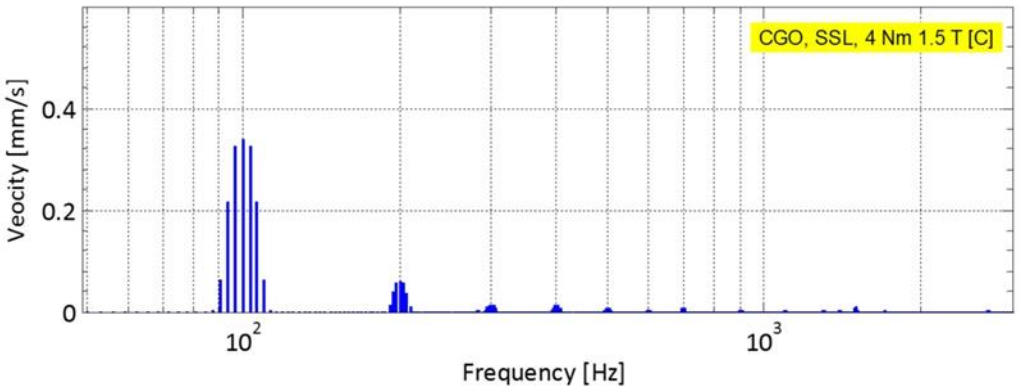

Fig. 5-102: Frequency distribution of vibration velocity on core No.24, 3 phase SSL CGO, at position C with clamping torque 4 Nm at 1.5 T, 50 Hz.

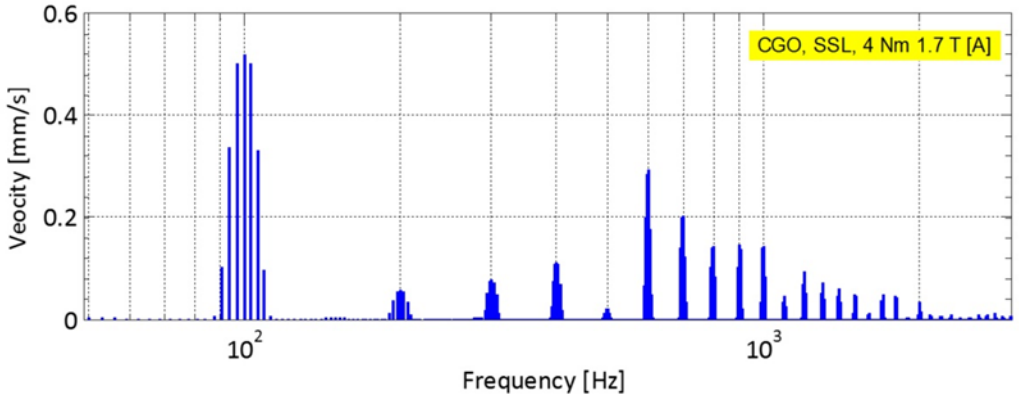

Fig. 5-103: Frequency distribution of vibration velocity on core No.24, 3 phase SSL CGO, at position A with clamping torque 4 Nm at 1.7 T, 50 Hz.

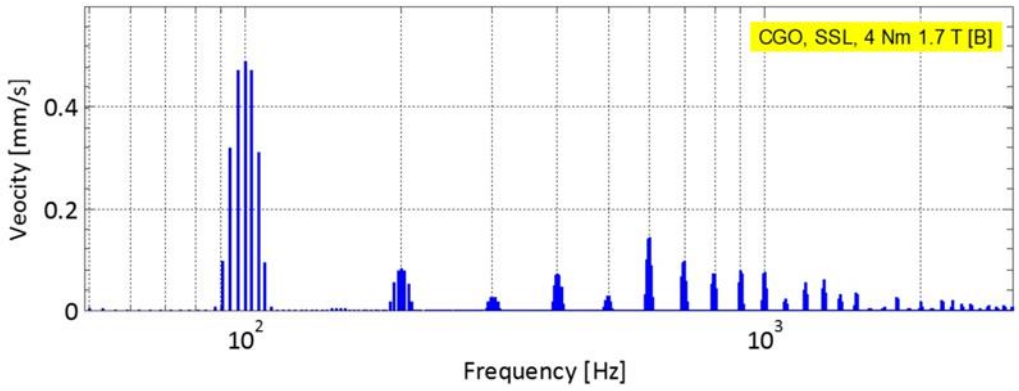

Fig. 5-104: Frequency distribution of vibration velocity on core No.24, 3 phase SSL CGO, at position B with clamping torque 4 Nm at 1.7 T, 50 Hz.

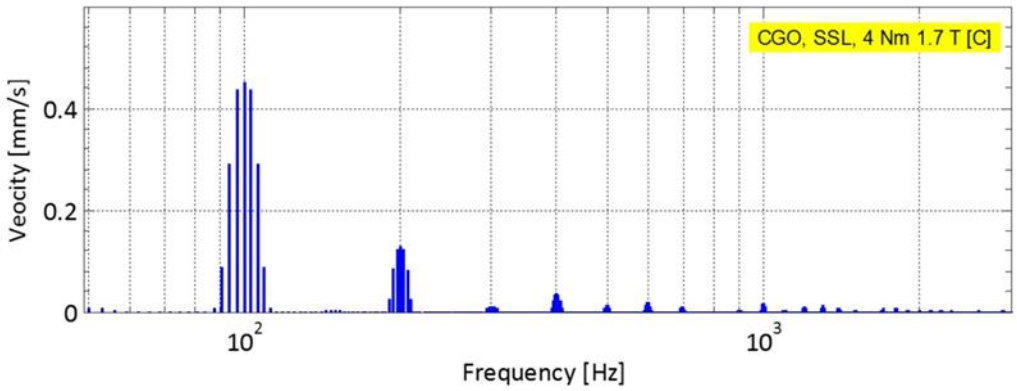

Fig. 5-105: Frequency distribution of vibration velocity on core No.24, 3 phase SSL CGO, at positions C with clamping torque 4 Nm at 1.7 T, 50 Hz.

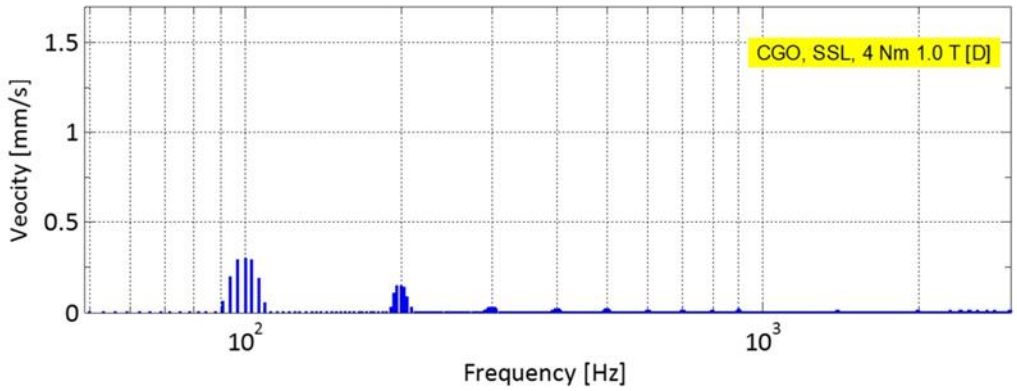

Fig. 5-106: Frequency distribution of vibration velocity on core No.24, 3 phase SSL CGO, at position D (T-joint) with clamping torque 4 Nm at 1.0 T, 50 Hz.

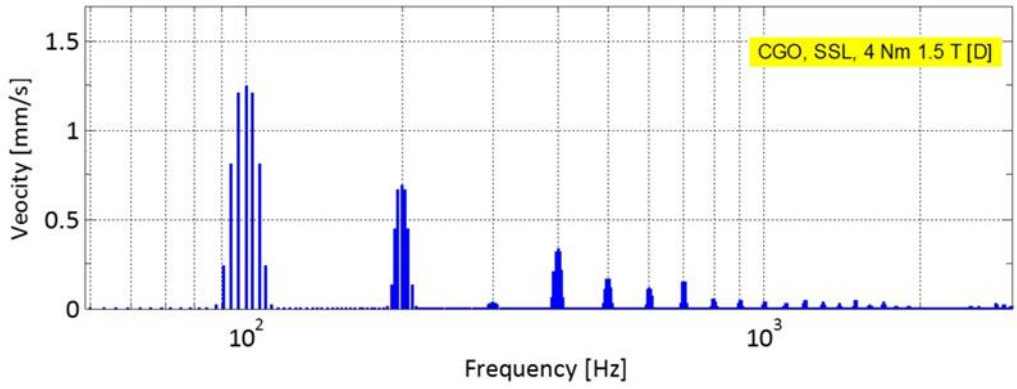

Fig. 5-107: Frequency distribution of vibration velocity on core No.24, 3 phase SSL CGO, at position D (T-joint) with clamping torque 4 Nm at 1.5 T, 50 Hz.

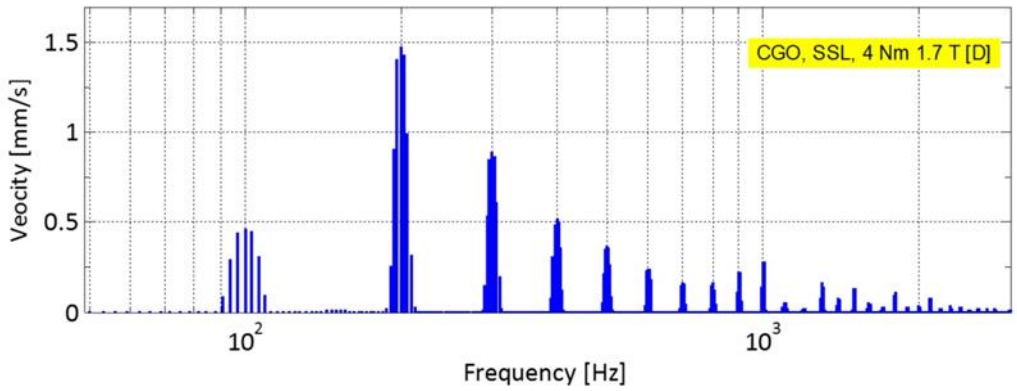

Fig. 5-108: Frequency distribution of vibration velocity on core No.24, 3 phase SSL CGO, at position D (T-joint) with clamping torque 4 Nm at 1.7 T, 50 Hz.

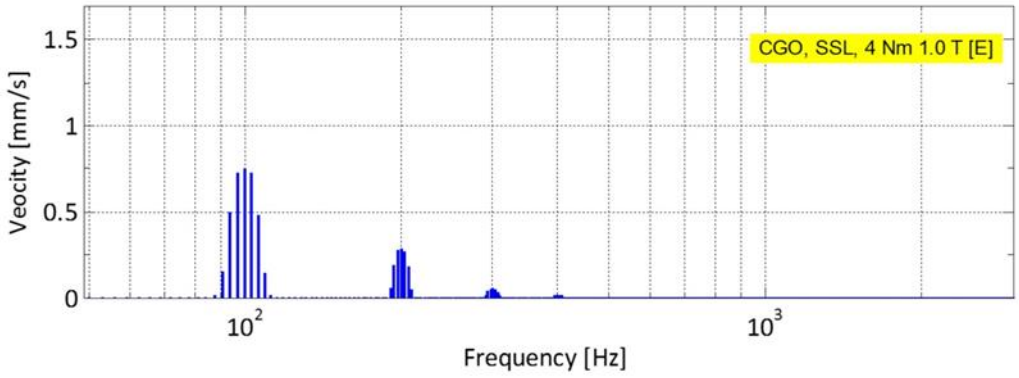

Fig. 5-109: Frequency distribution of vibration velocity on core No.24, 3 phase SSL CGO, at position E (Corner) with clamping torque 4 Nm at 1.0 T, 50 Hz.

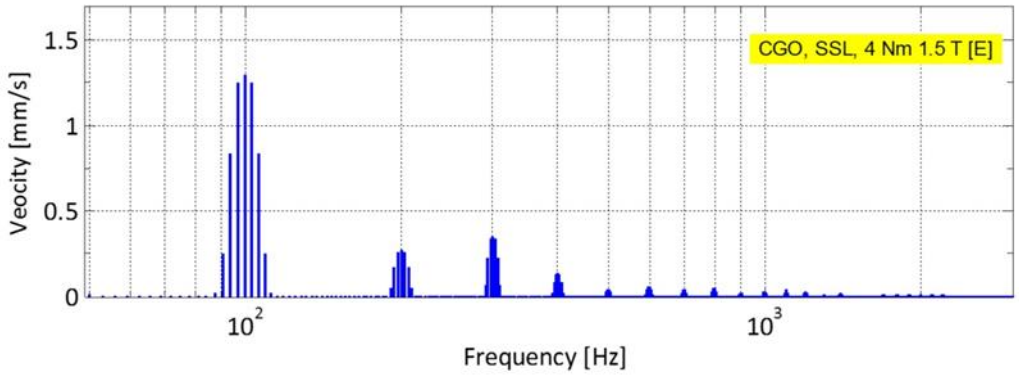

Fig. 5-110: Frequency distribution of vibration velocity on core No.24, 3 phase SSL CGO, at position E (Corner) with clamping torque 4 Nm at 1.5 T, 50 Hz.

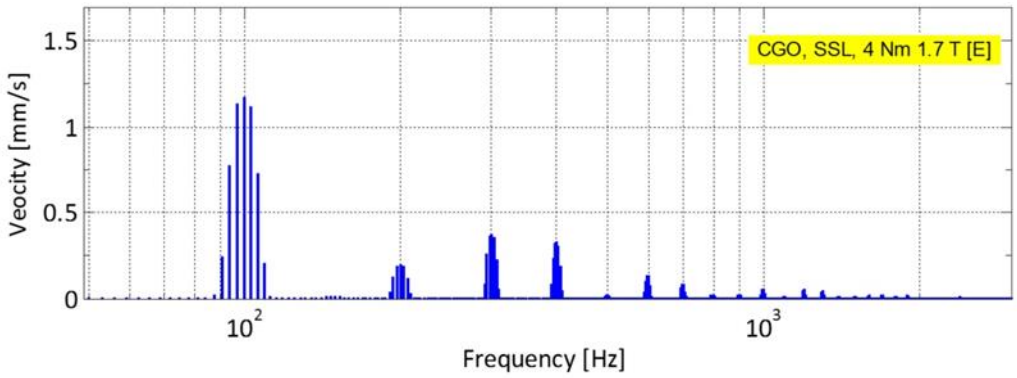

Fig. 5-111: Frequency distribution of vibration velocity on core No.24, 3 phase SSL CGO, at position E (Corner) with clamping torque 4 Nm at 1.7 T, 50 Hz.

5.10 Influence of Core Building on Transformer Core Noise

Skilled workers are required for transformer core assembly process. Although there are jigs and pins for holding the lamination located in desired positions, gaps between the laminations at the joints can be subject to significant variation. The gaps not only affect core losses but also core noise.

To investigate the effect of core building on transformer core noise, A-weighted sound power level from two identical cores were compared. Figs.5-112 to 5-117 shows comparison of A-weighted sound power level of six pairs of 3 phase identical cores built with different materials and step lap configurations with clamping torque 4 Nm at magnetic flux density from 1.5 T to 1.8 T. The error bars in the Figs.5-112 to 5-117 represent variation of sound pressure level on microphone positions which were located on a prescribed contour.

The results show the variation of A-weighted sound power level between each build is up to 2 dB, 4 dB and 6 dB at 1.5 T, 1.7 T and 1.8 T whereas the variation of A-weighted sound power level between each material is up to 2 dB for all levels of flux density. From these results, it can be concluded that core building is another factor affecting transformer core noise. A core assembled from low magnetostriction

material can produce higher noise than one with high magnetostriction material if the building tolerances are poorer.

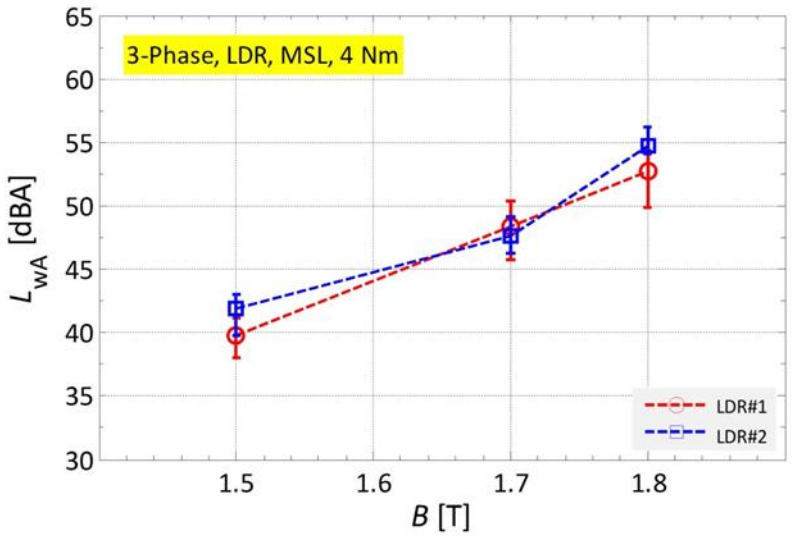

Fig. 5-112: Comparison of A-weighted sound power level of two 3 phase MSL LDR transformer cores with clamping torque 4 Nm at 1.5 T to 1.8 T, 50 Hz.

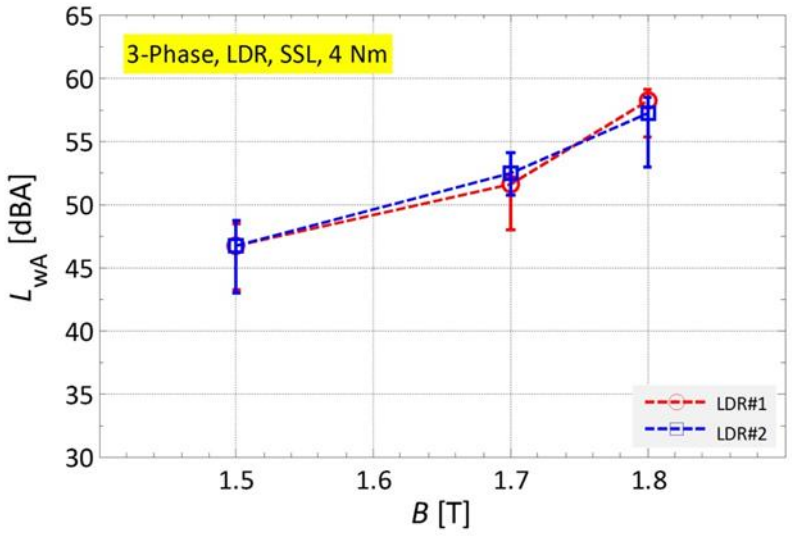

Fig. 5-113: Comparison of A-weighted sound power level of two 3 phase SSL LDR transformer cores with clamping torque 4 Nm at 1.5 T to 1.8 T, 50 Hz.

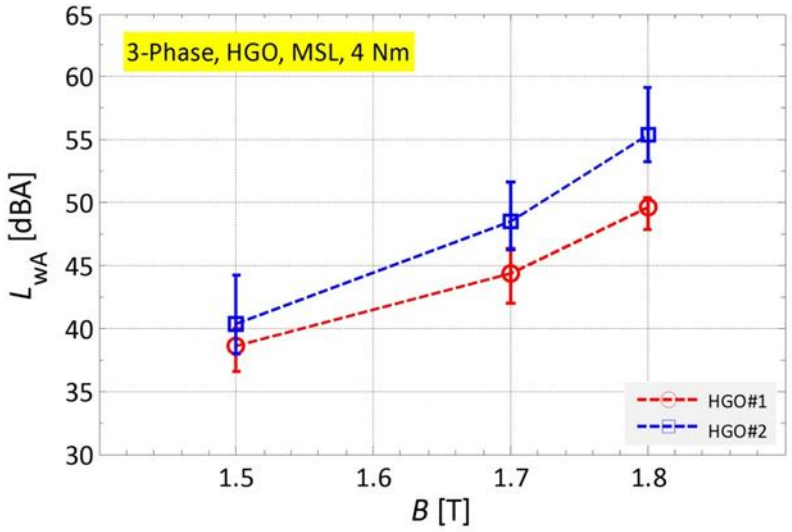

Fig. 5-114: Comparison of A-weighted sound power level of two 3 phase MSL HGO transformer cores with clamping torque 4 Nm at 1.5 T to 1.8 T, 50 Hz.

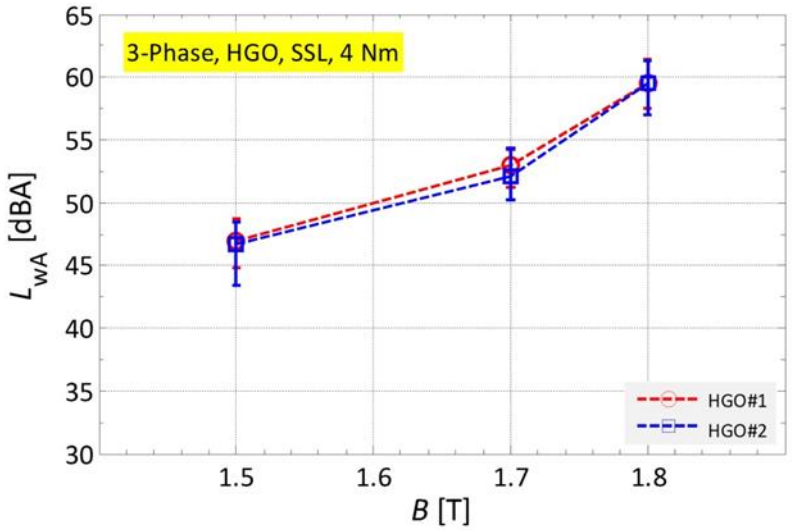

Fig. 5-115: Comparison of A-weighted sound power level of two 3 phase SSL HGO transformer cores with clamping torque 4 Nm at 1.5 T to 1.8 T, 50 Hz.

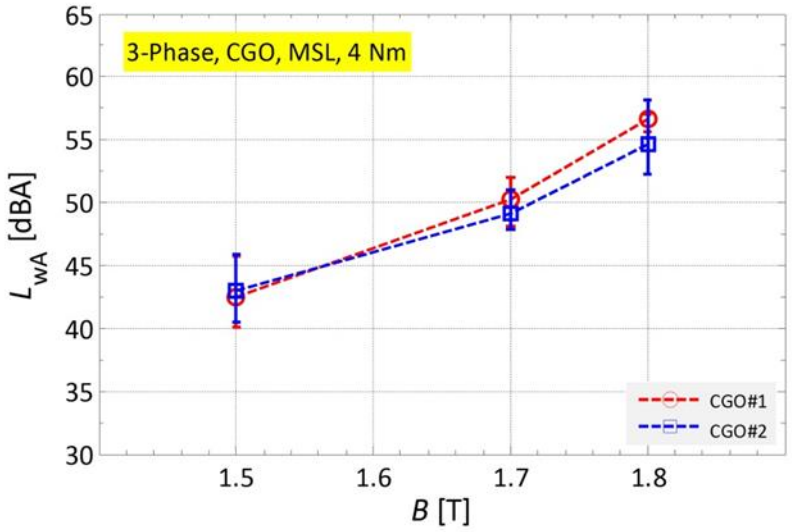

Fig. 5-116: Comparison of A-weighted sound power level of two 3 phase MSL CGO transformer cores with clamping torque 4 Nm at 1.5 T to 1.8 T, 50 Hz.

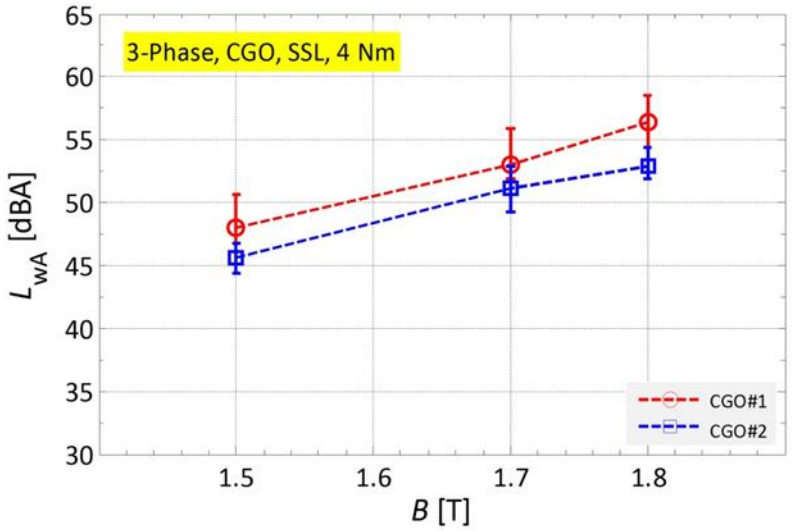

Fig. 5-117: Comparison of A-weighted sound power level of two 3 phase SSL CGO transformer cores with clamping torque 4 Nm at 1.5 T to 1.8 T, 50 Hz.

5.11 Effect of Bonding on Transformer Core Noise

An investigation on flexible bonding of laminations in a 20 kVA single phase single step lap transformer core by Moses [80] has shown the noise at operating flux density 1.5 T is reduced 3 dB after bonding. To investigate the effect of bonding on transformer core noise, a single phase core No.5 (single phase multistep lap configuration with CGO material) was measured as a reference followed by a varnishing stage as described in Chapter 4. Fig.5-118 shows a comparison of the A-weighted sound power level for the core before and after bonding. Despite the resin being applied only to the outer surfaces of the fully built core, Fig.5-119 shows how capillary action has led to approximately 80 % of the lamination surface being bonded. The results show an average from 3 measurements. The error bars represent the variation of the measurements due to microphone positions. The bonding significant reduces the core noise. At 1.5 T, the noise reduced from 44 dBA to 34 dBA (approximately 23 %) while at 1.7 T the noise reduced from 51 dBA to 47 dBA (approximately 8 %). Because operating the core below B_c has higher interlaminar stress in the normal direction than above B_c therefore the reduction on the noise at 1.5 T is higher than at 1.7 T. The critical induction of the core is approximately 1.6 T. Bonding the stack of laminations creates a more homogeneous structure. If a transformer core has a homogeneous structure, there is only in-plane vibration due to magnetostriction forces [62].

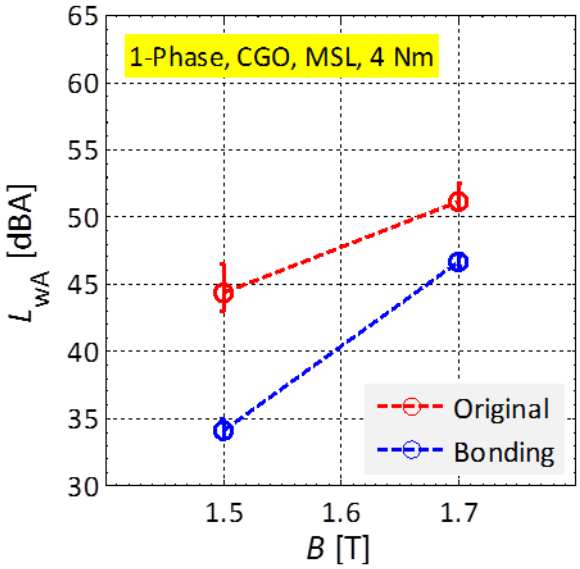

Fig. 5-118: Comparison of A-weighted sound power level of the effect of–with original core at clamping torque 4 Nm, magnetic flux density 1.5 T to 1.7 T, 50 Hz.

Fig. 5-119: Laminations surface with bonded area.

5.12 Investigation of Localised Magnetic Flux Density

Magnetostriction and magnetic forces strongly depend on the magnetic flux density. In addition, the amplitude and phase of the harmonics of magnetic flux density affect the magnetostriction [81]. The fundamental of magnetostriction of grain oriented material decreases or increases depending on phase shift of the harmonic; phase shift between approximately 0-60° (lagging) decreases the fundamental of magnetostriction while between approximately 90-180° (lagging) leads to an increase [82]. To investigate behaviour of localised magnetic flux density on the three phase transformer core, the search coil technique was used. The positions of localised search coils are shown in Chapter 4. The localised magnetic flux densities were obtained from a three phase MSL CGO core by using the search coil technique described in Section 4.5.

In the experiment, the magnetic flux density signal on the middle limb was used as a reference. Figs.5-120 to 5-122 show the frequency distribution components of localised magnetic flux density along the rolling direction at the corner and T-joint. It can be seen that the amplitude of the 3^{rd} harmonic is more than 10 % of the fundamental component. The local flux in some positions show an amplitude difference with the reference since the localised measurements are highly dependent on local grain and domain structures. Table 5-6 shows the phase shift of the 3^{rd} harmonics with reference to their fundamental. It can be seen that at the corner, phase difference between the 3^{rd} harmonic and fundamental is lagging between 0-60° therefore the amplitude of the fundamental of magnetostriction in this region decreases. While, at position 29 which was located at near the end of the middle limb there is a phase shift over 90°, hence, the fundamental of magnetostriction at this point is increased. Although the amplitude of fundamental component of magnetostriction is one of the causes of fundamental component of vibration, it does not have much effect on the human ear.

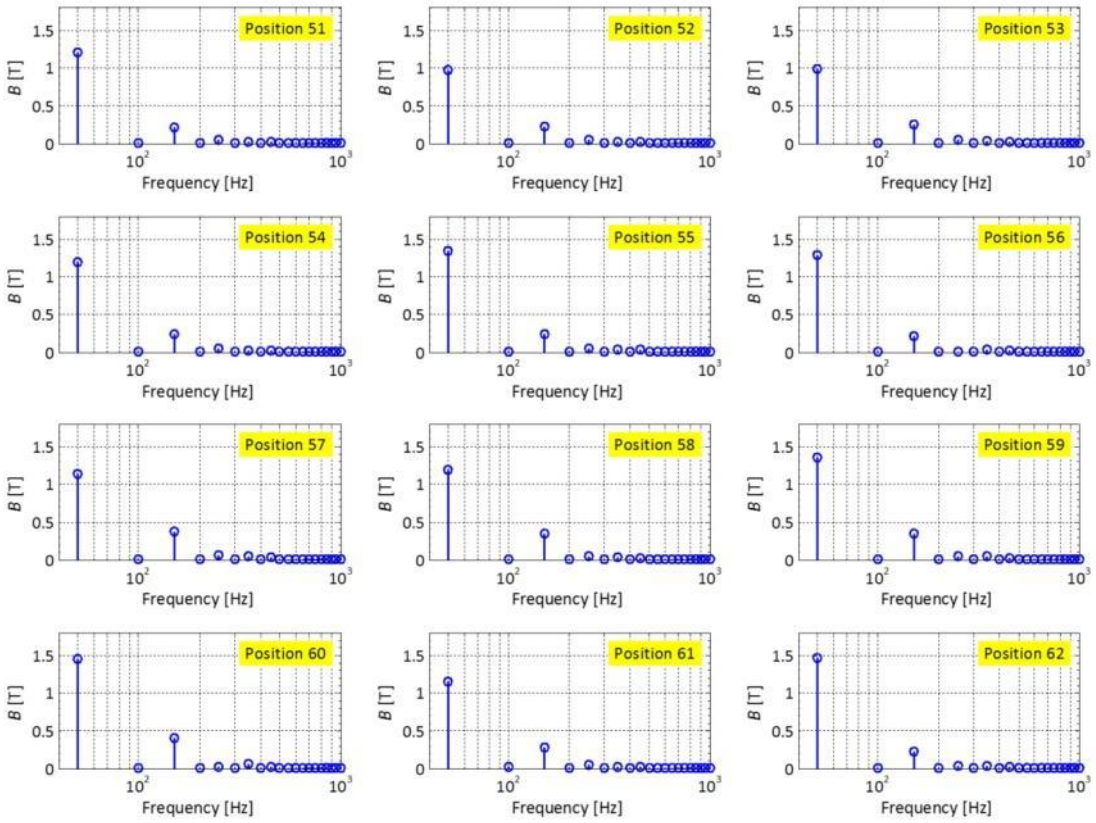

Fig. 5-120: Frequency distribution components of localised magnetic flux density along the rolling direction at the corner between limb C and top yoke with average maximum flux density 1.7 T, 50 Hz.

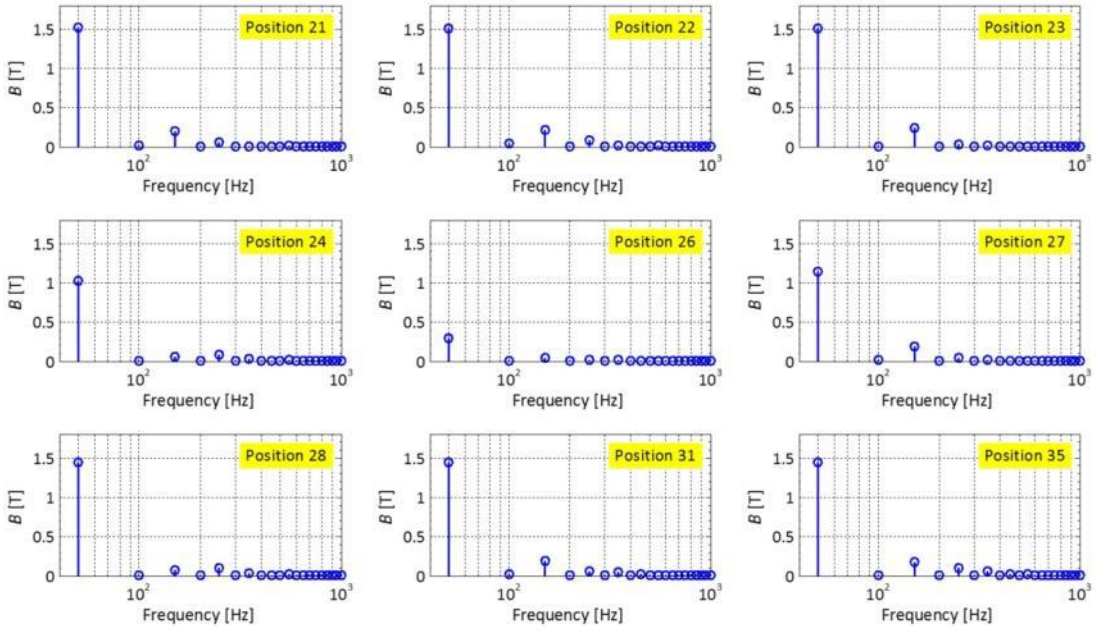

Fig. 5-121: Frequency distribution components of localised magnetic flux density along the rolling direction at the T-joint on top yoke with average maximum flux density 1.7 T, 50 Hz.

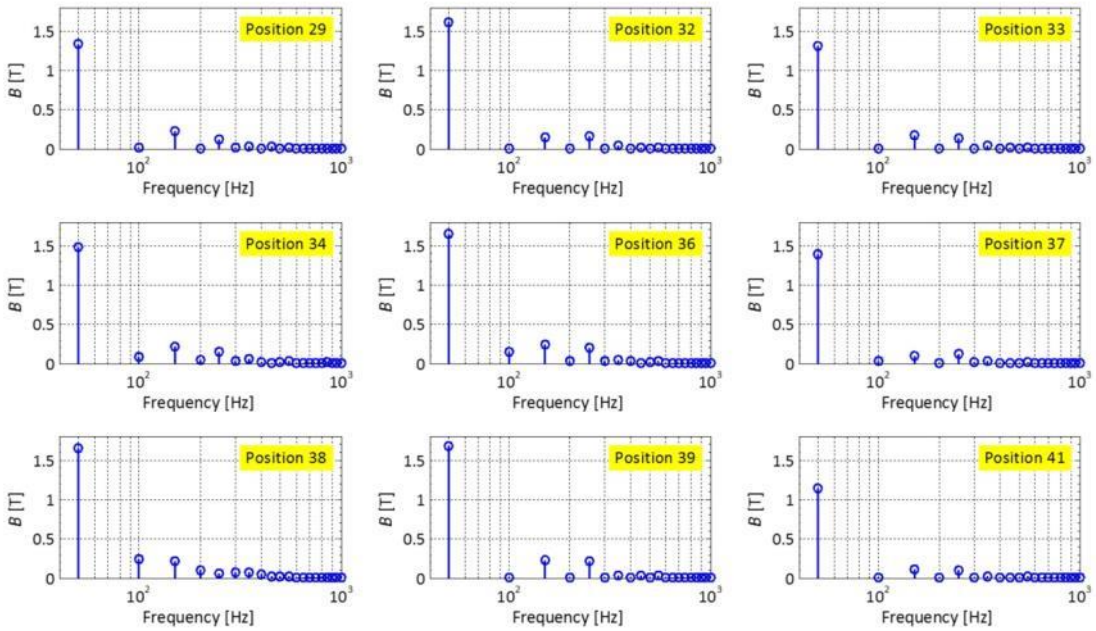

Fig. 5-122: Frequency distribution components of localised magnetic flux density along the rolling direction at the T-joint on the middle limb with average maximum flux density 1.7 T, 50 Hz.

Table 5-6: Phase difference of fundamental and third harmonics of localised flux density on three phase MSL CGO transformer core

Corner		T-joint [on yoke]		T-joint [on limb]	
Position	phase shift [°]	Position	phase shift [°]	Position	phase shift [°]
51	-17	21	59	29	96
52	-40	22	38	32	35
53	-46	23	24	33	73
54	-43	24	161	34	93
55	-54	26	147	36	10
56	-79	27	-33	37	-4
57	-46	28	-139	38	73
58	-36	31	-90	39	115
59	-47	35	187	41	75
60	-58				
61	-32				
62	-42				

5.13 Discussions

The experimental results shown in sections 5.1 to 5.12 are discussed in this section. The model of the transformer core (ref. section 5.1) showed that the deformation of the core was due to the longitudinal magnetostriction. It also showed that the middle limb exhibited the highest strain when the magnetic flux was increased to the maximum. The core laminations continually deform twice in a period of magnetic flux density. The transverse magnetostriction was not considered in the model because: (a) the magnetic flux was assumed to flow uniformly along the rolling direction; and (b) the lamination width was significantly shorter than the length. However, in reality the magnetic flux flows across grains at the joints, therefore, the deformation due to transverse magnetostriction is required to be taken into account to improve the model further.

The experimental noise and vibration results of the transformer cores showed that the highest noise was observed in the CGO core for the same step lap configuration and the lowest noise in the HGO core. The noise from the LDR core was lower than the CGO core but higher than the HGO core. The noise from the LDR core remained nearly constant at lower flux density; however at higher magnetic flux densities it increased significantly. This was because at lower flux densities the closure domains near the laser scribing lines were not activated, whereas at high flux densities the closure domains were activated and made a significant contribution to the magnetostriction. The experimental vibration results show that there is a higher vibration at the core joint. The core joint was subjected to: (a) higher magnetostriction from closure domains; and (b) repelling stress due to the magnetic flux flowing in the normal direction, which is the transverse direction for the domain.

Interestingly, the A-weighted sound power level for the single phase core type transformer was higher than that of the three phase three limb transformer core. Although the three phase core had higher mass and underwent rotational

magnetisation at the T-joint, which increases magnetostriction, the single phase has higher noise. This was because in the three phase core the noise was cancelled due to the phase difference of the vibrations between the limbs.

In the vibration separation model, the deformed middle limb was assumed as a segment of a circle. To improve the model, it was required to validate the assumption. The experimental noise and vibration results of the MSL and SSL in a three phase three limb transformer core showed that the noise of the MSL was lower but its vibration was higher. This difference in the behaviour can be explained by the higher harmonics of vibration in the SSL due to the unsymmetrical dimensions of the lamination in the middle limb which the MSL did not have.

The noise measured from the cores that were built using the same material was not constant. The variation of noise between each build of the core with the same material can be higher than the variation between the materials. Therefore, if care was not taken during the core building process, a core assembled using a low magnetostriction material could lead to higher noise than the core build with high magnetostriction material. To reduce the noise generated from the core, the manufacturers and designer should not only choose the low magnetostriction material but also consider the building process. Core vibration could also be minimised by bonding the laminations of the core because it helps to eliminate the interlaminar stress between the laminations.

Chapter 6

Conclusions and Future Work

6.1 Conclusions

The A-weighted sound power level of single phase transformer cores is higher than 3 phase cores with the same core cross sectional area per phase and core window size although the 3 phase core is larger in volume and greater in mass and has high out of plane vibration. This is due to the effect of phase difference of the vibration on each limb of the three phase core.

Magnetostriction is more significant when a core is operated at low flux density. Magnetic forces have the more significant effect on transformer core vibration when the operating flux density is high due to increased air gap flux density in the joints.

When a transformer core is operated at low magnetic flux density, higher core noise is generated from in-plane direction of the laminations on its side surface than from the front and the top surfaces. However, at high flux density, higher noise is generated from the out of plane direction of the laminations due to an increase of both magnetostriction and magnetic forces.

Although A-weighted sound power level is gaining acceptance as a reference quantity for quantification and comparison of noise generated from transformer cores, it is not suitable for investigating the relationship between noise and vibration because the A-weighting scale is applied to the sound pressure signal. Sound pressure and the vibration signal in the frequency domain are the most appropriate parameters for studying the relationship between transformer core noise and vibration.

Louder noise can be generated from a core built with low magnetostriction material than higher magnetostriction if the building tolerances are worse. Thus for low noise transformers tight control of corner air gaps is required.

Bonding laminations together in a core are shown to lead to a reduction in core noise due to the resulting effect of interlaminar magnetic forces between the overlap regions

and flapping of the laminations. The bonding is the most effective when the core is operated below the critical induction of the core.

6.2 Suggested Future Work

From the findings of this study it can be deduced that the future research on the following two themes would be highly beneficial to transformer core design and electrical steel produce for quantifying the deformation of the core due to magnetostriction.

Magnetostriction characteristics under rotational magnetisation should be investigated in order to better understand the in-plane strains at the joints. These can be carried out using experimental localised magnetic flux orthogonal component results as an input of magnetostriction measurement of the 2D magnetisation system. Also magnetic domain behaviour at the ends of the lamination and joints needs to be investigated. Results of such a study should lead to improvement in the core deformation model due to magnetostriction.

More detailed analysis of strains and flux paths at the joints would enhance the understanding of the vibration generation mechanism allowing the models developed here to be validated. The university has recently purchased a 3D laser scanning vibrometer which will enable this study to take place.

References

[1] U.S. Energy Information Administration. (18 July 2013). *International Energy Statistics*.Available:http://www.eia.gov/cfapps/ipdbproject/IEDIndex3.cfm?tid=44&pid=44&aid=2

[2] European Commitee for Electrotechnical Standardization, "Three-phase oil-immersed distribution transformers 50 Hz from 50 kVA to 2 500 kVA with highest voltage for equipment not exceeding 36 kV General requirements," 2007.

[3] S. V. Kulkarni and S. A. Khaparde, *Transformer engineering : design and practice*. New York: Marcel Dekker, Inc., 2004.

[4] M. J. Heathcote and D. P. Franklin, *The J & P transformer book : a practical technology of the power transformer*, 13th ed. Burlington, MA: Newnes, 2007.

[5] M. Mizokami, M. Yabumoto, and Y. Okazaki, "Vibration analysis of a 3-phase model transformer core," *Electrical Engineering in Japan*, vol. 119, pp. 1-8, 1997.

[6] B. Weiser, H. Pfützner, and J. Anger, "Relevance of magnetostriction and forces for the generation of audible noise of transformer cores," *IEEE Transactions on Magnetics*, vol. 36, pp. 3759-3777, 2000.

[7] Bharat Heavy Electricals Limited, *Transformers*, 2 ed. New Delhi: Tata mcGraw-Hill, 2008.

[8] I. Dasgupta, *Power transformers quality assurance*: New Age International Limited, 2009.

[9] S. Chikazumi, *Physics of Ferromagnetism*: Oxford Science Publications, 2010.

[10] E. Reiplinger, "Assessment of grain-oriented transformer sheets with respect to transformer noise," *Journal of Magnetism and Magnetic Materials*, vol. 21, pp. 257-261, 1980.

[11] S. L. Foster and E. Reiplinger, "Charcteristics and Control of Transformer Sound," *IEEE Transactions on Power Apparatus and Systems*, vol. PAS-100, pp. 1072-1077, 1981.

[12] D. J. Mapps and C. White, "Longitudinal and transverse magnetostriction harmonics in (110)[001] silicon-iron," *IEEE Transactions on Magnetics*, vol. 20, pp. 1566-1568, 1984.

[13] Z. Valkovic, "Effect of electrical steel grade on transformer core audible noise," *Journal of Magnetism and Magnetic Materials*, vol. 133, pp. 607-609, 1994.

[14] Z. Valkovic, "Investigations of core noise levels using a dry-type transformer model," *Journal of Magnetism and Magnetic Materials*, vol. 160, pp. 205-206, 1996.

[15] A. Ilo, B. Weiser, T. Booth, and H. Pfützner, "Influence of geometric parameters on the magnetic properties of model transformer cores," *Journal of Magnetism and Magnetic Materials,* vol. 160, pp. 38-40, 1996.

[16] F. Loffler, T. Booth, H. Pfützner, C. Bengtsson, and K. Gramm, "Relevance of step-lap joints for magnetic characteristics of transformer cores," *IEE Proceedings Electric Power Applications,* vol. 142, pp. 371-378, 1995.

[17] Z. Valkovic, "Effects of transformer core design on noise level," *J. Phys. IV France,* vol. 08, pp. Pr2-603-Pr2-606, 1998.

[18] M. Ishida, S. Okabe, and K. Sato, "Analysis of Noise Emitted from Three-Phase Stacked Transformer Model Core," Kawasaki Steel Technical Report, 1998.

[19] P. I. Anderson, A. J. Moses, and H. J. Stanbury, "Assessment of the Stress Sensitivity of Magnetostriction in Grain-Oriented Silicon Steel," *IEEE Transactions on Magnetics,* vol. 43, pp. 3467-3476, 2007.

[20] M. Ishida, S. Okabe, T. Imamura, and c. Komatsubara, "Model Transformer Evaluation of High-Permeability. Grain-Oriented Electrical Steels," *Journal of Materials Science &Technology,* vol. 16, 2000.

[21] D. Snell, "Measurement of noise associated with model transformer cores," *Journal of Magnetism and Magnetic Materials,* vol. 320, pp. e535-e538, 2008.

[22] D. Snell, "Noise generated by model step lap core configurations of grain oriented electrical steel," *Journal of Magnetism and Magnetic Materials,* vol. 320, pp. e887-e890, 2008.

[23] R. S. Girgis, Bernesjo, x, M. S., S. Thomas, J. Anger, D. Chu, and H. R. Moore, *Development of Ultra-Low-Noise Transformer Technology* vol. 26, 2011.

[24] L. Lahn, W. Chaoyong, A. Allwardt, T. Belgrand, and J. Blaszkowski, "Improved Transformer Noise Behavior by Optimized Laser Domain Refinement at ThyssenKrupp Electrical Steel," *IEEE Transactions on Magnetics,* vol. 48, pp. 1453-1456, 2012.

[25] B. Weiser, A. Hasenzagl, T. Booth, and H. Pfützner, "Mechanisms of noise generation of model transformer cores," *Journal of Magnetism and Magnetic Materials,* vol. 160, pp. 207-209, 1996.

[26] B. Weiser and H. Pfützner, "Relevance of magnetostatic forces for transformer core vibrations," *J. Phys. IV France,* vol. 08, pp. Pr2-591-Pr2-594, 1998.

[27] L. Vandevelde and J. A. A. Melkebeek, "Modeling of magnetoelastic material," *IEEE Transactions on Magnetics,* vol. 38, pp. 993-996, 2002.

[28] L. Vandevelde and J. A. A. Melkebeek, "Magnetic forces and magnetostriction in electrical machines and transformer cores," *IEEE Transactions on Magnetics,* vol. 39, pp. 1618-1621, 2003.

[29] L. Vandevelde, J. Gyselinck, M. A. C. De Wulf, and J. A. A. Melkebeek, "Finite-element computation of the deformation of ferromagnetic material taking into account magnetic forces and magnetostriction," *IEEE Transactions on Magnetics*, vol. 40, pp. 565-568, 2004.

[30] T. Hilgert, L. Vandevelde, and J. Melkebeek, "Comparison of Magnetostriction Models for Use in Calculations of Vibrations in Magnetic Cores," *IEEE Transactions on Magnetics*, vol. 44, pp. 874-877, 2008.

[31] Q. Li, X. Wang, L. Zhang, J. Lou, and L. Zou, "Modelling methodology for transformer core vibrations based on the magnetostrictive properties," *IET Electric Power Applications*, vol. 6, pp. 604-610, 2012.

[32] L. Zhu, Q. Yang, R. Yan, Y. Li, X. Zhang, W. Yan, and J. Zhu, "Numerical computation for a new way to reduce vibration and noise due to magnetostriction and magnetic forces of transformer cores," *Journal of Applied Physics*, vol. 113, pp. 17A333-17A333-3, 2013.

[33] M. Javorski, G. Cepon, J. Slavic, and M. Boltezar, "A Generalized Magnetostrictive-Forces Approach to the Computation of the Magnetostriction-Induced Vibration of Laminated Steel Structures," *IEEE Transactions on Magnetics*, vol. 49, pp. 5446-5453, 2013.

[34] J. R. Hassall and K. Zaveri, *Acoustic Noise Measurements*, 3rd ed.: Brüel & Kjær, 1978.

[35] British Standard, "Electroacoustics. Sound level meters. Specifications," 2003.

[36] Brüel & Kjær, "Microphone Handbook." vol. 1, 1996.

[37] Brüel & Kjær, "Measurement Microphones," 1994.

[38] Brüel & Kjær, "Microphone Handbook : For the Falcon™ Range of Microphone Products," 1995.

[39] Brüel & Kjær, "Measuring Vibration," 1982.

[40] M. Serridge and T. R. Licht, *Piezoelectric Accelerometer and Vibration Preamplifier Handbook*: Brüel & Kjær, 1987.

[41] M. P. Norton and D. G. Karczub, *Fundamentals of noise and vibration analysis for engineers*, 2nd ed. Cambridge, UK ; New York, NY: Cambridge University Press, 2003.

[42] Clarence W. de Silva, *Vibration : Fundamentals and Practice*: CRC Press LLC, 1999.

[43] PolyTec, "Operating Instructions and Specifications, PSV-400 Scanning Vibrometer", 2012.

[44] G. Loisos and A. J. Moses, "Critical evaluation and limitations of localized flux density measurements in electrical steels," *IEEE Transactions on Magnetics*, vol. 37, pp. 2755-2757, 2001.

[45] H. Pfützner and G. Krismanic, "The needle method for induction tests: sources of error," *IEEE Transactions on Magnetics*, vol. 40, pp. 1610-1616, 2004.

[46] T. Phophongviwat, A. J. Moses, P. I. Anderson, and J. P. Hall, "Simultaneous measurement of magnetostriction, vibration and noise of distribution transformer cores," presented at the Soft Magnetic Materials Conference 2011 (SMM20), Kos Island, Greece, 2011.

[47] British Standard, "*Power transformers-Part 10: Determination of sound level*," 2001.

[48] Brüel & Kjær, "Product Data : TEDS Microphones," 2012.

[49] National Instruments, "Operating instructions and specifications, NI 9215 4-Channel, ±10 V, 16-Bit Simultaneous Analog Input Module", 2011.

[50] UKAS-M3003, "The Expression of Uncertainty and Confidence in Measurement," 2012.

[51] S. Bell, *A beginner's guide to uncertainty in measurement*. Teddington, Middlesex, United Kingdom: National Physical Laboratory 2001.

[52] LEM NORMA GmbH, "Wide Band Power Analyzer D6000 Operating Instructions."

[53] H. Stanbury, "The treatment of uncertainties in magnetic measurements," Unpublished, Wolfson Centre for Magnetics, School of Engineering, Cardiff University, 2011.

[54] LEM NORMA GmbH, "Power Analyzer D 4000 Operating Instructions."

[55] Brüel & Kjær, "16-channel DeltaTron® Conditioning Amplifiers — Types 2694," 2011.

[56] National Instruments, "NI 9215 Operating Instructions and Specifications," 2011.

[57] PolyTec, "Manufacturer Calibration Procedure for Laser Vibrometer," 2002.

[58] B. D. Cullity and C. D. Graham, *Introduction to magnetic materials*, 2nd ed. USA: Hoboken, N.J. : Wiley 2009.

[59] Nippon steel & Sumitomo Metal, "Technical Data on Domain Refined ORIENTCORE HI-B ZDKH", 2013.

[60] S. Tabrizi, "Study of effective method of characterisation of magnetostriction and its fundamental effect on transformer core noise and vibration," Wolfson Centre for Magnetics, School of Engineering, Cardiff University, Technical report, 2013.

[61] D. Jiles, *Introduction to magnetism and magnetic materials*, 1st ed. London ; New York: Chapman and Hall, 1991.

[62] M. G. Say, *Alternating current machines*, 5th ed. Harlow: Longman Scientific and Technical, 1986.

[63] AK Steel Corporation, "TRAN-COR® H GRAIN ORIENTED ELECTRICAL STEELS", 2013.

[64] Cogent Power Ltd., "Electrical Steel Grain Oriented Unisil, Unisil-H", 2010.

[65] ThyssenKrupp Electrical Steel GmbH, "Grain oriented electrical steel PowerCore®", 2013.

[66] RS Components Ltd., "Insulating Vanish, RS 199-1480", 2010.

[67] T. P. P. Phway and A. J. Moses, "Magnetisation-induced mechanical resonance in electrical steels," *Journal of Magnetism and Magnetic Materials*, vol. 316, pp. 468-471, 2007.

[68] A. Lundgren, "On measurement and modelling of 2D magnetization and magnetostriction of SiFe sheets," PhD Thesis, Royal Institute of Technology, Sweden, 1999.

[69] M. N. O. Sadiku, *Elements of electromagnetics*, 5th ed. New York: Oxford University Press, 2011.

[70] H. Pfutzner, E. Mulasalihovic, H. Yamaguchi, D. Sabic, G. Shilyashki, and F. Hofbauer, "Rotational Magnetization in Transformer Cores-A Review," *IEEE Transactions on Magnetics,*, vol. 47, pp. 4523-4533, 2011.

[71] K. Senda, M. Ishida, K. Sato, M. Komatsubara, and T. Yamaguchi, "Localized magnetic properties in grain-oriented electrical steel measured by needle probe method," *Electrical Engineering in Japan*, vol. 126, pp. 1-11, 1999.

[72] E. G. teNyenhuis, G. F. Mechler, and R. S. Girgis, "Flux distribution and core loss calculation for single phase and five limb three phase transformer core designs," *IEEE Transactions on Power Delivery*, vol. 15, pp. 204-209, 2000.

[73] T. Nakata, M. Nakano, and K. Kawahara, "Effects of Stress Due to Cutting on Magnetic Characteristics of Silicon Steel," *IEEE Translation Journal on Magnetics in Japan,*, vol. 7, pp. 453-457, 1992.

[74] D. Mapps and C. White, "Longitudinal and transverse magnetostriction harmonics in (110)[001] SiFe," *IEEE Transactions on Magnetics*, vol. 20, pp. 1566-1568, 1984.

[75] H. D. Young, R. A. Freedman, and L. Ford, *University physics with modern physics.*, 13th ed. Boston, Mass. ; London : Addison-Wesley, 2011.

[76] R. M. D. Vecchio, B. Piulin, P. T. Feghali, D. M. Shah, and R. Ahuja, *Transformer design principles : with applications to core-form power transformers*, 2nd ed. Boca Raton, FL: CRC Press, 2010.

[77] R. G. Budynas, Nisbett, J. Keith, *Shigley's mechanical engineering design*, 9th ed. New York: McGraw-Hill, 2011.

[78] Röchling. (2011). *Durostone® Fasteners*. Available: http://www.roechling-plastics.co.uk/en/products/composites/fibre-reinforced-plastics/fasteners.html

[79] D. Ray and R. Gnanamoorthy, "Friction and wear behavior of vinylester resin matrix composites filled with fly ash particles," *Journal of Reinforced Plastics and Composites,* vol. 26, pp. 5-13, 2007.

[80] A. J. Moses and S. M. Pegler, "The effects of flexible bonding of laminations in a transformer core," *Journal of Sound and Vibration,* vol. 29, pp. 103-112, 1973.

[81] D. J. Mapps and C. White, "Phase-shifted flux harmonics and magnetostriction in (110)[001] SiFe," *IEEE Transactions on Magnetics,* vol. 18, pp. 1505-1507, 1982.

[82] S. G. Ghalamestani, L. Vandevelde, J. J. J. Dirckx, and J. A. A. Melkebeek, "Magnetostriction and the Influence of Higher Harmonics in the Magnetic Field," *IEEE Transactions on Magnetics,* vol. 48, pp. 3981-3984, 2012.

Appendix A

Uncertainty in the Measurements

The uncertainty in the measurements of magnetic flux densities on three phase and single phase cores, noise, vibration and localised magnetic flux density were calculated at a confidence level of 95 %. The details of the uncertainty budget are described in Chapter 3. To apply a single uncertainty value for all measurements, the values of source of uncertainty were taken from the value which yields the maximum uncertainty. The results are shown in Tables A-1 to A-5.

Table A-1: Uncertainty budget in the measurement of *B* on the three phase cores

Source of uncertainty	**± %**	**Probability distribution**	**Divisor**	C_i	U_i **± %**
Accuracy of D6000 (reading)	0.050	Normal	2.0000	1	0.02500
Accuracy of D6000 (range)	0.005	Normal	2.0000	1	0.00250
Lamination width	0.010	Rectangular	1.7321	1	0.00577
Stack depth	0.010	Rectangular	1.7321	1	0.00577
Frequency	0.100	Normal	2.0000	1	0.05000
Drift between calibrations	0.020	Rectangular	1.7321	1	0.01155
Type A uncertainty, V_A	0.029	Normal	2.0000	1	0.01450
Type A uncertainty, V_B	0.029	Normal	2.0000	1	0.01450
Type A uncertainty, V_C	0.029	Normal	2.0000	1	0.01450
Combined uncertainty					0.06294
Expanded uncertainty at a confidence level of 95 %					**0.2**

Table A-2: Uncertainty budget in the measurement of B on the single phase cores

Source of uncertainty	**± %**	**Probability distribution**	**Divisor**	C_i	U_i ± %
Accuracy of D400 (reading)	0.100	Normal	2.0000	1	0.05000
Accuracy of D400 (range)	0.100	Normal	2.0000	1	0.05000
Lamination width	0.010	Rectangular	1.7321	1	0.00577
Stack depth	0.010	Rectangular	1.7321	1	0.00577
Frequency	0.100	Normal	2.0000	1	0.05000
Drift between calibrations	0.020	Rectangular	1.7321	1	0.01155
Type A uncertainty, V	0.029	Normal	2.0000	1	0.01450
Combined uncertainty					0.08894
Expanded uncertainty at a confidence level of 95 %					**0.2**

Table A-3: Uncertainty budget in the measurement of noise

Source of uncertainty	**± %**	**Probability distribution**	**Divisor**	C_i	U_i ± %
Accuracy of B&K 4188-A-021	0.645	Normal	2.0000	1	0.32258
Accuracy of B&K 2694	0.125	Normal	2.0000	1	0.06250
Accuracy of NI 9215 (reading)	0.020	Normal	2.0000	1	0.01000
Accuracy of NI 9215 (range)	0.014	Normal	2.0000	1	0.00700
Drift between calibrations	0.020	Rectangular	1.7321	1	0.01155
Type A uncertainty	0.070	Normal	2.0000	1	0.03500
Combined uncertainty					0.33087
Expanded uncertainty at a confidence level of 95 % (k_{95}=2)					**0.7**

Table A-4: Uncertainty budget in the measurement of vibration

Source of uncertainty	**± %**	**Probability distribution**	**Divisor**	C_i	U_i ± %
Accuracy of Vibrometer	1.300	Normal	2.0000	1	0.65000
Drift between calibrations	0.020	Rectangular	1.7321	1	0.01155
Type A uncertainty, V	0.000	Normal	2.0000	1	0.00000
Combined uncertainty					0.65010
Expanded uncertainty at a confidence level of 95 %					**2**

Table A-5: Uncertainty budget in the measurement of localised magnetic flux density

Source of uncertainty	**± %**	**Probability distribution**	**Divisor**	C_i	U_i **± %**
Accuracy of NI 9215 (reading)	0.020	Normal	2.0000	1	0.01000
Accuracy of NI 9215 (range)	0.014	Normal	2.0000	1	0.00700
Lamination width	0.010	Rectangular	1.7321	1	0.00577
Lamination thick	0.010	Rectangular	1.7321	1	0.00577
Frequency	0.100	Normal	2.0000	1	0.05000
Drift between calibrations	0.020	Rectangular	1.7321	1	0.01155
Type A uncertainty, V	0.045	Normal	2.0000	1	0.02250
Combined uncertainty					0.05792
Expanded uncertainty at a confidence level of 95 %					**0.2**

Appendix B

List of Publications

International Conferences

A.J. Moses, P.I. Anderson, **T. Phophongviwat**, S. Tabrizi. "Contribution of magnetostriction to transformer noise" Universities Power Engineering Conference (UPEC), 2010 45th International, Cardiff, UK, Aug. 31 2010-Sept. 3 2010.

T. Phophongviwat, A.J. Moses, P.I. Anderson, and J.P. Hall. "Simultaneous measurement of magnetostriction, vibration and noise of distribution transformer cores" Soft Magnetic Materials Conference 2011 (SMM20), Kos Island, Greece, Sep. 18-22, 2011.

T. Phophongviwat, P.I. Anderson and A.J. Moses. "Relationship between Vibration and Acoustic Noise of 3 Phase 3 Limb transformer Cores." Soft Magnetic Materials Conference 2011 (SMM21), Budapest, Hungary, Sep. 1-4, 2013.

Due to the sponsorship conditions, journal publications have to date been restricted while partners disseminate results. Drafts with the following title have been prepared for publication in 2014 subject to sponsors approved.

- Relationship between Vibration and Acoustic Noise of transformer Cores
- Model for Separation the Effect of Magnetostriction and Magnetic Forces on Transformer Core Vibration